NASA CONTRACTOR REPORT

NASA CR-309

CURRENT SHEATH DYNAMICS AND MAGNETOSONIC OSCILLATIONS IN MAGNETOPLASMAS

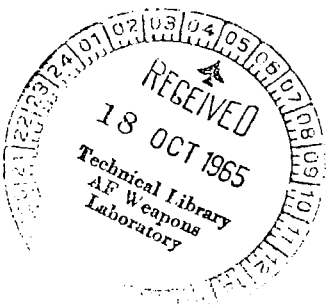

by Otto M. Friedrich, Jr., and Arwin A. Dougal

Prepared under Grant No. NsG-353 *by*
UNIVERSITY OF TEXAS
Austin, Texas
for

NATIONAL AERONAUTICS AND SPACE ADMINISTRATION • WASHINGTON, D. C. • OCTOBER 1965

CURRENT SHEATH DYNAMICS AND MAGNETOSONIC OSCILLATIONS IN MAGNETOPLASMAS

By Otto M. Friedrich, Jr., and Arwin A. Dougal

Prepared under Grant No. NsG-353 by
UNIVERSITY OF TEXAS
Austin, Texas

for

NATIONAL AERONAUTICS AND SPACE ADMINISTRATION

For sale by the Clearinghouse for Federal Scientific and Technical Information
Springfield, Virginia 22151 – Price $4.00

ABSTRACT

The electrical breakdown, current sheath formation, and acceleration of current sheaths in deuterium, hydrogen, and argon plasmas are investigated analytically and experimentally. A system of partial differential equations is written from the Maxwell's electromagnetic field equations and plasma equations to describe the current density, resistivity, electron temperature, ion temperature, and degree of ionization as functions of position and time. The plasma equations include: an energy balance equation, an equation relating resistivity to collisions, an ionization equation, and an energy transfer equation. The resulting set of partial differential equations is coded for electronic digital computation on The University of Texas' Control Data Corporation 1604 high speed, electronic digital computer using finite difference techniques. Theoretical results are obtained for initial deuterium gas pressures of 1 micron, 100 microns, and 1 mm Hg.

The subsequent motion of dynamic current sheaths in a parallel plate accelerator is calculated using a finite difference technique on an equation of motion based on a snowplow model. The dynamics of current sheaths produced and accelerated in a stabilized inverse pinch are determined using a Runge-Kutta method of integration on an equation of motion based on the snowplow model. Magnetosonic oscillations are predicted and the frequency of these oscillations is determined by a perturbation calculation. The position of the peak density vs time for a

theta pinch with reverse bias magnetic fields of 2 and 4 kilogauss is calculated for a hydrodynamic model with the Hain-Roberts computer code. Radial hydrodynamic oscillations are predicted for the 2 kilogauss reverse bias field.

Three experimental geometries are employed to produce and accelerate dynamic current sheaths: 1) a parallel plate accelerator with 50,000 amperes peak driving current, 5 microsecond quarter period, 6 cm wide x 8 cm long electrodes spaced 3.4 cm apart; 2) a stabilized inverse pinch with 100,000 amperes peak driving current, 3.5 microsecond quarter period, 18 cm OD x 6.6 cm long circular cylindrical discharge tube immersed in a stabilizing magnetic field of 0 to 5 kilogauss; and 3) an extremely high temperature theta pinch with peak magnetic fields as high as 75 kilogauss and bias fields of 0 to 10 kilogauss in a discharge tube 5 cm ID and over 20 cm long.

Diagnostic techniques employed to investigate the formation, acceleration, and oscillations of dynamic current sheaths includes the following: a 3.39 micron coupled infrared maser resonator technique; double electrode, unbiased, electrostatic probes; high speed Kerr cell photography; piezoelectric pressure sensitive probes; small magnetic probes; and high voltage-current input measurements. The infrared maser interferometry technique is employed to determine space and time resolved electron densities during formation and acceleration of current sheaths in the parallel plate accelerator. Peak electron densities the order of

10^{17}/cc are measured. The onset of current sheaths is readily observed. The electric fields established by radially expanding current sheaths in the stabilized inverse pinch are measured with double electrode, unbiased, electrostatic probes. From radial electric fields, estimates for the ion energy of 30 ev are obtained for argon plasma under certain conditions. The self-luminous fronts produced in the parallel plate accelerator, the stabilized inverse pinch, and the theta pinch are photographed with a high speed Kerr cell system. Radial hydrodynamical oscillations in the theta pinch are indicated. Electrical breakdown, current sheath formation, and acceleration are observed in all three experimental arrangements employed. The pressure fronts produced in the stabilized inverse pinch are investigated with small piezoelectric probes. Magnetic probes are employed to determine the current sheath onset time vs radius, to investigate the magnetosonic oscillations developed, and to study macroscopic stability, and/or to search for oscillations of the current sheath.

Electrical breakdown and current sheath formation occur near the paths of minimum impedance. Measured electron densities indicate a high degree of ionization in the current sheath for current densities the order of 10^4 amp/cm^2 and initial gas pressures of several hundred microns. Effective sweeping (good snowplowing) of the electrons as the current sheath moves down the parallel plate accelerator is observed. Experimental results of the dynamics of the current sheath produced and accelerated in the parallel plate accelerator and the stabilized inverse pinch compare

favorably with calculated results based on a snowplow model. The initial radial pinch and hydrodynamical oscillations predicted by the Hain-Roberts analytical results agree, in general, with the observed motion of the dynamic current sheath produced in the theta pinch.

TABLE OF CONTENTS

Page

Abstract iii

List of Figures ix

Chapter

I. INTRODUCTION 1

II. THEORETICAL ANALYSIS 7

A. Initial Electrical Breakdown and Formation of Current Sheaths 7

B. Dynamics of Current Sheaths 12

III. EXPERIMENTAL ARRANGEMENTS 39

A. Parallel Plate Accelerator 39

B. Stabilized Inverse Pinch 42

C. Extremely High Temperature Theta Pinch 46

IV. INSTRUMENTATION 54

A. Infrared Maser Interferometry 54

B. Electrostatic Probes 58

C. Kerr Cell High Speed Photography 59

D. Piezoelectric Pressure Sensitive Probes 61

E. Magnetic Probes 61

F. Voltage-Current Input Measurements 63

G. Other Diagnostics Employed 65

V. EXPERIMENTAL FINDINGS 66

A. Plasma Breakdown and Current Sheath Formation Between Planar Electrodes 66

B. Space and Time Resolved Electron Densities in the Parallel Plate Geometry 67

C. Electric Fields Associated with Current Sheaths Formed in an Inverse Pinch 75

D. Self-Luminous Fronts Formed and Accelerated Between Planar Electrodes 80
E. Pressure Fronts Associated with Current Sheaths in an Inverse Pinch Geometry 86
F. Magnetic Fields in an Inverse Pinch Geometry 90
G. Macroscopic Behavior of Current Sheaths Formed Between Planar Electrodes 94

VI. CONCLUSIONS 95
A. Breakdown, Formation, and Structure 95
B. Electron Densities in a Parallel Plate Accelerator 97
C. Acceleration, Propulsion, and Dynamics 98
D. Magnetosonic Oscillations and Macroscopic Stability 99

APPENDICES
A. Initial Conditions for Stabilized Inverse Pinch (Equations and Computer Code) 101
B. Theoretical Models (Equations) 106
C. Current Sheath Dynamics Calculations for Parallel Plate Accelerator (Equations and Computer Code) 109
D. Current Sheath Dynamics Calculations for Stabilized Inverse Pinch (Equations and Computer Code) 114
E. Hain-Roberts Calculations (Equations) 119

BIBLIOGRAPHY 125

LIST OF FIGURES

Figure		Page
I-1	Parallel Plate Accelerator Geometry	5
I-2	Stabilized Inverse Pinch Geometry	5
I-3	Theta Pinch Geometry	5
II-1	Current Density vs Radius for Various Times During Formation of the Inverse Pinch (1 micron, Deuterium)	13
II-2	Resistivity, Degree of Ionization, Electron Temperature, and Ion Temperature as a Function of Time, Near the Central Axis (1 Micron, Deuterium)	13
II-3	Resistivity, Degree of Ionization, Electron Temperature, and Ion Temperature as a Function of Radius for Time = 0.05 microseconds (1 micron, Deuterium)	14
II-4	Resistivity, Degree of Ionization, Electron Temperature, and Ion Temperature as a Function of Radius for Time = 0.5 microseconds (1 micron, Deuterium)	14
II-5	Current Density vs Radius for Various Times During Formation of the Inverse Pinch (100 microns, Deuterium)	15
II-6	Resistivity, Degree of Ionization, Electron Temperature, and Ion Temperature as a Function of Time, Near the Central Axis (100 microns, Deuterium)	15
II-7	Resistivity, Degree of Ionization, Electron Temperature, and Ion Temperature as a Function of Radius for Time = 0.05 microseconds (100 microns, Deuterium)	16
II-8	Resistivity, Degree of Ionization, Electron Temperature, and Ion Temperature as a Function of Radius for Time = 0.5 microseconds (100 microns, Deuterium)	16
II-9	Current Density vs Radius for Various Times During Formation of the Inverse Pinch (1 mm , Deuterium)	17

II-10 Resistivity, Degree of Ionization, Electron Temperature, and Ion Temperature as a Function of Time, Near the Central Axis (1 mm, Deuterium) 17
II-11 Resistivity, Degree of Ionization, Electron Temperature, and Ion Temperature as a Function of Radius for Time = 0.05 microseconds (1 mm, Deuterium) 18
II-12 Resistivity, Degree of Ionization, Electron Temperature, and Ion Temperature as a Function of Radius for Time = 0.5 microseconds (1 mm, Deuterium) 18
II-13 Snowplow Model 22
II-14 Quasi-Steady or Hydrodynamic Model 22
II-15 Slug Model 25
II-16 Gasdynamic Model 25
II-17 Axial Position of Current Sheath vs Time 29
II-18 Radius of Current Sheath vs Time 32
II-19 Calculated Position of Peak Density in a Theta Pinch, 2 kilogauss Reverse Bias Field 38
II-20 Calculated Position of Peak Density in a Theta Pinch, 4 kilogauss Reverse Bias Field 38

III-1 Parallel Plate Accelerator Discharge Tube 41
III-2 Parallel Plate Accelerator Electrical Circuit 41
III-3 Photograph of Parallel Plate Accelerator Arrangement 43
III-4 Stabilized Inverse Pinch Discharge Tube 47
III-5 Stabilized Inverse Pinch Systems Diagram 48
III-6 Photograph of Stabilized Inverse Pinch 49
III-7 Close-Up Photograph of Stabilized Inverse Pinch Discharge Tube in Electromagnet 50
III-8 Extremely High Temperature Theta Pinch System Diagram 52
III-9 Photograph of Extremely High Temperature Theta Pinch Experiment 53

IV-1 Photograph of He-Ne Gaseous Maser 56
IV-2 IR Maser Excited Coupled Resonator System 57
IV-3 Sketch of Electrostatic Probes, (E_r) and (E_z, E_θ) Probes 60
IV-4 Construction of Piezoelectric Probe 62
IV-5 Dynamic Response of Piezoelectric Probe 62
IV-6 Construction of Magnetic Probes 64

V-1 Infrared Maser Interferometry Signals 68
V-2 Plasma Inside Laser Cavity Signals 68
V-3 Current Sheath Position vs Time (35,000 amperes) 72
V-4 Current Sheath Position vs Time (50,000 amperes) 72
V-5 Electron Density vs Time (200 microns, z = 0, 5 cm)..... 73
V-6 Electron Density vs Time (200 microns, z = 10 cm, 15 cm)..... 73
V-7 Electron Density vs Time (700 microns, z = 0, 5 cm) 74
V-8 Electron Density vs Time (700 microns, z = 10 cm, 15 cm)..... 74
V-9 Radial Electric Field vs Time (B_{zo} = 0 gauss) 76
V-10 Radial Electric Field vs Time (B_{zo} = 500 gauss) 77
V-11 Radial Electric Field vs Time (B_{zo} = 4,000 gauss) 78
V-12 Kerr Cell Photographs (Parallel Plate Accelerator, 1000 microns, Deuterium)..... 82
V-13 Kerr Cell Photographs (Parallel Plate Accelerator, 500 microns, Argon)..... 84
V-14 Kerr Cell Photographs (Stabilized Inverse Pinch, 100 gauss)..... 85
V-15 Kerr Cell Photographs (Stabilized Inverse Pinch, 2000 gauss) 85
V-16 Luminous Front Radius vs Time in Theta Pinch (2 kilogauss Reverse Bias).....87
V-17 Luminous Front Radius vs Time in Theta Pinch (4 kilogauss Reverse Bias) 87
V-18 Pressure Front Position vs Time as Measured with a Piezoelectric Probe in a Stabilized Inverse Pinch 89

V-19 Actual Response of Piezoelectric Probe to Pressure Fronts Produced in a Stabilized Inverse Pinch 89
V-20 Experimental Magnetic Probe Traces 91
V-21 Experimentally Measured Current Sheath Radius vs Time 91
V-22 Magnetosonic Oscillation in a Stabilized Inverse Pinch. Frequency of Oscillation is Plotted vs Pressure (Density)..... 93

CHAPTER I

INTRODUCTION

There are many reasons for investigating dynamic current sheaths produced in magnetoplasmas. Space propulsion systems with specific impulses several times that presently available from chemical rockets are required for optimum lunar and interplanetary missions. Pulsed plasma accelerators based on $\overline{J} \times \overline{B}$ body forces show promise for high specific impulse, moderate thrust space propulsion units. Continued research on the formation and subsequent dynamics of plasmas produced in pulsed plasma accelerators is needed to evaluate and to design an efficient electric space propulsion system. Pulsed electromagnetic plasma accelerators are being considered for use as hypervelocity sources in controlled aerodynamic studies. Plasma phenomena encountered during orbital and explorer space missions can be simulated in a laboratory system employing pulse plasma accelerators and spacecraft models. To fully benefit from such simulated space flights, knowledge of the basic properties of the accelerated plasma media are required. Also, magnetohydrodynamic (MHD), direct energy conversion generators employ $\overline{J} \times \overline{B}$ plasma accelerators. Therefore, knowledge of the formation and subsequent dynamics of a moving plasma is required for efficient design and evaluation of proposed MHD generators. Some phenomena observed with earth stationed equipment and deep space probing explorer rockets can be described and demonstrated

with much smaller laboratory size plasmas. For example, many electromagnetic wave properties (reflection, attenuation, scattering, and resonance) observed in the upper atmosphere can be studied in laboratory produced plasmas. The interaction of solar wind with the earth's magnetic field can be investigated employing a $\bar{J} \times \bar{B}$ plasma accelerator and a dipole magnetic field. In order to design and evaluate proposed controlled thermonuclear fusion reactors, a complete understanding of the dynamics of energetic current sheaths produced in magnetoplasmas is necessary.

Problems of forming, accelerating, and/or confining plasmas are common to propulsion systems, MHD generators, and proposed thermonuclear fusion machines. Basic to the problems associated with plasma confinement and heating is a knowledge of the formation, structure, and dynamics of current sheaths in magnetoplasmas. Details of the formation of a dynamic ionized media from an initially cold gas must be well understood before new and more efficient heating methods can be developed. The structure of current sheaths at all points, points near the cathode, near the anode, and in the middle of the discharge, is necessary to predict performance of plasma accelerators, MHD generators, and most proposed fusion devices. The question, "What charged particles carry the large current densities in high current discharges?", must be answered. The current sheath structure influences the model designated for evaluation of the system under study. The measured dynamics of a current sheath are compared with analytical solutions for the model employed.

Ampere was the first to observe that when electric currents flow in

the same direction through two parallel conductors, the conductors are attracted together. Similarly, when an electric current flows in an ionized gas (which may be thought of as an infinite number of filamentary currents flowing in the same direction), there are mutual attractive forces. If the currents are large enough, the ionized gas may be compressed. This phenomena is commonly called the "pinch" phenomena. There are two major types of pinches being extensively studied today in hopes of finding a controlled thermonuclear fusion reactor and in constructing an efficient plasma propulsion unit; they are the axial pinch and the theta pinch.

A current sheath may be considered to be formed in a gas in the following manner. An electrical discharge begins with a Townsend shower, which proceeds to a glow discharge, and then finally progresses to an arc discharge. This arc discharge initiates the formation of the current sheath. When the magnetic pressure on one side of the current sheath exceeds the gas pressure (and any other pressures) on the other side of the current sheath, a dynamic motion results.

When large currents flow in a gas discharge tube, dynamic shocks may also occur due to the interaction of the self-induced magnetic fields with the currents. Shock waves are pressure disturbances of finite amplitude that move at speeds greater than the speed of sound. Examples of shock waves are the sonic booms from supersonic aircraft, and blast waves from chemical and nuclear explosions. There are presently two methods widely used to produce shock waves in the laboratory. The first is the breakable diaphragm method. In this method, a breakable diaphragm is

located in a pipe between two pressure chambers, the driver gas and the expansion gas. Secondly, there is the electromagnetically driven shock tube method which is being presently studied at Oklahoma University, Naval Research Laboratory, AVCO-Everett Research Laboratory, Massachusetts Institute of Technology, Jet Propulsion Laboratory, and at other research laboratories.

Three different geometries were employed to investigate dynamic current sheaths. Fig. I-1 shows a sketch of a parallel plate accelerator in which current sheaths are formed in the breech ($z = 0$) between the plate electrodes. These sheaths are then propelled outward along the z axis between the electrodes by $j_y \times B_x$ body forces. In Fig. I-2, a sketch of a stabilized inverse pinch is given. Current sheaths are formed near the central hard-core conductor between the two electrodes. Due to $j_z \times B_\theta$ body forces, the current sheaths are driven radially outward into the stabilizing magnetic fields, B_{zo}. The total current I_o flows along the central conductor, in the top electrode, in the gas, and in the bottom electrode. A theta pinch coil is sketched in Fig. I-3. Due to currents in the one turn coil, j_θ currents and B_z fields are produced inside the gas within the coil. Current sheaths produced along the inside wall of the coil are accelerated radially inward by $j_\theta \times B_z$ body forces.

Chap. II presents a theoretical analysis of the formation of dynamic current sheaths. A brief summary of several models often considered is given. Calculations for a parallel plate accelerator and a stabilized inverse pinch are presented. Calculations for a hydromagnetic model developed by

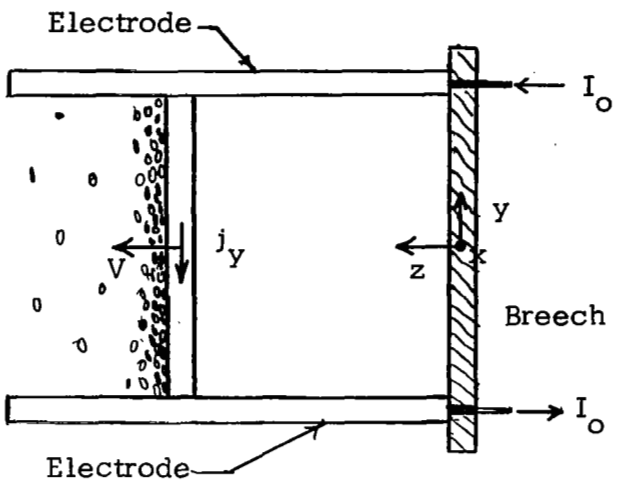

Fig. I-1. Parallel Plate Accelerator Geometry

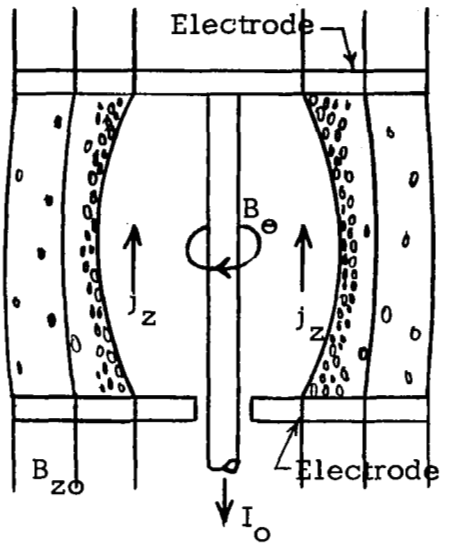

Fig. I-2. Stabilized Inverse Pinch Geometry

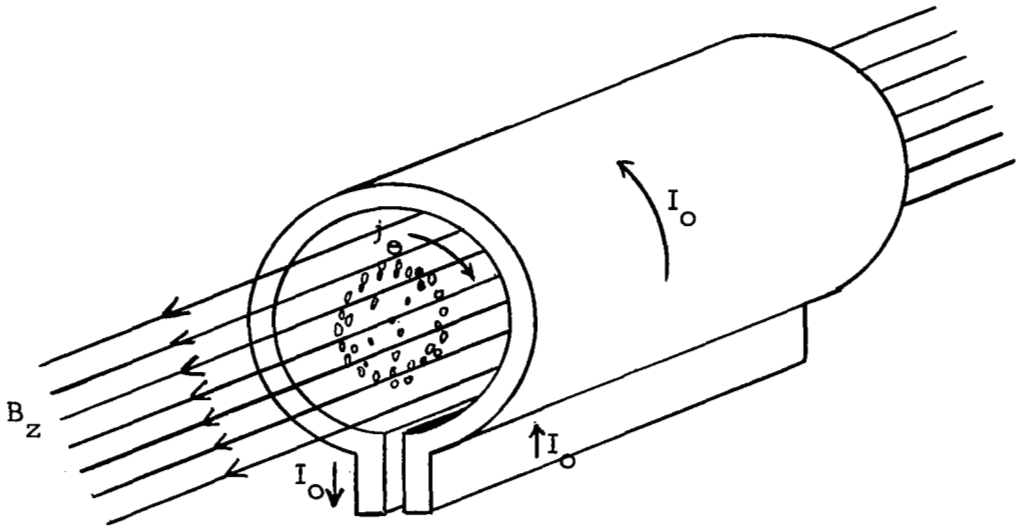

Fig. I-3. Theta Pinch Geometry

Drs. Hain and Roberts for a theta pinch are also given in Chap. II. Chap. III describes the experimental apparatus employed to investigate dynamic current sheaths. A parallel plate accelerator (or parallel plate "rail" gun), a stabilized inverse pinch (or hard-core pinch), and an extremely high temperature theta pinch are described. Chap. IV describes the instrumentation employed to quantitatively investigate the properties of dynamic current sheaths. These include an infrared maser interferometer, electrostatic probes, Kerr cell high speed photography, piezoelectric pressure probes, magnetic probes, and voltage-current measurements. The experimental findings are presented in Chap. V. Current sheath formation, space and time resolved electron densities, electric fields, self-luminous fronts, pressure fronts, and magnetic fields associated with dynamic current sheaths are measured. Chap. VI presents conclusions made about breakdown, formation, the snowplow model, propulsion efficiency, electron density, and oscillations of the current sheath.

CHAPTER II

THEORETICAL ANALYSIS

The initial electrical breakdown of a cold gas by strong electric fields and the formation of current sheaths in the resulting gaseous plasma are investigated in the first part of this chapter. Several proposed models to describe the dynamics of current sheaths formed and accelerated in parallel electrode geometries are then examined. Based on a snowplow model, the current sheath's position, velocity, and acceleration are examined and analytically determined for: 1) a parallel plate accelerator, and 2) a stabilized inverse pinch. Results based on the Hain-Roberts model for a theta pinch are also presented.

A. Initial Electrical Breakdown and Formation of Current Sheaths

The location of the initial electrical breakdown of the cold gas and subsequent formation of the current sheaths between parallel, planar electrodes determine the starting conditions for all analytical methods which are to be employed to compute the position, velocity, and acceleration of the current sheaths produced and accelerated. The formation process and the resulting current sheath's structure influence the model which is to be employed to describe the dynamic current sheaths.

The initial breakdown path is determined by the physical arrangement of electrodes and insulators. For parallel, planar electrode geometries,

this is the path of least electrical impedance. Initially the inductive effects dominate in the geometries employed and to be described in more detail later. Therefore, the breakdown path is the path of least inductance. For the parallel plate accelerator, initial electrical breakdown occurs along the insulator wall in the breech of the gun. For the inverse pinch geometry, initial electrical breakdown occurs along the outside of the insulation covering the axial return conductor at the center of the circular cylindrical geometry.

The formation of a plasma when an electric field is applied to a cold gas for the parallel plate accelerator and the inverse pinch geometries is described by Maxwell's electromagnetic field equations and the other equations including the plasma properties. With the assumptions of initially negligible mass motion, particle diffusion, heat diffusion, bremsstrahlung, and charge-exchange during the formation process, the current density, plasma resistivity, electron temperature, ion temperature, and degree of ionization are determined for two geometries mentioned earlier, the parallel plate accelerator and the inverse pinch.

N. W. Wyld and K. M. Watson[1] considered the ionization and formation of a plasma due to uniform current flow through an initially cold deuterium gas. Their analytical results show that almost 100% ionization

---

[1] Wyld, N. W., and Watson, K. M., "Ionization and Heating of a Plasma in a Magnetic Field", Conference on Controlled Thermonuclear Reactions, June 4-7, 1956, Gatlinburg, Tennessee, U.S.A.E.C. Report TID-7520 (Part 2), 1956.

is possible in the initially cold gas within the current sheath after a very short time. Later, in 1959, J. Killeen, G. Gibson, and S. A. Colgate[2] considered the case of a non-uniform current flow through an initially cold deuterium gas. (The current layer's formation is calculated instead of assuming a uniform current.)

The parallel plate accelerator closely approximates a one (space) dimensional problem. The results of Killeen, Gibson, and Colgate's analysis applies, with minor modifications, to this geometry. From the two Maxwell's electromagnetic field equations

$$\bar{\nabla} \times \bar{E} = -\frac{\partial \bar{B}}{\partial t} \qquad \text{(II-1)}$$

and

$$\bar{\nabla} \times \bar{H} = \bar{j} \qquad \text{(II-2)}$$

and Ohm's law of the form $\bar{E} = \eta \bar{j}$, a nonlinear, partial differential equation for the current density j is obtained. The necessary boundary conditions are: 1) the current density j approaches zero as the space coordinate approaches infinity, and 2) the electric field at the plasma boundary is the applied electric field minus the self-induced electric field.

The remaining equations to specify the plasma formation are obtained from the following plasma relations: 1) an energy balance relating the ohmic heating (source) with the energy used to ionize neutrals (sink), and to heat charged particles (sink), 2) an electrical resistivity due to electron-ion and electron-neutral collisions for the partially ionized gas, 3) an

---

[2]Killeen, J., Gibson, G., and Colgate, S. A., "Boundary-Layer Formation in the Pinch", Phys. Fluids, 3, 387, 1960.

ionization equation, and 4) an equation for the elastic transfer of energy from the electrons to the ions.

The resulting set of partial differential equations defining the current density, plasma resistivity, electron temperature, ion temperature, and degree of ionization was solved simultaneously by employing finite difference equations and a digital computer by Killeen, Gibson, and Colgate, (Ref. 2). For example, consider the case of an applied electric field E_o = 100 volts/cm and an initial gas density of $n_o = 10^{15}$/cc. Killeen, Gibson, and Colgate, "Boundary-Layer Formation in the Pinch", (Ref. 2) considered a typical, fast, linear pinch device similar to those employed at Los Alamos Scientific Laboratory, Lawrence Radiation Laboratory (Livermore), and elsewhere. (This holds where the inductance parameter "a" defined in their article is 1 cm.) Their calculations show that at the location where breakdown occurs and the plasma current sheath is formed (the "wall"), the fraction of ionization f is essentially unity, i.e. 100% ionization by the time 0.25 microseconds. Also, the resistivity is less than 10^{-4} ohm-cm, the ion energy (temperature) is larger than 0.1 ev, the electron energy (temperature) is larger than 50 ev, and the current density j is the order of 10^5 amp/cm^2. The current sheath formed is fairly narrow with the majority of the current flowing within a 1 cm layer. As time progresses, the current spreads and the sheath becomes thicker. (This is still neglecting mass motion effects.) Further details of their calculations and results appear in Ref. 2.

In order to investigate the formation of a cylindrical plasma formed

in a cold deuterium gas in the inverse pinch geometry, Maxwell's electromagnetic field equations are written in circular cylindrical coordinates. Due to symmetry, these equations reduce to

$$\frac{\partial E_z(r,t)}{\partial r} = \mu_0 \frac{\partial H_\theta(r,t)}{\partial t} \tag{II-3}$$

$$H_\theta(r,t) = \frac{I_0}{2\pi r} - \frac{1}{r}\int_{r'=b}^{r'=r} j'_z(r',t)\,[r'dr'] \tag{II-4}$$

and $$E_z(r,t) = \eta_z(r,t)\, j'_z(r,t) \tag{II-5}$$

The plasma equations employed for the inverse pinch geometry are basically those used by Killeen, Gibson, and Colgate mentioned earlier. They are

$$\eta j^2 = a\epsilon_0 \frac{\partial n_e}{\partial t} + \frac{\partial}{\partial t}\left[\tfrac{3}{2} n_e k T_e + \tfrac{3}{2} n_i k T_i\right] \tag{II-6}$$

$$\eta = \frac{m}{n_e e^2}\left(\nu_i + \nu_n\right) \tag{II-7}$$

$$\frac{\partial n_e}{\partial t} = n_e(n_0 - n_e)\,\overline{\sigma_i v_e} \tag{II-8}$$

and $$\frac{\partial \theta_i}{\partial t} = \frac{8}{3}\sqrt{2\pi}\, e^4 \frac{n_e\sqrt{m}}{M} \frac{\theta_e - \theta_i}{\theta_e^{3/2}} \ln\left(\frac{b_{max}}{b_{min}}\right). \tag{II-9}$$

The above set of partial differential equations are re-written into a set of finite difference equations and solved on a high speed digital computer, a CDC 1604. Calculations for a deuterium plasma of 1 micron initial gas pressure show that the current density near the central axis of the

stabilized inverse pinch increases to almost 10^9 amp/m^2 in 0.5 microseconds. The major portion of the current flows within 2 cm of the central axis for time less than 0.005 microseconds, less than 10^4 amp/m^2 flows at a 2 cm radius. The current spreads outward with time and for times larger than 0.5 microseconds, sizeable current densities (10^4 to 10^5 amp/m^2) flow at radii larger than 7 cm. Near the central axis, the degree of ionization reaches 100% within 0.1 microseconds for a deuterium plasma of 100 microns. At 0.4 microseconds, the resistivity has decreased from 10^{-4} ohm-meters for a 1 micron plasma to 10^{-8} ohm-meters, to 5×10^{-7} ohm-meters for a 100 micron pressure, and 3×10^{-6} ohm-meters for a 1 mm pressure. Also near the central axis, the electron energy is larger than 100 ev for times greater than 0.05 microseconds for a pressure of 1 micron. The electron energy is less than 20 ev for a pressure of 1 mm at 0.1 microsecond. At the time t = 0.50 microseconds, the ionization is greater than 90% up to a radius of 2 cm for a 1 micron plasma, but only to a radius of 1 cm for a 1 mm plasma. As the pressure is increased, the electron temperature drops more rapidly with radius. Also, at the time t = 0.50 microseconds, the ion temperature increases with the pressure. Curves presenting these calculated results are shown in Fig. II-1 through Fig. II-12. Appendix A lists the computer code employed to obtain these calculations.

B. Dynamics of Current Sheaths

After describing several proposed models for the dynamic current sheath, the position, velocity, and acceleration of current sheaths formed

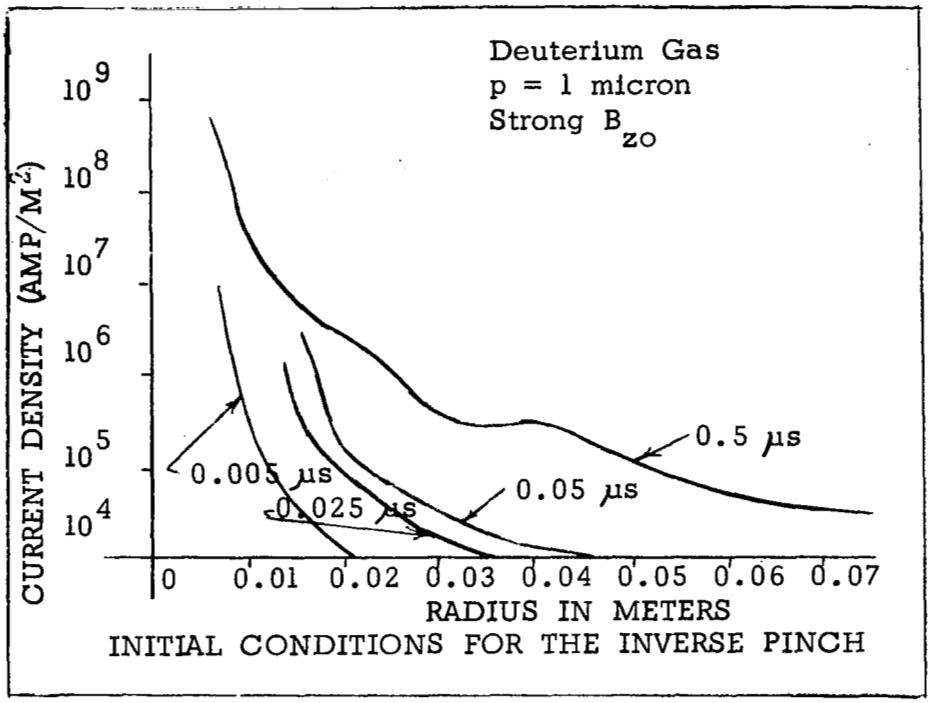

Fig. II-1. Current Density vs Radius for Various Times During Formation of the Inverse Pinch (1 micron, Deuterium)

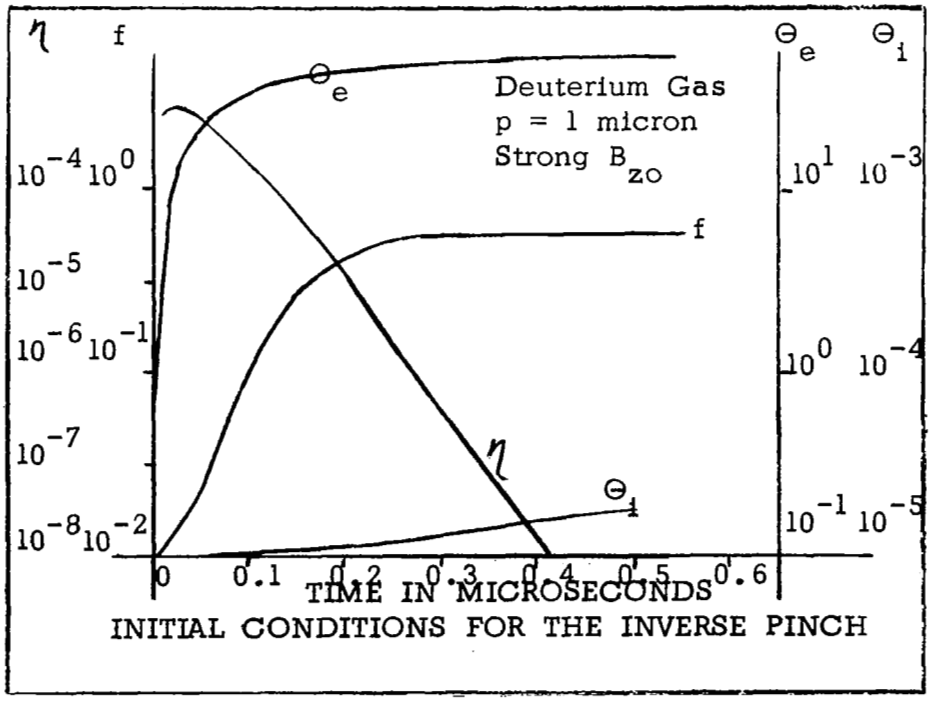

Fig. II-2. Resistivity, Degree of Ionization, Electron Temperature, and Ion Temperature as a Function of Time, Near the Central Axis (1 micron, Deuterium)

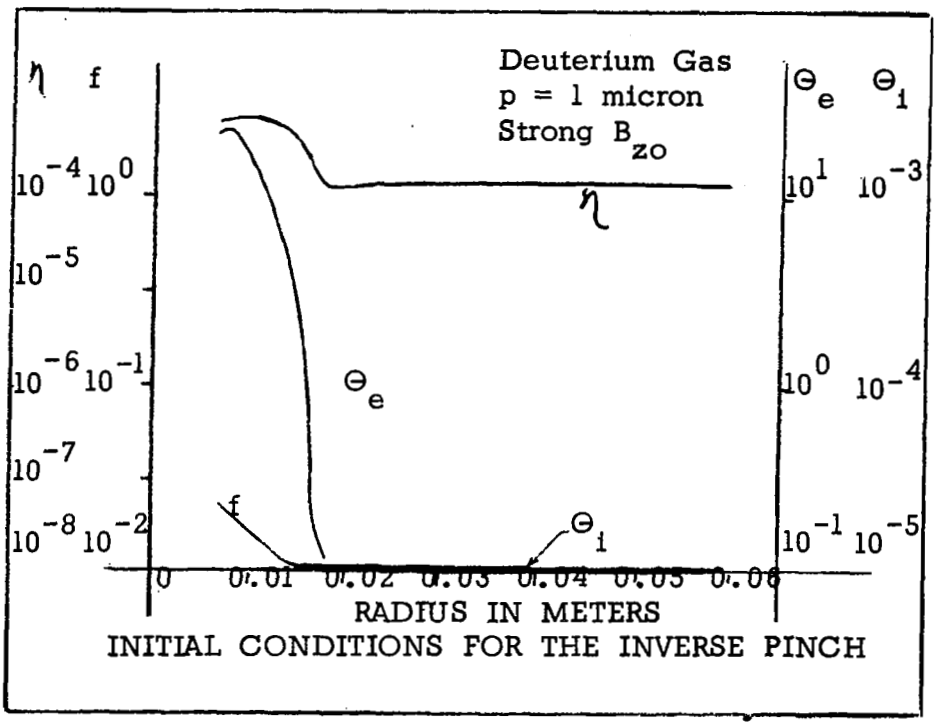

Fig. II-3. Resistivity, Degree of Ionization, Electron Temperature, and Ion Temperature as a Function of Radius for Time = 0.05 microseconds (1 micron, Deuterium)

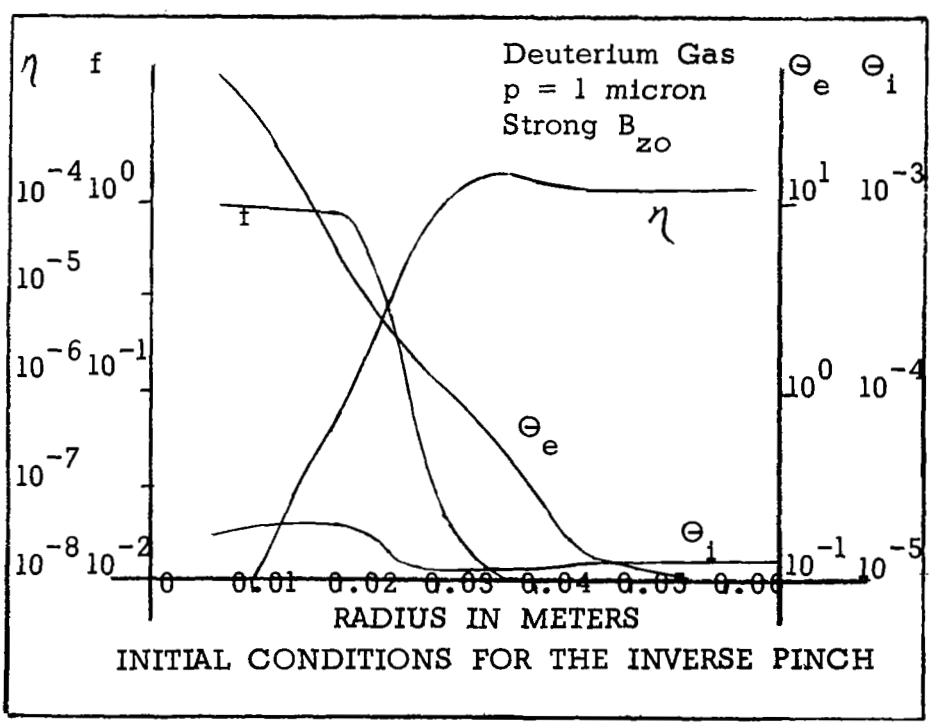

Fig. II-4. Resistivity, Degree of Ionization, Electron Temperature, and Ion Temperature as a Function of Radius for Time = 0.5 microseconds (1 micron, Deuterium)

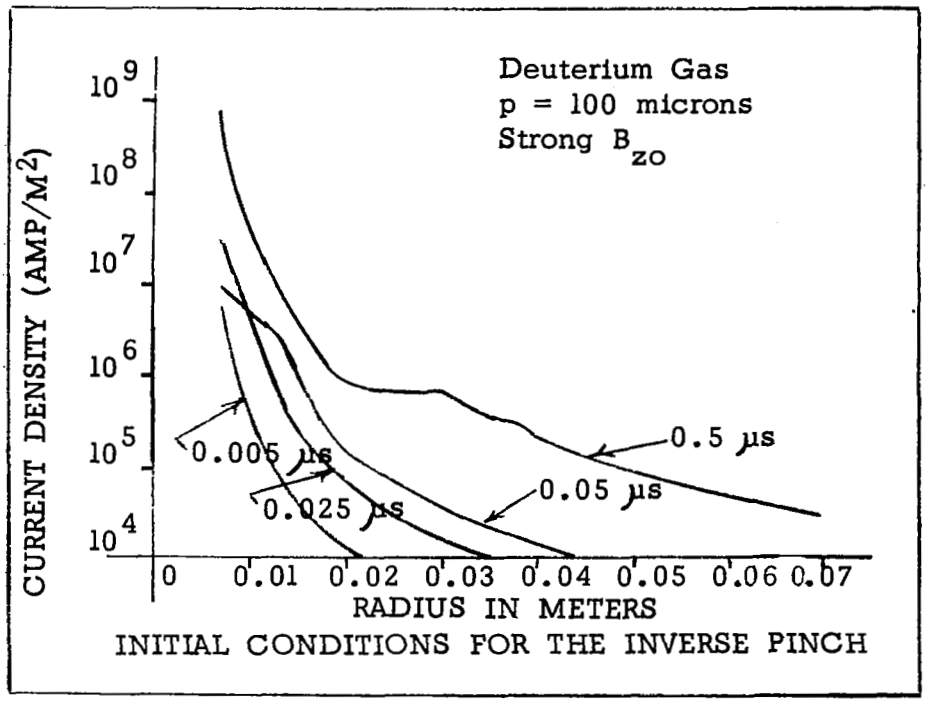

Fig.II- 5. Current Density vs Radius for Various Times During Formation of the Inverse Pinch (100 microns, Deuterium)

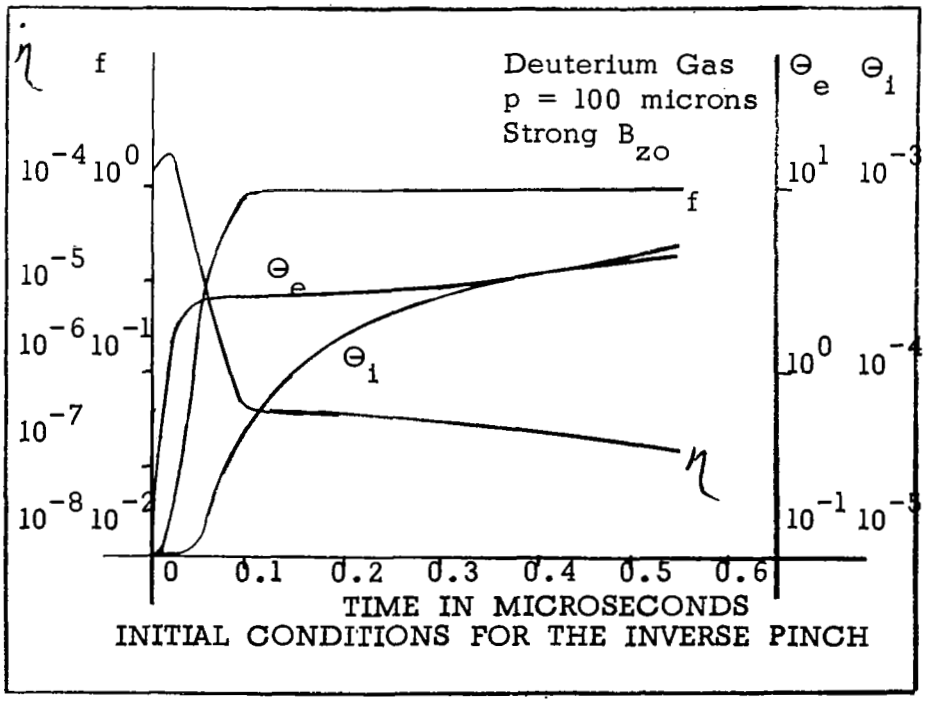

Fig.II- 6 . Resistivity, Degree of Ionization, Electron Temperature, and Ion Temperature as a Function of Time, Near the Central Axis (100 microns, Deuterium)

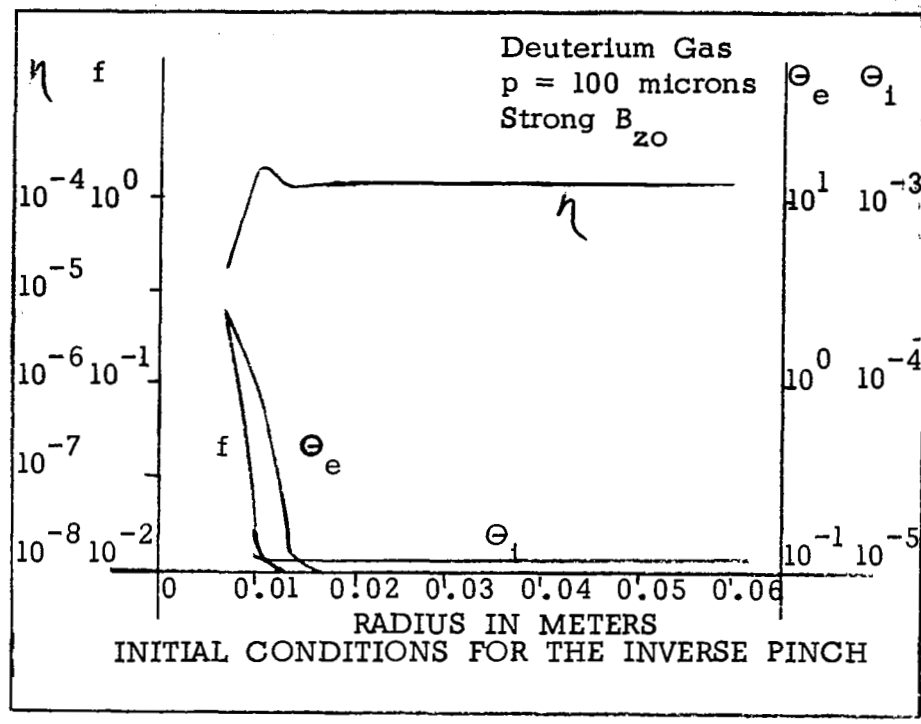

Fig.II- 7 . Resistivity, Degree of Ionization, Electron Temperature, and Ion Temperature as a Function of Radius for Time = 0.05 microseconds (100 microns, Deuterium)

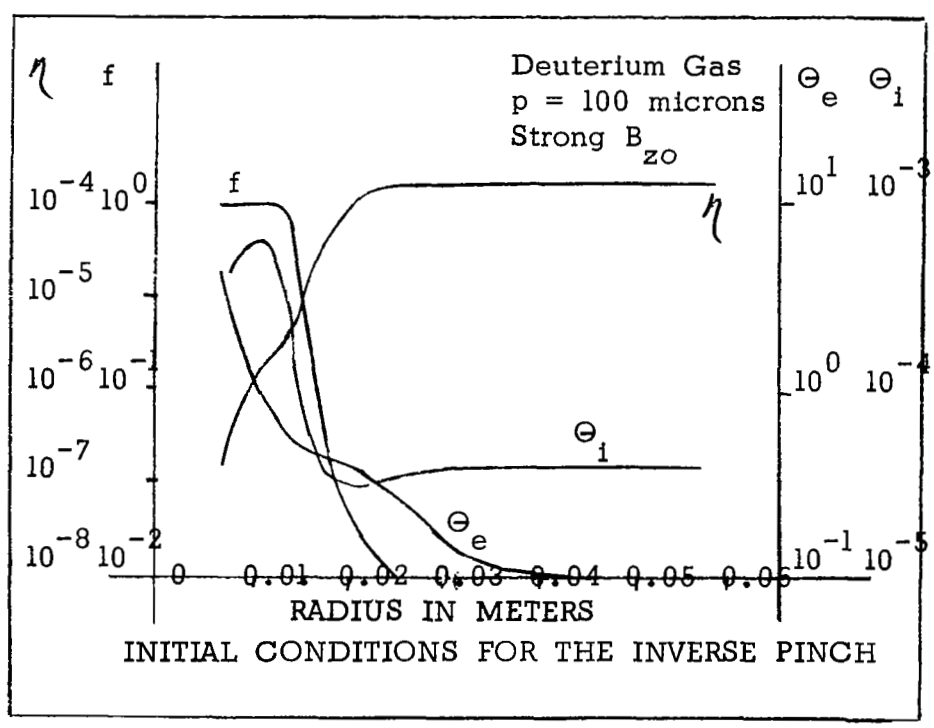

Fig.II- 8 . Resistivity, Degree of Ionization, Electron Temperature, and Ion Temperature as a Function of Radius for Time = 0.5 microseconds (100 microns, Deuterium)

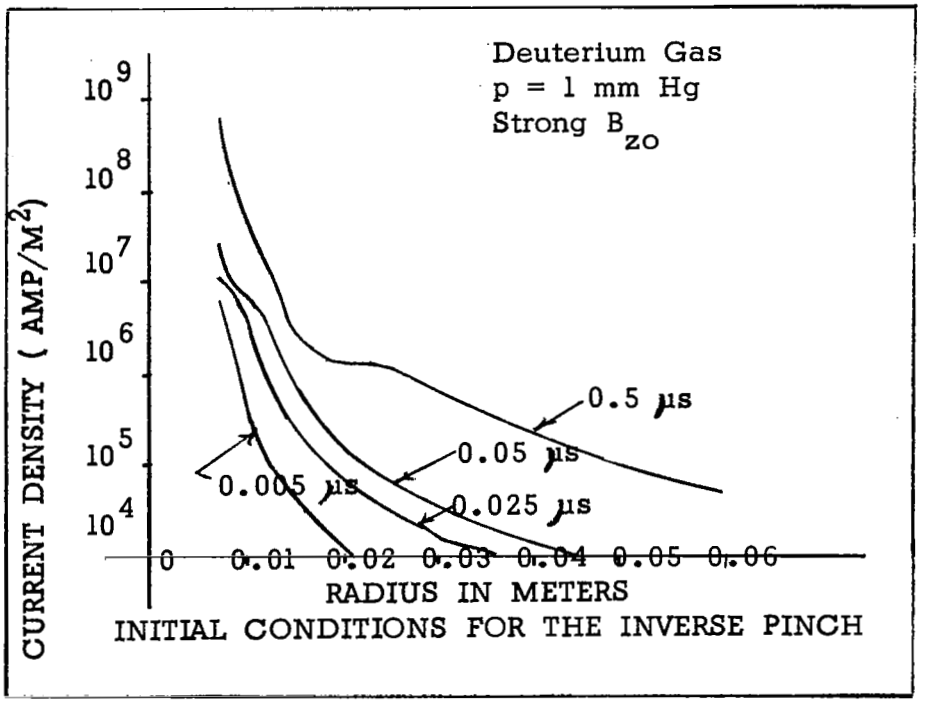

Fig. II- 9. Current Density vs Radius for Various Times During Formation of the Inverse Pinch (1 mm, Deuterium)

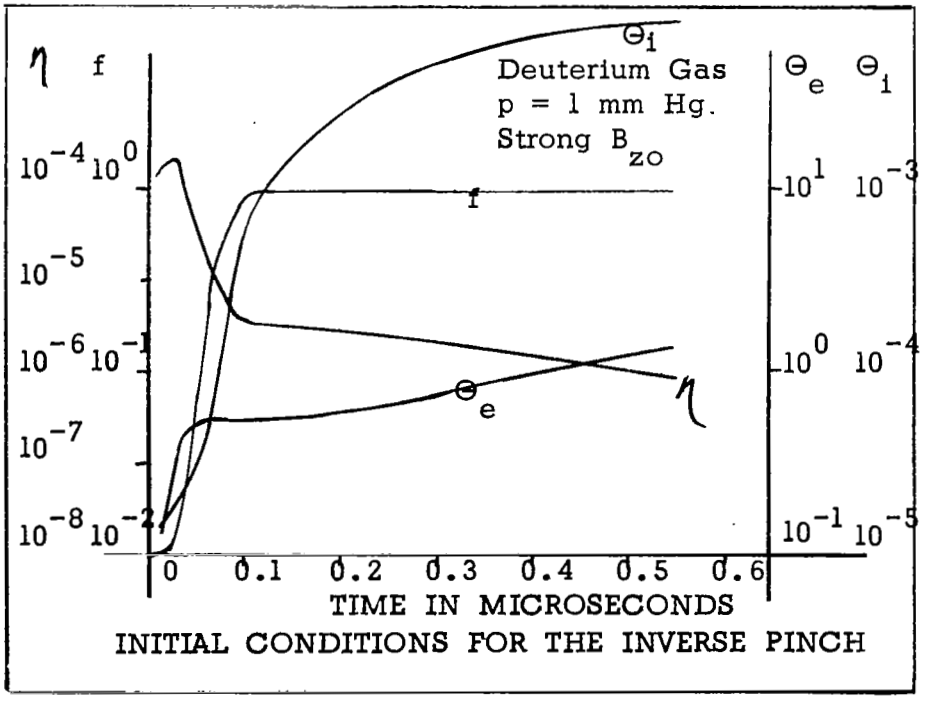

Fig. II-10. Resistivity, Degree of Ionization, Electron Temperature, and Ion Temperature as a Function of Time, Near the Central Axis (1 mm, Deuterium)

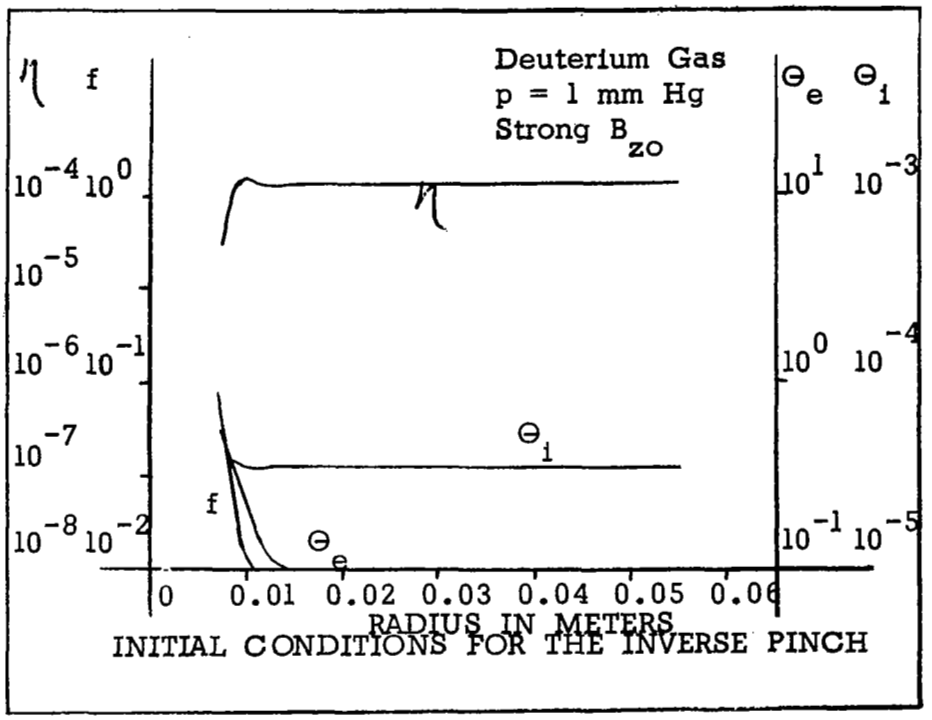

Fig. II- 11. Resistivity, Degree of Ionization, Electron Temperature, and Ion Temperature as a Function of Radius for Time = 0.05 microseconds (1 mm, Deuterium)

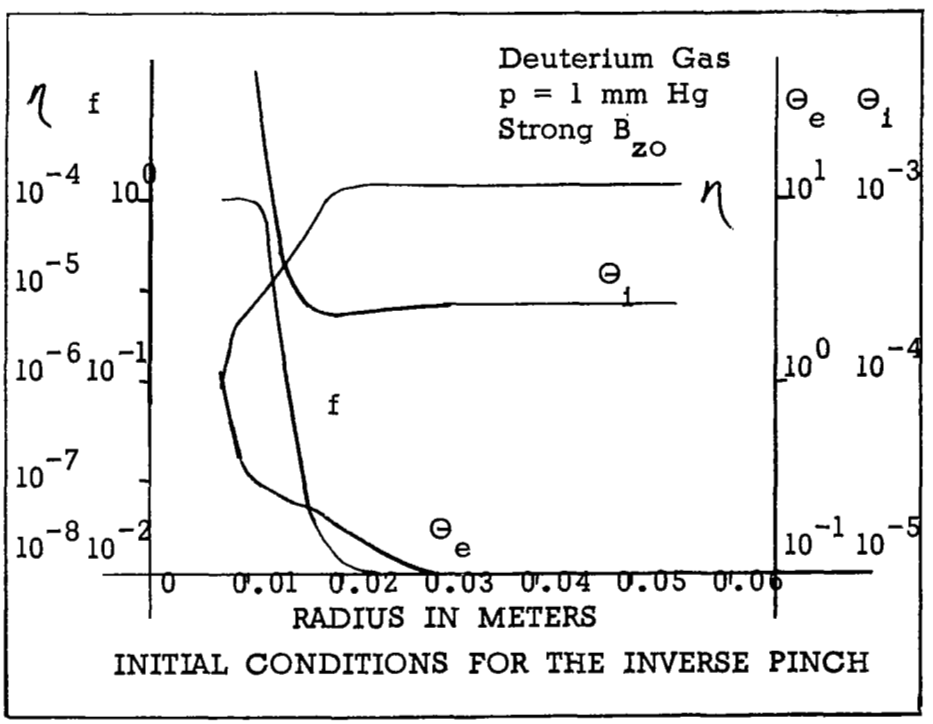

Fig. II- 12. Resistivity, Degree of Ionization, Electron Temperature, and Ion Temperature as a Function of Radius for Time = 0.5 microseconds (1 mm, Deuterium)

and accelerated in the parallel plate accelerator and the inverse pinch geometries are calculated based on a snowplow model. In order to accelerate plasma efficiently, the material in the current sheath must be sufficiently ionized and the sheath thick enough to prevent loss of neutral particles through the sheath. The ionization condition usually places an upper limit on the initial gas pressure and the sheath thickness places a lower limit on the initial gas pressure. If the current sheath forms near a material wall, the wall material's evaporation rate is critical. High evaporation of wall material often prevents the current sheath from leaving the wall, the so called wall breakaway problems.

Models

Depending on the gasdynamical and electrical properties of the system, dynamic current sheaths can often be represented by relatively simple models. There are many reasons why a model is considered. If a simple physical model is available, the electrical and the gasdynamical variables for the system can be determined analytically. For example, in the area of thermonuclear fusion research the spatial distribution of currents and magnetic fields, which are very important in determining the stability of the system, can be calculated. Similarly, in the investigation of plasma propulsion for spacecraft a simple model is required for a practical method of calculating the efficiency of the system.

Presently, there are two major types of models, the continuum and the non-continuum. The models to be considered are the following four

continuum models: [3,4,5] the snowplow, quasi-steady state, the slug, and the gasdynamic model. The models differ primarily in their method of representing the accumulation of mass near the driving magnetic piston.

In general, the coupled electrodynamic-gasdynamic equations used to describe the continuum fluid models which represent the system consist of the following four types of equations: 1) a continuity equation for the mass accumulated, 2) a momentum equation (an equation of motion), 3) a conservation of energy equation, and 4) an electrical circuit equation. In order to simplify the mathematics, some additional assumptions are often made. For example, assume infinite electrical conductivity, and inviscid fluids. Appendix B presents the equations for the four continuum models to be discussed next.

The snowplow model was developed by R. Garwin, A. Rosenbluth, and M. Rosenbluth[6] in the 1950's. This model was first presented in 1954

---

[3]Colgate, Stirling A., "Initial Conditions for the Dynamic Pinch", Lawrence Radiation Laboratory, University of California, Livermore, California, UCRL-4895, 1957.

[4]Granet, Irving and Guman, William J., "The Application of the Pinch Process for Space Propulsion", Z. Flugwiss. 10, Heft 3, 83, 1962.

[5]Granet, Irving and Guman, William J., "Some Engineering Aspects of the Magnetohydrodynamic Pinch Process for Space Propulsion", Republic Aviation Corporation, Farmingdale, N. Y., AFOSR TN 60-86, (PPL #120), November, 1959.

[6]Rosenbluth, M., Garwin, R., and Rosenbluth, A., "Infinite Conductivity Theory for the Pinch", Los Alamos Scientific Laboratory, Los Alamos, New Mexico, LA-1850, 1954.

in the classified report, "Infinite Conductivity Theory of the Pinch"; the report was declassified in 1957. In the snowplow model, all the media (fluid) is presumed to be swept up by the magnetic piston and piled up in a very thin layer at the piston and to travel with it. In this model, the gasdynamics of an ionized media are completely ignored. The only requirement is that the plasma pressure (and other pressures) at the layer must balance the driving magnetic pressure, thus resulting in coupling between the electromagnetics and hydrodynamics. (Refer to Fig. II-13 for a sketch of a one-dimensional model.) The distinguishing feature of the snowplow model is the assumption of mass being continuously picked up and accumulated in a thin layer at the advancing current sheath, tending toward infinite compression. The equations are simple enough so that the mass can be distributed in any manner initially. The thin layer at the magnetic piston is considered to be highly ionized so as to have infinite electrical conductivity and thus requiring no energy to ionize the fluid. Due to its simplicity, the snowplow model has been widely used by investigators of pinch (and/or shock) experiments to represent their experimental system. Since its introduction in 1954, the model has been used to describe linear axial, inverse axial, and theta pinches. Also, the breaking diaphragm and the electromagnetic shock tubes have used the snowplow, or a modified version, to study the shock phenomena. Guman and Granet[7]

---

[7] Guman, William J., and Granet, Irving, "Pinch Dynamics with Nonuniform Conditions", Republic Aviation Corporation, Farmingdale, N. Y., PPL-TR-60-6, January, 1960.

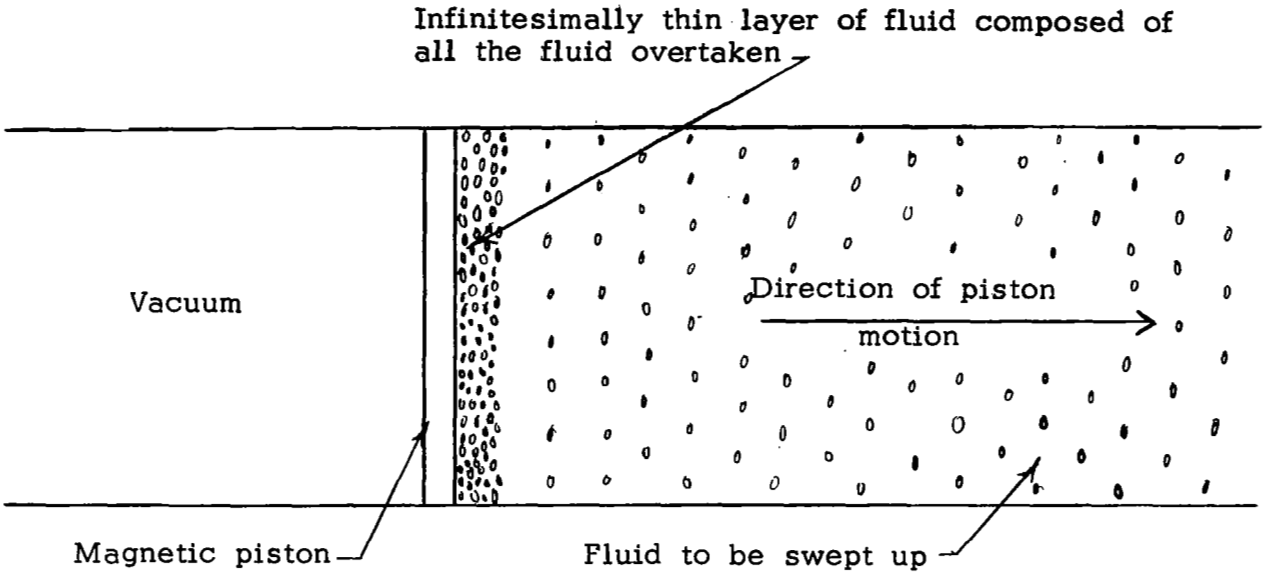

Fig. II-13. Snowplow Model

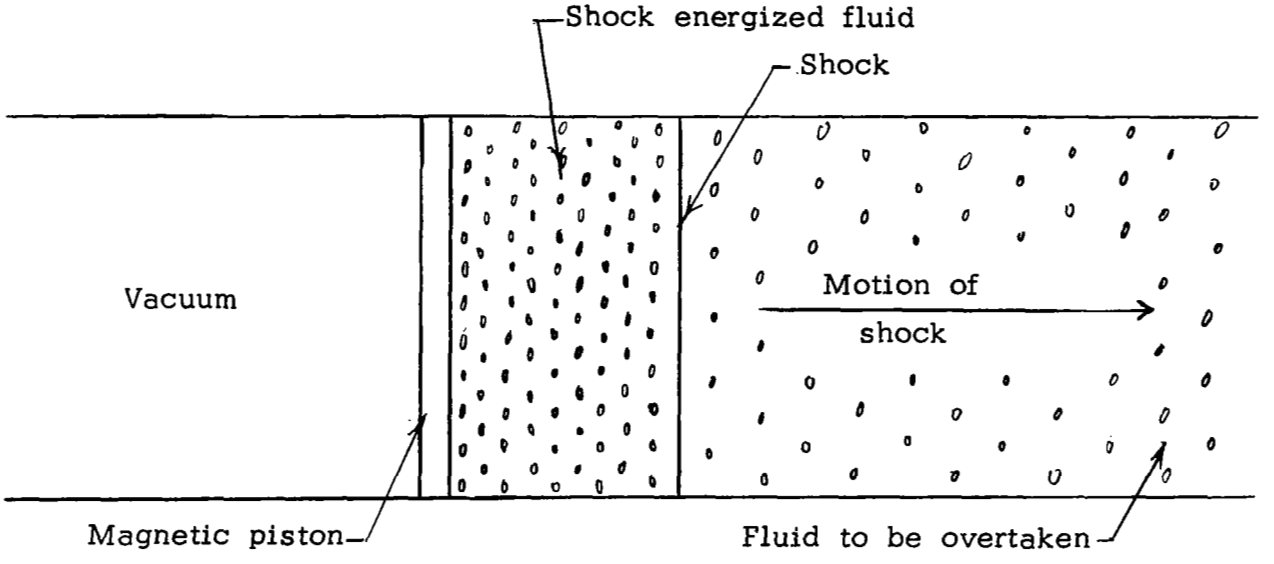

Fig. II-14. Quasi-Steady or Hydrodynamic Model

have applied the snowplow model (with uniform and non-uniform initial fluid conditions) to a linear pinch contoured to give axial thrust, i. e. an experimental plasma propulsion engine. As is so often the case, the simplest model does not always give satisfactory results. Burkhardt and Lovberg[8] in a recent publication, "Current Sheet in a Coaxial Plasma Gun", point out that the snowplow model does not give satisfactory correlation with experimental measurements for their coaxial plasma gun.

The quasi-steady state model takes into account some of the gas-dynamics of a shock by using Rankine-Hugoniot strong shock relations[9]. In this model, the advancing shock front overtakes the stationary fluid, and this overtaken fluid is then uniformly distributed between the shock front and the magnetic piston. This region of shocked fluid moves at the piston velocity, refer to Fig. II-14. Since the equations for the quasi-steady state model are more complete, and somewhat more complicated, the model has not been used as often as the simpler snowplow model. But, the results of recent experimental work by Burkhardt and Lovberg presented in their paper, "Current Sheet in a Coaxial Gun", (Ref. 8), indicates that the quasi-steady state model utilizing strong shock wave assumption may be a better model for the coaxial gun than the snowplow model. The quasi-steady state model is becoming more and more accepted

---

[8] Burkhardt, L. C., and Lovberg, R. H., "Current Sheet in a Coaxial Plasma Gun", Phys. Fluids, 5, 341, 1962.

[9] Pai, Shih-I, Magnetogasdynamics and Plasma Dynamics, Prentice-Hall, 1962.

for detailed studies of pinch phenomena, and of strong shock wave experiments where some gasdynamics must be employed.

The third continuum model to be described, the slug model, is the simplest to describe physically. This model postulates that the mass is a fixed quantity that is always located at the advancing current sheath. There is no mass ahead of this sheath, and no mass behind it. Fig. II-15 shows this model. In the slug model, one cannot consider the material to be a fluid, but rather it is regarded as an incompressible substance. The slug model is used in the study of high specific impulse drive units, fusion injection devices, plasmoid generators, and other experimental arrangements where the conducting media is considered non-deformable with a constant mass. For example, Mostov, Neuringer, and Rigney[10] have numerically solved the coupled equations describing an electromagnetically accelerated plasma slug. (The slug model should also be very useful in studying the exploding wire phenomena in a vacuum region.)

The gasdynamic model, sketched in Fig. II-16, makes an attempt to include the nonsteady gasdynamic motion which occurs between the shock front and the magnetic piston. In the gasdynamic model, the mass that is continuously overtaken by the advancing shock is assumed to be distributed between the shock and the current sheath so as to account for a nonsteady flow by using an artificial diffusion process. At present, the

---

[10] Mostov, Philip M., Neuringer, Joseph L., and Rigney, Donald, "Electromagnetic Acceleration of a Plasma Slug", Republic Aviation Corporation, Farmingdale, N. Y., PPL-TR-61-5, February, 1961.

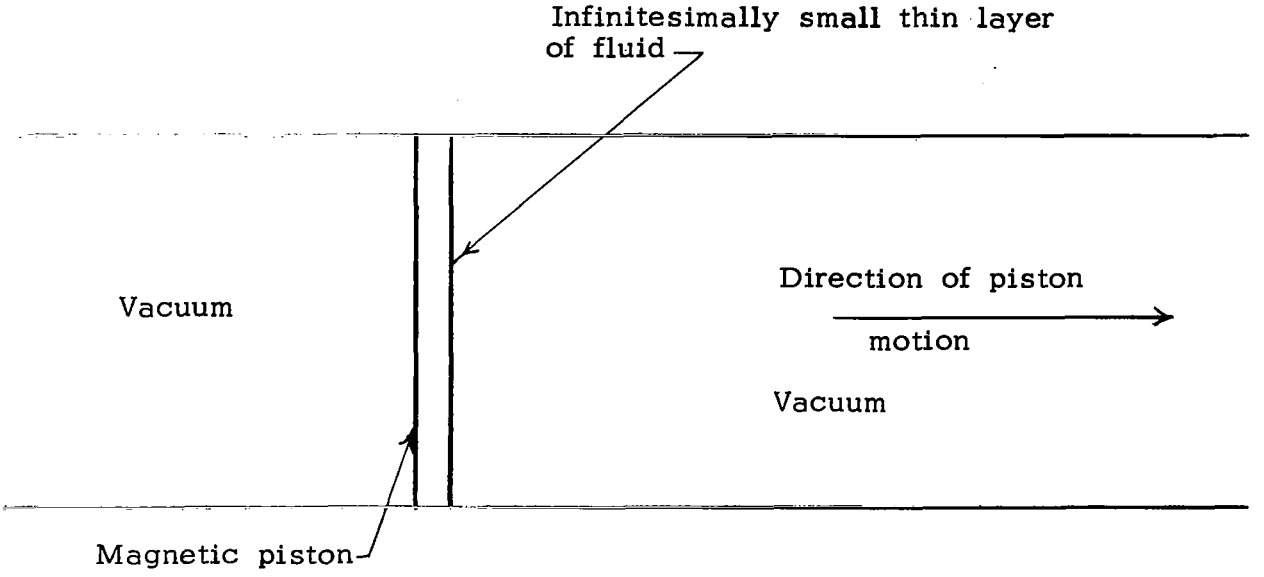

Fig. II-15. Slug Model

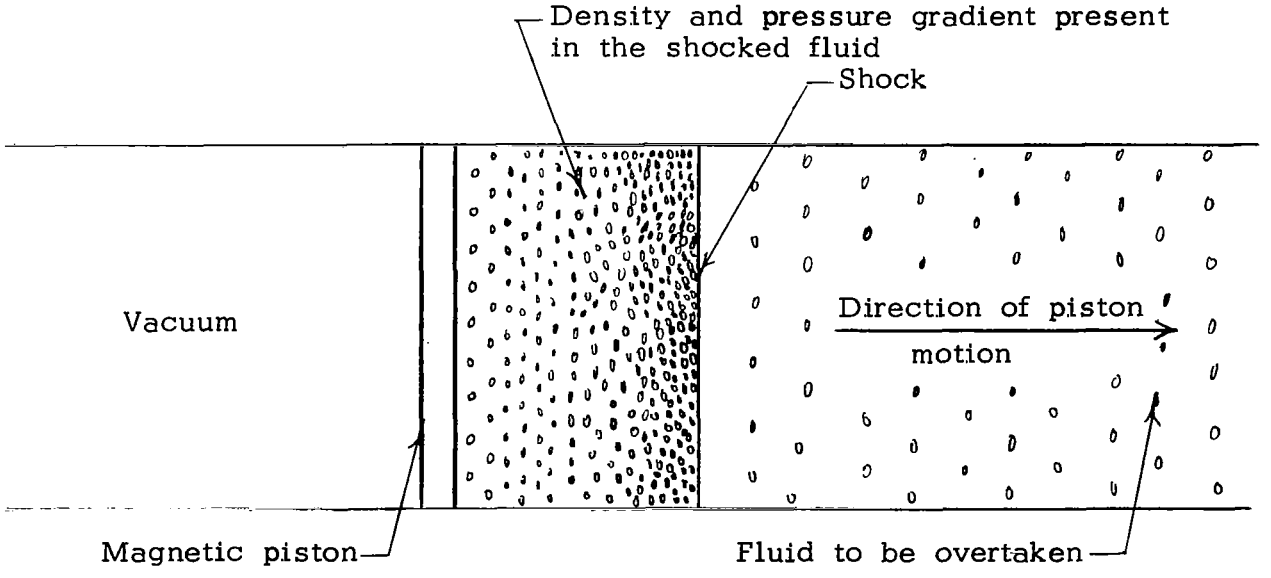

Fig. II-16. Gasdynamic Model

gasdynamic model is the only continuum model (of the four presented here) that could possibly account for pressure wave interactions.

After considering the relative advantages and the disadvantages of the four above mentioned continuum models, the snowplow model was selected to initially investigate the dynamics of current sheaths produced in a parallel plate accelerator and in a stabilized inverse pinch. The calculated position and velocity of the current sheath in these two geometries are usually in good agreement with experimentally measured properties associated with the current sheath. Calculations based on the snowplow model are presented for the parallel plate accelerator and the stabilized inverse pinch in the following paragraphs of this chapter. In order to obtain the gasdynamic properties associated with the current sheath in the theta pinch, a gasdynamic model was employed. Results obtained with the Hain-Roberts computer code are presented in this chapter.

Parallel Plate Accelerator

The equations describing the dynamics of current sheaths formed in a parallel plate accelerator are: 1) the electrical circuit equation coupled with 2) the equation of motion derived from Newton's second law. The electrical circuit equation can be written

$$V_{cap} = RI + \frac{d(LI)}{dt} \qquad \text{(II-10)}$$

where V_{cap} is capacitor voltage, I is current, R is circuit resistance, and

L is circuit inductance. From Newton's second law,

$$\frac{d(Mv)}{dt} = F \qquad \text{(II-11)}$$

where F is the total force acting on the element of mass M of the current sheath moving with velocity v. For a planar, highly conducting current sheath in a parallel plate accelerator, the inductance L and the mass M are linear functions of the displacement x.

Therefore,

$$L = L_o + L'x \qquad \text{(II-12)}$$

and $$M = \rho A x \qquad \text{(II-13)}$$

The force F is due to the magnetic pressure p_m acting on the area A where

$$p_m = \frac{B^2}{2\mu_o} \qquad \text{(II-14)}$$

The force equation can now be written

$$\frac{d}{dt}(\rho A x v) = A p_m = \frac{A B^2}{2\mu_o} \qquad \text{(II-15)}$$

or $$\frac{d(\rho x v)}{dt} = \frac{B^2}{2\mu_o}, \qquad \text{(II-16)}$$

where ρ is the initial mass density, B is the magnetic field density, x is the displacement, and v is the velocity of the current sheath.

The electrical circuit equation and the equation of motion form a set of two coupled ordinary differential equations which can be solved numerically for various mass densities and/or capacitor voltages. The above set of differential equations can be decoupled if the current is known

(e.g. measured experimentally). The equation of motion is then solved using the magnetic field B specified by this known current.

The axial positions of current sheaths formed in the experimental parallel plate accelerator employed (to be described in more detail in Chap. III) are determined for a range of initial pressures of deuterium (and argon) gases for driving currents of 35,000 amperes (and 50,000 amperes). A representative set of the results for a driving current of 35,000 amperes, deuterium (and argon) gases at 500 microns (and 1,000 microns) is given in Fig. II-17. The results show the typically small initial velocity and subsequently higher velocity as the driving current begins to build up. (Maximum driving current occurs at 5 microseconds.) Typical velocities (at the axial position, z = 5 cm) are 5×10^4 m/sec for deuterium current sheaths and 10^4 m/sec for argon current sheaths. As the initial gas pressure is increased, the current sheaths require a longer time to reach any given axial location. Similarly, if a heavier gas is employed (e.g. argon instead of deuterium), the current sheaths require longer times to reach a preset location. Thus, with regard to plasma propulsion engines, there exists an optimum propellant mass for maximum $(1/2)m\ v^2$ leaving the accelerator. Appendix C presents the FORTRAN computer code employed to calculate the positions and velocities of the current sheath.

Stabilized Inverse Pinch

An equation of motion for an inverse pinch with stabilizing axial

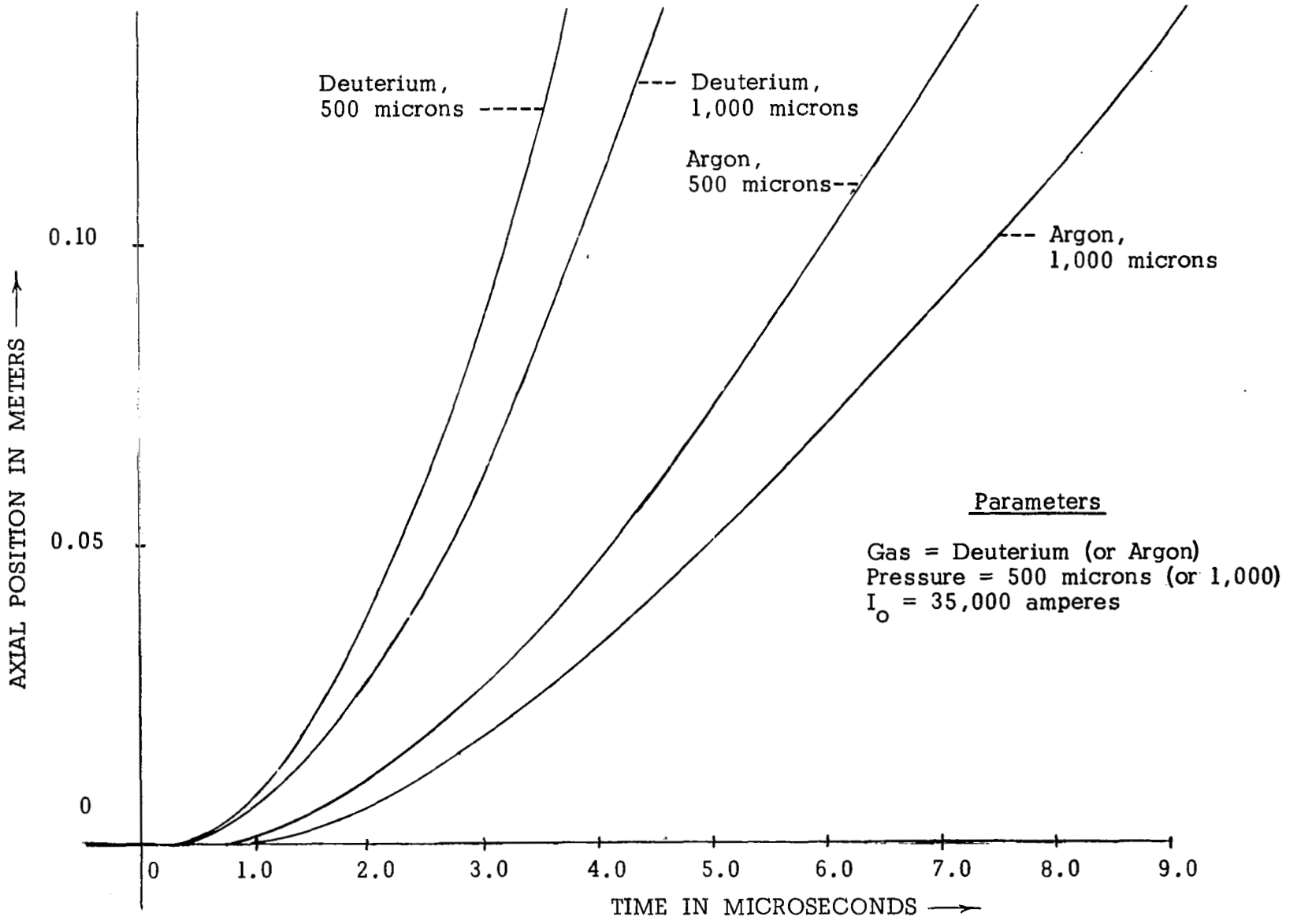

Fig. II-17. Axial Position of Current Sheath vs Time

magnetic fields is derived next employing the snowplow model. The inverse pinch geometry is such that cylindrical coordinates are natural to use. As a result of the total current going along the center return conductor (the hard-core), plasma sheaths formed near the central axis are accelerated radially outward by $j_z \times B_\theta$ body forces. A stabilizing magnetic field B_{zo} is applied to constrain the radially expanding current sheaths.

Starting with Newton's second law

$$F = \frac{d(Mv)}{dt} \tag{II-17}$$

where $M = \rho$ (volume of sheath) (II-18)

or $M = \rho(\pi r^2 - \pi R^2)$ length (II-19)

and ρ is initial mass density of the gas,

R is initial radius,

r is radius of expanding sheath,

an equation of motion for the stabilized inverse pinch is

$$\rho\pi\frac{d}{dt}\left[(r^2-R^2)\frac{dr}{dt}\right] = \frac{\mu_o I_o^2 \sin^2\omega t}{4\pi r} - \frac{4\pi B_{zo}^2}{\mu_o L}\frac{(R_m^2-R^2)^2(r-R)r}{(R_m^2-r^2)^2} + \frac{\pi B_{zo}^2}{\mu_o}\left[\frac{(R_c^2-R^2)^2 r}{(r^2-R_c^2)^2} - \frac{(R_m^2-R^2)^2 r}{(R_m^2-r^2)^2}\right] \tag{II-20}$$

The term on the left side of the equation is the time rate of change of linear momentum. The first term on the right is the sinusoidal, driving magnetic force. The second term on the right is the restoring force due to the increase in tension of stretched magnetic flux lines. The last term is the force due to displacement of axial magnetic flux lines.

This nonlinear, second order, differential equation is solved

numerically by using the Runge-Kutta method with Gill's coefficients on a high speed digital computer (a CDC 1604)[11]. The position, velocity, and acceleration are computed for a range of initial gas densities and accelerating currents. Magnetosonic oscillations of the current sheath are predicted by the numerical integration. A listing of the computer code is given in Appendix D.

The radial position of current sheaths produced and accelerated in the stabilized inverse pinch employed (to be described in more detail in Chap. III) is calculated. Typical results are presented in Fig. II-18. The initial gas pressure is 150 microns, the gas is deuterium, and the driving current's peak is 100,000 amperes. Three stabilizing magnetic fields are presented, namely 0, 1000, and 3000 gauss. The curve for zero stabilizing field shows the usual high velocities of the order of 5×10^4 m/sec. With a stabilizing magnetic field of 1000 gauss, the radially expanding current sheaths are slowed down, stopped, and magnetosonic oscillations are predicted. For still larger stabilizing fields, the current sheath is stopped earlier and confined.

For the case of zero stabilizing magnetic fields, and after linearizing the equation of motion for the current sheath (e.g. consider only the initial portion of the driving current's period) the radial position of the current

---

[11] Friedrich, Otto M., Jr., "Analysis of the Plasma Current Sheath's Motion for an Inverse or 'Hard-Core' Pinch", Master's Thesis, The University of Texas, 1962.

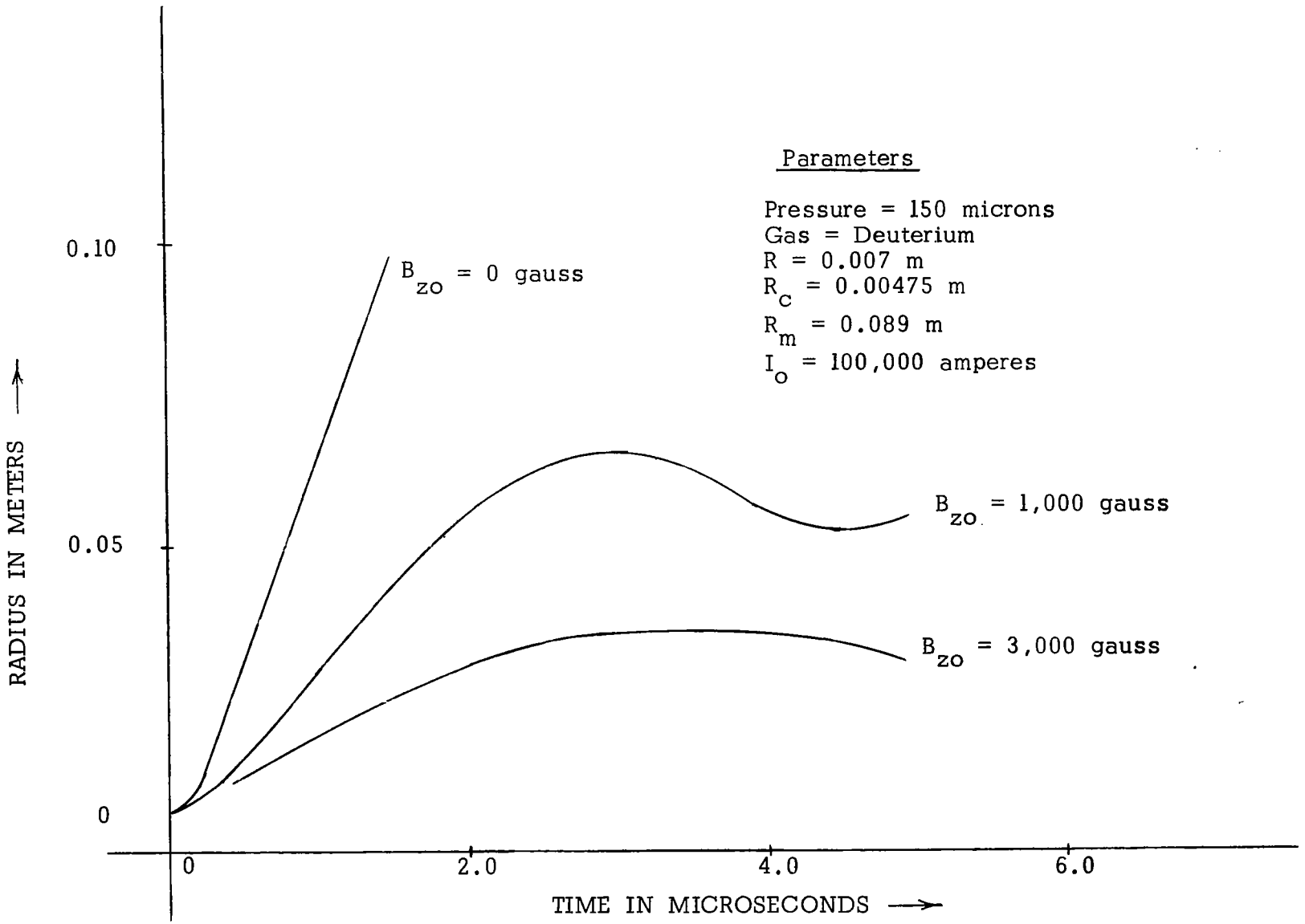

Fig. II-18. Radius of Current Sheath vs Time

sheath varies as

$$\left(I_o^2 / \rho \right)^{1/4} \qquad \text{(II-21)}$$

where I_o is the peak driving current, and ρ is the initial gas density. An expression based on a perturbation calculation for the frequency of magnetosonic oscillations is derived next in this chapter. For very large stabilizing magnetic fields, the equation of motion reduces to a simpler form. The time rate of change of the momentum term is then relatively small and can be neglected. The resulting equation of motion is an algebraic expression (not a differential equation) which can be readily solved.

Magnetosonic Oscillation Frequency

A numerical solution of the differential equation describing the motion of dynamic current sheaths in the stabilized inverse pinch indicates oscillations of the current sheath. (These oscillations will be referred to as magnetosonic oscillations.) An approximation for the steady state frequency of oscillation for the current sheath may be found by assuming

$$r = r_o + \delta r \qquad \text{(II-22)}$$

where r_o is a constant, δr is a small perturbation of r, and r is the total instantaneous radius. A more general expression for the dynamics of current sheaths in a stabilized inverse pinch was obtained earlier and presented in "Analysis of the Plasma Current Sheath's

Motion for an Inverse or Hard-Core Pinch".[12] A normalized radius y is defined as

$$y \equiv r/R \tag{II-23}$$

and a normalized time as

$$\tau \equiv kt \tag{II-24}$$

where

$$k = \left[\frac{\mu_0 I_0^2 \omega^2}{4\pi^2 \rho R^4} \right]^{1/4} . \tag{II-25}$$

Now, the approximation for the current sheath's steady state frequency of oscillation is found by assuming

$$y = y_0 + \delta y , \tag{II-26}$$

where y_0 is a constant, δy is a small perturbation of y. Using the above approximation, neglecting second order terms, and assuming $y_0 >> \delta y$, the equation of motion for the current sheath in a stabilized inverse pinch can be simplified to an expression that resembles the equation for a harmonic oscillator, i.e.

$$\frac{d^2 \delta y}{d\tau^2} + \omega_{osc}^2 \delta y = \text{constant} \tag{II-27}$$

where

$$\omega_{osc}^2 = \frac{K_3 \frac{4R}{L} \left[\left(\frac{R_m}{R}\right)^2 - 1 \right]^2}{\left[\left(\frac{R_m}{R}\right)^2 - y_0^2 \right]^3} \left[4y_0 - 4 + \frac{L}{R} \right] \tag{II-28}$$

where

$$K_3 = \frac{B_{z0}^2}{\mu_0 k^2 \rho R^2} . \tag{II-29}$$

---

[12] Friedrich, Otto M., Jr., "Analysis of the Plasma Current Sheath's Motion for an Inverse or 'Hard-Core' Pinch", Master's Thesis, The University of Texas, p. 50, 1962.

R is inner, or initial radius,

R_m is outer tube radius,

and, L is tube length.

Thus, knowing the parameters of the inverse pinch tube and the constant y_o, the frequency of oscillation can be calculated. For example, consider the following case: hydrogen gas at an initial pressure of 500 microns, peak driving current of 100,000 amperes with a period of 14 microseconds, and a stabilizing magnetic field of 500 gauss. Using the parameters for the inverse tube employed, R_m = 0.089 m, L = 0.066 m, R_c = 0.00475 m, and R = 0.007 m. Using 0.076 m for the constant r_o, the calculated frequency of the magnetosonic oscillations is approximately 350 kc.

Theta Pinch

Recently, several researchers have been investigating dynamic plasmas using the hydromagnetic models and large digital computers. In the mid 1950's, a joint effort between A.E.R.E. (Harwell, England) and Max-Planck-Institute (Germany) was begun. Dr. K.V. Roberts and S.J. Roberts of A.E.R.E. (Harwell) and Dr. K. Hain and G. Hain of Max-Planck-Institute performed much of these early analytical studies[13,14]. During the past several years major experimental studies have been performed to determine the merit of analytical results based on a hydro-

---

[13]Hain, K., Hain, G., Roberts, K. V., and Roberts, S.J., "Fully Ionized Pinch Collapse", Z. Naturforschg. 15a, 1039-1050, 1960.

[14]Roberts, K.V., Hertweck, F., and Roberts, S.J., "Thetatron, A Two-Dimensional Magnetohydrodynamic Computer Programme, Part 1, General Discussion", Culham Laboratory, UKAEA, CLM-R 29, 1963.

magnetic model. Today, the effect of trapped magnetic fields in theta pinches is of major concern and is being investigated analytically and experimentally.

The model employed by Hain and Roberts is the two fluid model. A set of equations is written describing the electrons and the ions. Most of the computer codes written to date are based on a one-dimensional space variation. For example, in cylindrical geometry the variables are functions only of radius r and time t. A fully ionized, quasi-neutral plasma is usually assumed. Electrons are assumed to be heated by joule, or ohmic, heating and the ions by shock heating. Only a thermal conductivity for ions and electrons perpendicular to the magnetic field is employed. Often an artificial shockwave term introduced by von Neumann is used to allow computation through the shock fronts. Also, fictitious wall sources of low density plasma are assumed so as to limit the Alfvén velocity at the walls.

The equations employed are: conservation of particles by an equation of continuity, conservation of momentum, an equation of state, an equation relating the energy gains and losses by the electron fluid, an equation relating energy gains and losses by the ion fluid, an Ohm's Law relation and Maxwell's electromagnetic field equations. The density, electron temperature, ion temperature, and other properties of the dynamic plasma are calculated using finite difference methods on a digital computer. Numerical calculations based on the Hain-Roberts computer codes for a theta pinch presently in operation in the Plasma Dynamics Research Laboratory at The University of Texas were made on the National Aeronautics and Space Administration's large digital computers

at the Langley Research Center [15]. Appendix E presents the equations employed in the Hain-Roberts codes.

The calculated position of the peak density vs time for the theta pinch at The University of Texas for two bias magnetic fields is shown in Fig. II-19 and Fig. II-20. The gas is deuterium at an initial pressure of 100 microns. The voltage on the main compression capacitor bank of ten 15 μf, 20 kv, capacitors is 15 kv. The bias field in Fig. II-19 is only - 2 kilogauss. The analytical calculations performed at Langley Research Center, National Aeronautics and Space Administration shows the initial pinch's first radial minimum at 0.4 microseconds. Subsequent radial hydrodynamic oscillations are predicted. Fig. II-20 presents the calculated results for a - 4 kilogauss bias field. The first pinch is predicted with the first radial minimum occurring at approximately 0.5 microseconds. (Notice the peak density does not leave the wall until the time 0.2 microseconds.)

---

[15]We wish to acknowledge the assistance given by Dr. G. Oertel of NASA, Langley Research Center in obtaining these computer calculations.

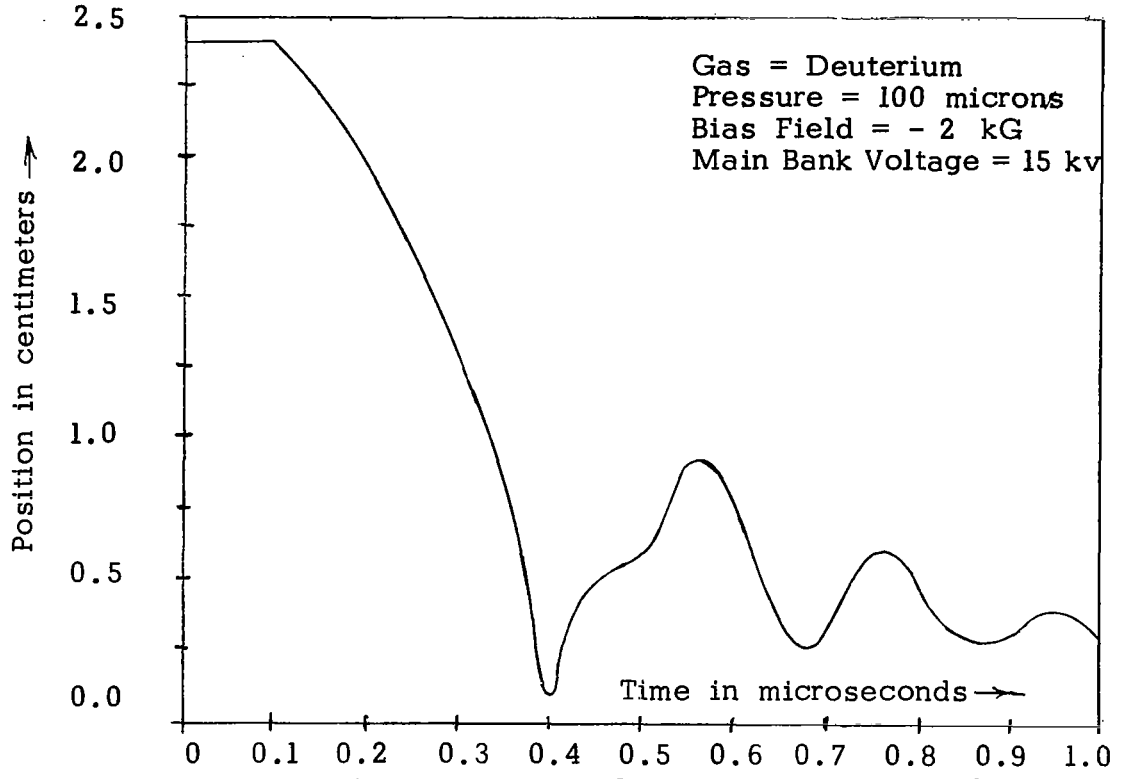

Fig. II-19. Calculated Position of Peak Density in a Theta Pinch, 2 kilogauss Reverse Bias Field.

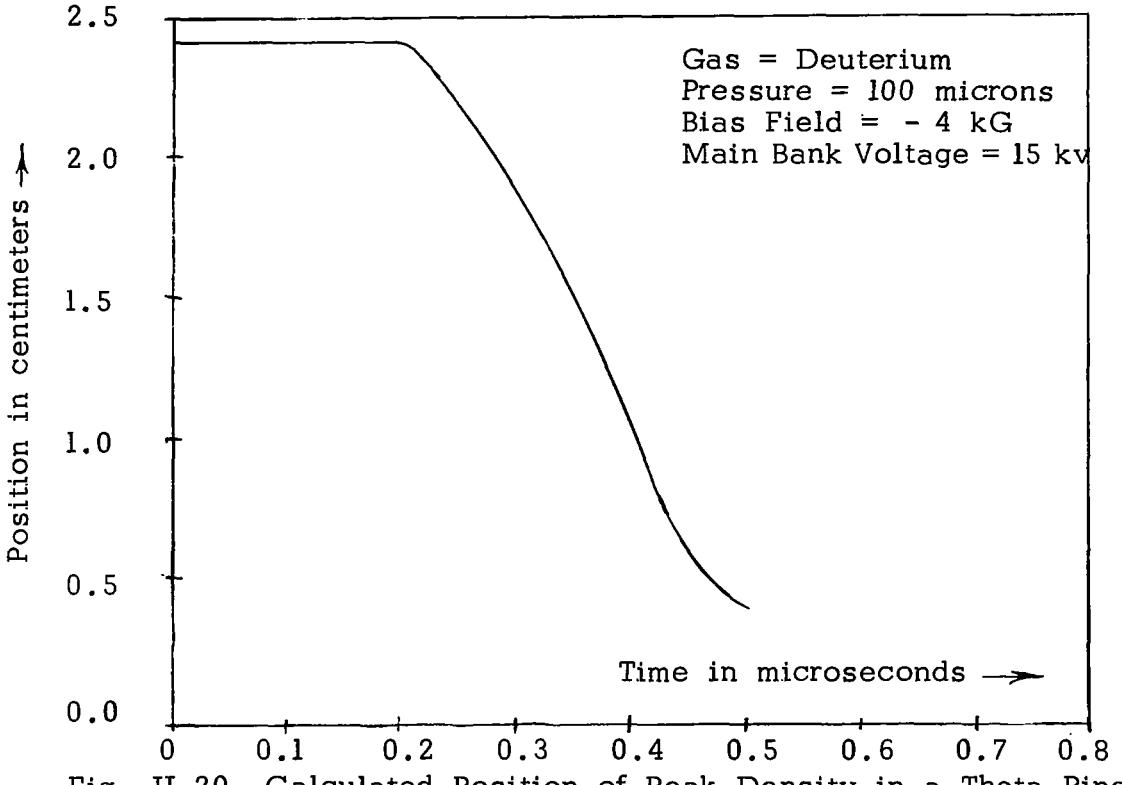

Fig. II-20. Calculated Position of Peak Density in a Theta Pinch, 4 kilogauss Reverse Bias Field.

CHAPTER III

EXPERIMENTAL ARRANGEMENTS

Several experimental arrangements employed to produce and accelerate current sheaths in magnetoplasmas are described in this chapter. First a parallel plate accelerator, or parallel plate "rail" gun, that produces flat, one dimensional current sheaths is described. Second, a stabilized inverse pinch, or stabilized hard-core pinch, used to produce radially expanding current sheaths is discussed. And third, a theta pinch used to produce extremely high temperature plasmas and dynamic current sheaths is briefly described.

A. Parallel Plate Accelerator

A parallel plate accelerator, or parallel plate "rail" gun, was recently investigated with magnetic and electric probes by R.H. Lovberg [1] and found to produce extremely flat current sheaths for certain conditions during the initial acceleration process. In order to use infrared maser probing techniques to further investigate flat current sheaths, a parallel plate accelerator enclosed in a rectangular quartz container was constructed at The University of Texas. An initially clean system and a rapidly rising driving current are required to form and accelerate flat current sheaths. An external magnetic field in the form of a multipole is employed to aid in confining and guiding the current sheaths down the

---

[1] Lovberg, R.H., "Acceleration of Plasma by Displacement Currents Resulting from Ionization", VI^e Conference Internationale sur les Phenomenes D'Ionisation dans les Gaz, vol. IV, 235, S.E.R.M.A., Paris, France, 1963.

accelerator.

The rectangular discharge tube enclosing the parallel plate accelerator electrodes was constructed from ground flat quartz plates 1/4" thick x 3" wide x 6" long. The quartz plates are joined together by using a vacuum grade epoxy (Torr seal by Varian). The insulator through which the drive current feeds to the electrodes is a 4" diameter x 1/4" thick ceramic (Al_2O_3) disc. This insulator at the breech of the accelerator is also sealed to the quartz plates with vacuum grade epoxy. The electrodes of the accelerator are stainless steel plates 1/4" thick x 2 and 3/4" wide x 3" long and are separated approximately 1.3" (3.4 cm). The electrodes are threaded onto the current feeds. Fig. III-1 shows a sketch of the discharge tube.

In order to obtain a good initial base vacuum, a two stage mechanical pump and a three stage oil diffusion pump are used. Since the discharge tube is sealed with epoxy, the system is not bakeable. The gas employed in the experiment is supplied from either a small (1 or 1.5 liter) commercial cylinder or from a large 244 cu ft cylinder. The gas pressure from the cylinder is reduced to several psi gauge pressure by a two stage regulator and then flowed into the discharge tube through a Granville-Phillips Type C valve. Since the gas filling-vaccum system is a continuously flowing system, the pressure inside the discharge tube as read on a Pirani gauge tube can be controlled with the Type C valve in the gas filling system.

The current sheaths are produced and accelerated between the parallel plate electrodes by discharging two 15 μf, 20 kv, 3000 joule energy storage capacitors through two GL 7703 ignitron switches and two low inductance coaxial cables per capacitor. Typically the capacitors

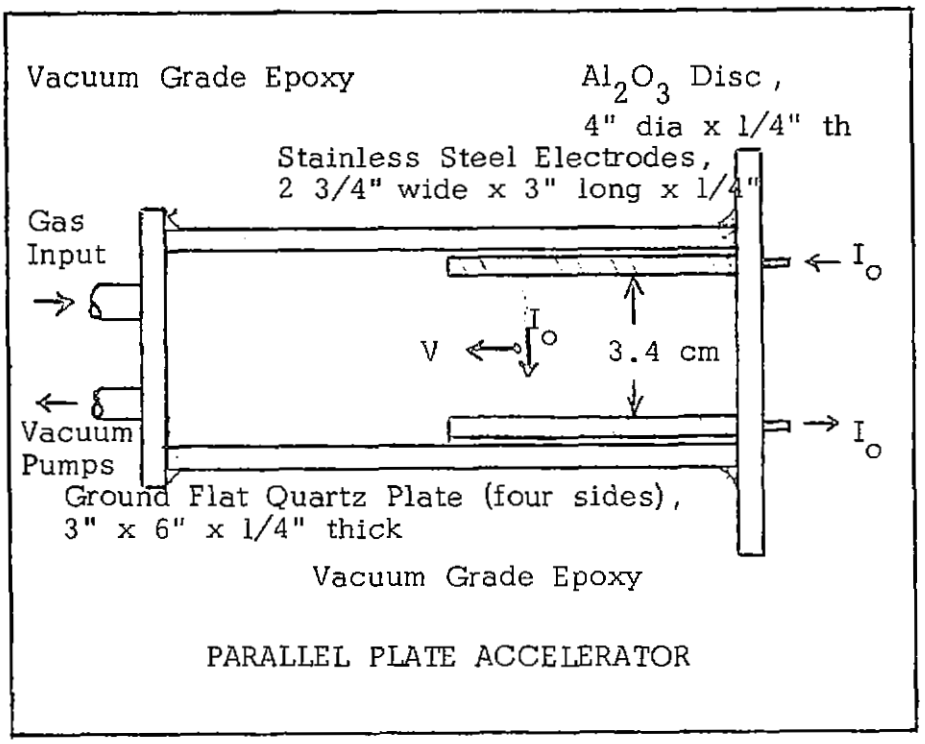

Fig. III-1. Parallel Plate Accelerator Discharge Tube

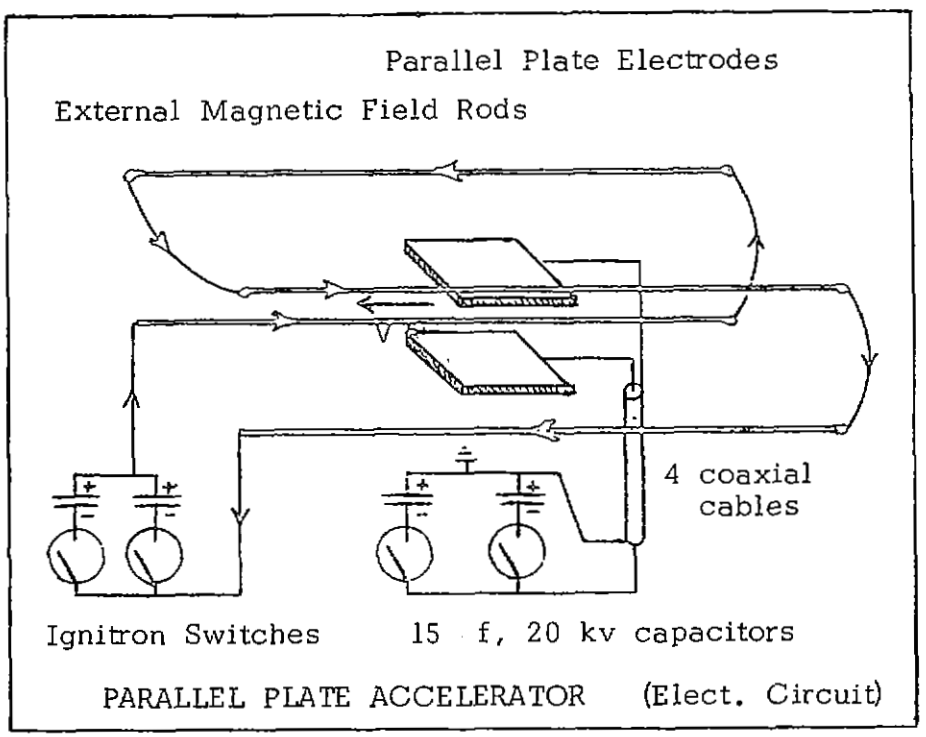

Fig. III-2. Parallel Plate Accelerator Electrical Circuit

are only charged to 4 or 6 kv resulting in peak currents of the order of 35,000 or 50,000 amperes with a quarter period of approximately 5 u sec.

The confining and guiding external magnetic field is produced by discharging two 15 uf, 20 kv, 3000 joule energy storage capacitors through two GL 7703 ignitron switches and two low inductance coaxial cables per capacitor, through four 3/16" diameter brass rods forming the multipole. Peak currents of the order of 10,000 amperes with a full period of 150 u sec result. Fig. III-2 shows a sketch of the electrical circuit for the parallel plate accelerator.

Mechanical and electrical timing circuits are employed to control the charging and discharging of the accelerator capacitor bank and the external magnetic field capacitor bank. The capacitor banks require less than 15 seconds to charge from a 20 kv, 100 ma power supply. An optical meter relay switches the power supply off when the preset operating voltage is reached. After the capacitor banks are charged, an electrical pulse is generated to initiate the discharge cycle. Electronic delay generators are used to control the sequence of discharging the accelerator bank w.r.t. the magnetic field bank. Oscilloscopes and other equipment are triggered from delay generators, from probe signals which monitor the accelerating current, and/or probe signals which monitor the external magnetic field. Fig. III-3 shows a photograph of the parallel plate accelerator experimental arrangement.

B. Stabilized Inverse Pinch

A metal and glass stabilized inverse pinch (or hard-core pinch) discharge tube is used to produce dynamic current sheaths in a crossed, steady, stabilizing magnetic field. The discharge tube is constructed

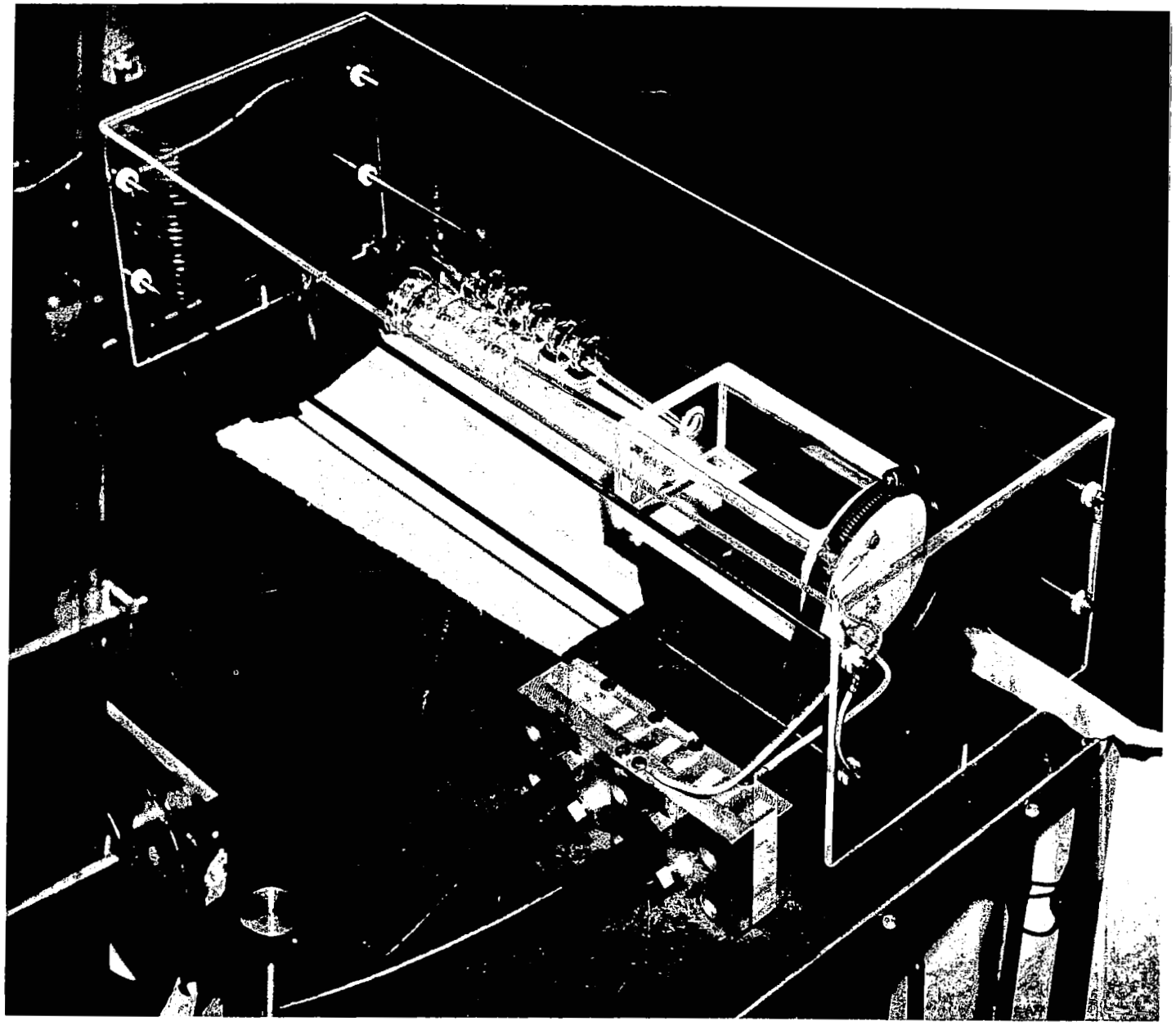

Fig. III-3. Photograph of Parallel Plate Accelerator Arrangement

with two stainless steel electrodes 9 and 1/2" O.D. and 1/2" thick connected at each end of a 7" O.D., 2 and 9/16" long glass cylinder. Two small ridges are machined inside of a groove on a 7" O.D. in the stainless steel electrodes for a seal from metal to glass. Neoprene rubber seals and later viton O-rings were used for the seal. The 7" O.D. glass cylindrical shell has three radial 15 mm I.D. glass tubulations and two radial 10 mm I.D. glass tubulations. One of the 15 mm tubes is connected to a 3 stage oil diffusion vacuum pump through a glass stop-cock. A second of the 15 mm tubes is used to measure the pressure in the discharge tube with a Pirani gauge tube. The third 15 mm tubulation is used for flowing gas into the discharge region. The two 10 mm glass tubulations (attached radially and located with a 90 degree angular separation) are used for probing the current sheath with magnetic, electrostatic, and piezoelectric probes. A 0.375" O.D. brass "hard-core" current return is located on the central axis of the cylindrical arrangement and is used to establish the magnetic fields to drive the current sheaths formed at the center radially outward. The metal core is covered with a teflon cylinder for making a vacuum seal. The teflon is then shielded with a quartz tube inside the active plasma region between the stainless steel electrodes.

The main accelerating current input is through a 1/8 inch brass strap and the current return is through a 1/16 inch brass strap. A quick-coupling coaxial cable header with positions for 10 low inductance cables is used to couple the capacitor bank to the discharge tube's input and output straps.

After trying several radio frequency methods to preionize the cold gas, a linear discharge was constructed and used for preionization. Two 15 μf, 20 kv, 3000 joule energy storage capacitors are charged from

4 to 8 kv and discharged through a 30 μh inductor into the discharge tube via the stainless steel electrodes. One side of the capacitors when switched by ignitrons is connected by several No. 10 wires to one electrode; the other side of the capacitor is connected through the input cable header assembly also used for the main acceleration feeds to the other electrode. Peak currents of the order of 10,000 amperes and with a ringing frequency of 10 kc are obtained.

The main capacitor bank for forming and then driving the current sheaths uses two 15 μf, 20 kv, 3000 joule low inductance energy storage capacitors. Peak currents of more than 100,000 amperes and with a full period of 14 μ sec are obtained. These large currents are switched through two GL 7703 ignitron tubes per capacitor and are triggered by hydrogen thyratron tubes. The high voltage charging supply is a 20 kv, 100 ma unit designed and constructed in our laboratory.

In order to effectively study the dynamics of current sheaths, a vacuum system capable of a base pressure of 10^{-5} mm Hg or better is required. The present limitation in the ultimate vacuum base pressure is the metal to glass seals made with neoprene or viton. The forepump used is a two stage mechanical pump capable of 0.05 microns. A three stage oil diffusion pump capable of 8×10^{-8} mm Hg is also used. The control valves used are high vacuum, glass stopcocks. The base vacuum is monitored on a Veeco Type RG-75 ionization gauge.

The gas used to form the current sheaths is supplied from small (1 or 1.5 liter) commercial gas cylinders or large 244 cu ft cylinders. A two stage reducer and regulator is used to supply the gas at several psi gauge to a Granville-Phillips Type C valve. The system is a continuously flowing system. The operating pressure in the discharge tube is measured on a Pirani gauge tube.

A Harvey-Wells Model L-75A laboratory electromagnet is used to supply the 3 to 5 kilogauss fields across a 4 and 1/2" air gap which is 7" in diameter. A UR-1050 power supply manufactured also by Harvey-Wells is used to power the magnet.

Mechanical timers and electronic delay generators are used to control the charging, discharging, and sequencing. The long charge and delay times of the order of seconds are controlled by mechanical timers. The short delays of several to several hundred microseconds that are required between preionization, main acceleration, and initiation of electronic recording instruments are generated by electronic delay units. Typically, 10 to 20 seconds are required to charge the capacitors to the preset operating voltage. An electronic pulse is then generated to fire the preionization bank. Approximately 100 microseconds later, the main accelerator bank is fired. Electronic recording instruments are triggered from delay generators or probe signals generated by the main accelerator current. Fig. III-4 shows a sketch of the discharge tube for the stabilized inverse pinch. A systems diagram is shown in Fig. III-5. Fig. III-6 is a photograph of the overall experimental arrangement. A close-up view of the discharge tube inside the electromagnet is pictured in Fig. III-7.

C. Extremely High Temperature Theta Pinch

Dynamic current sheaths are produced in an extremely high temperature theta pinch[2]. The plasma is formed in a 2" O.D. Pyrex

---

[2]Gribble, R.F., Roberts, H.N., and Dougal, Arwin A., "Diagnostics of Experimental Extreme Temperature Plasma", Quarterly Progress Report No. 1 on Research on Plasma Diagnostic Methods for High Temperature Plasma Research, (Contract No. AF 33(657)-11073), Plasma Dynamics Research Laboratory, The University of Texas, Austin, Texas, July 15, 1963.

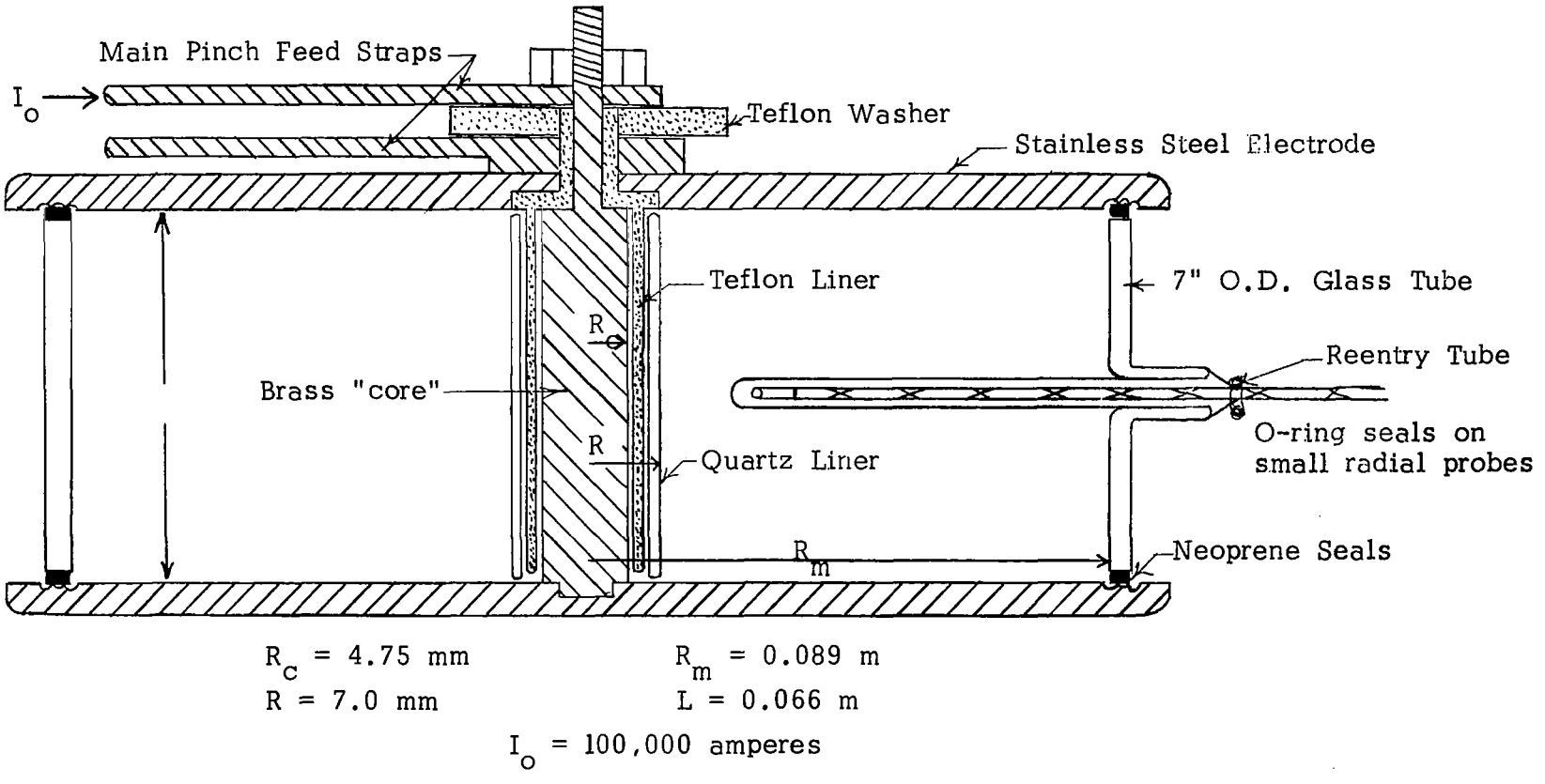

Fig. III-4. Stabilized Inverse Pinch Discharge Tube

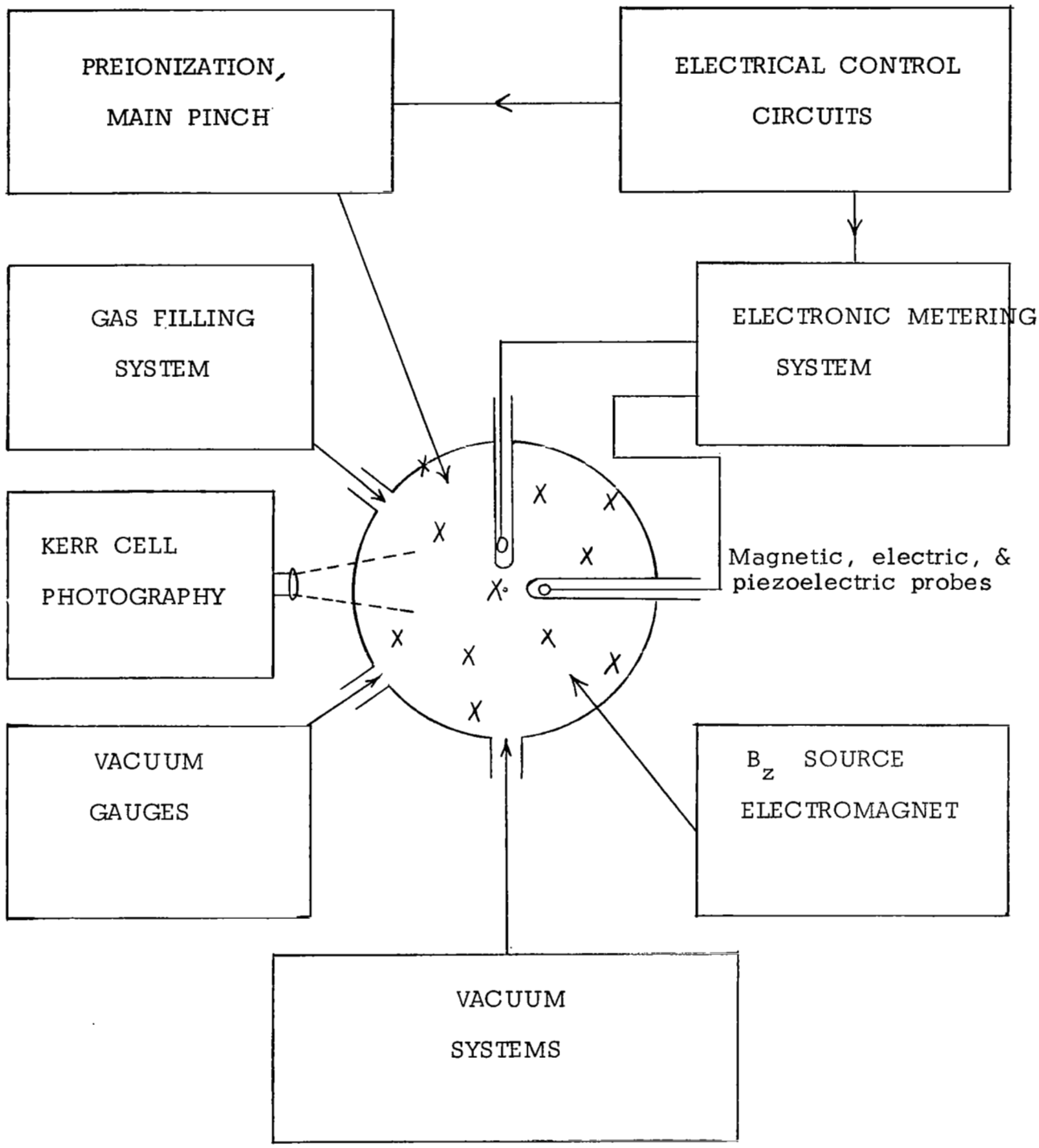

Fig. III-5. Stabilized Inverse Pinch Systems Diagram

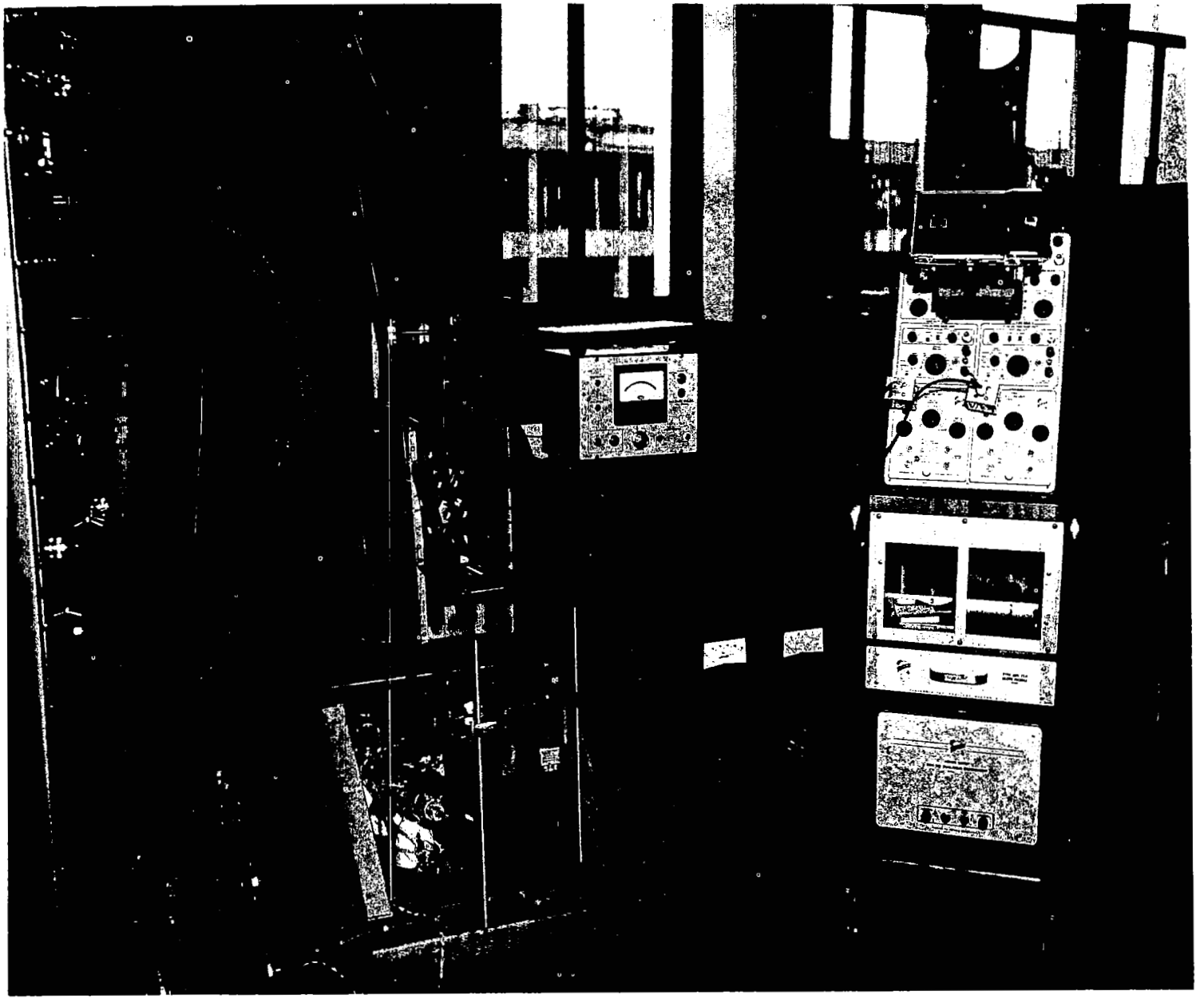

Fig. III-6. Photograph of Stabilized Inverse Pinch

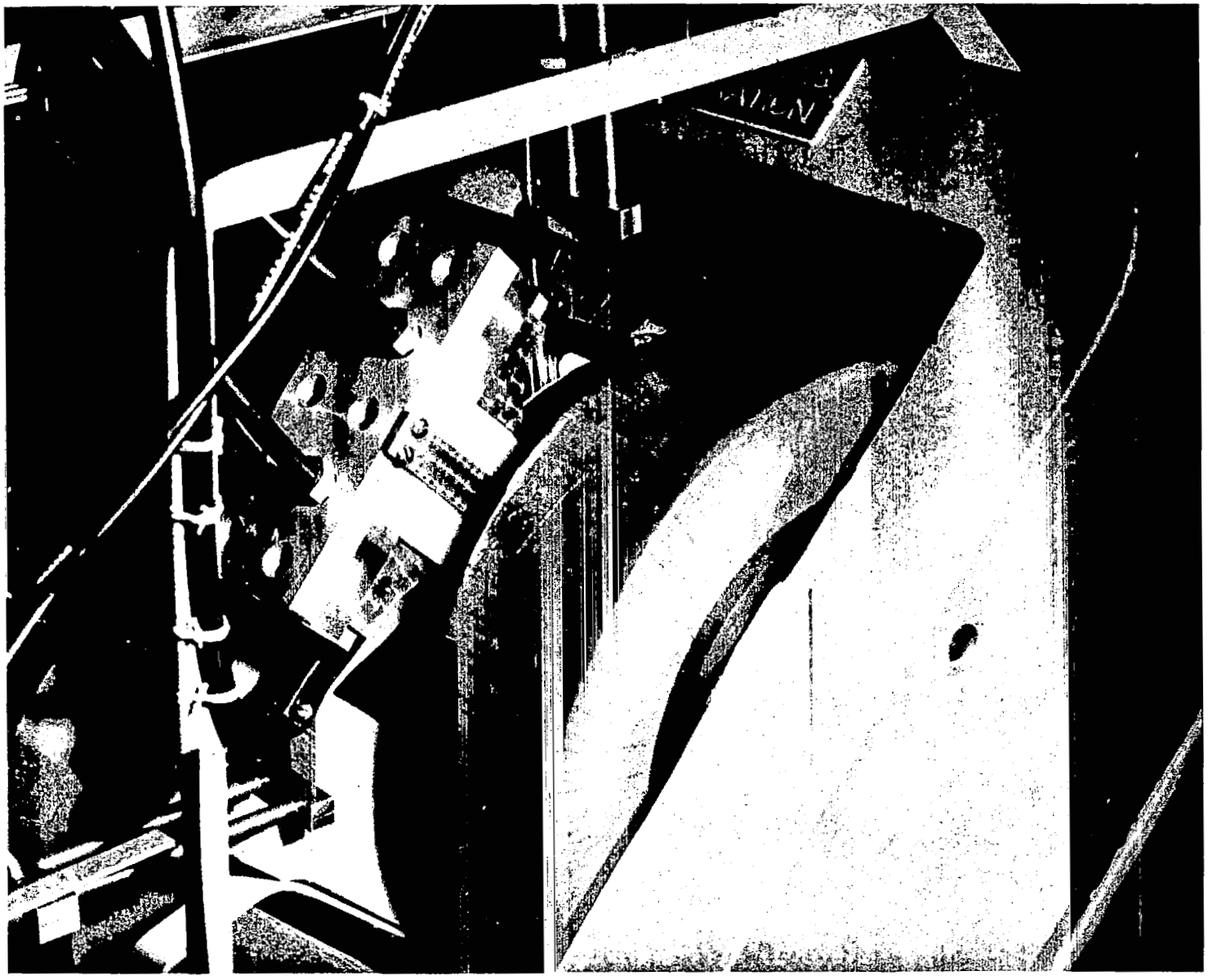

Fig. III-7. Close - Up Photograph of Stabilized Inverse Pinch Discharge Tube in Electromagnet

discharge tube approximately 10" long. A one turn coil surrounding the discharge tube is used with a super high power preheater capacitor bank, a magnetic bias field capacitor bank, and a main compression capacitor bank. The high temperatures are produced in four stages. First, a 10 kw, 1 ms, 16 Mc radio frequency oscillator pulse breaks the gas down. Next a 3 kv, 120 μf, 36 μ sec rise time capacitor bank capable of producing magnetic fields of +10 kilogauss or -10 kilogauss is connected to the one turn coil. Third, a super high power preheater capacitor bank with 0.16 μf, 20 kv, 50 megawatts peak power is switched with a spark gap into the one turn coil. Finally, the main fast compression bank consisting of ten 15 μf, 20 kv, 3000 joule low inductance energy storage capacitors is switched with twenty ignitrons onto the one turn coil. Fig. III-8 shows a system diagram of the extremely high temperature theta pinch. A photograph of the experiment is presented in Fig. III-9.

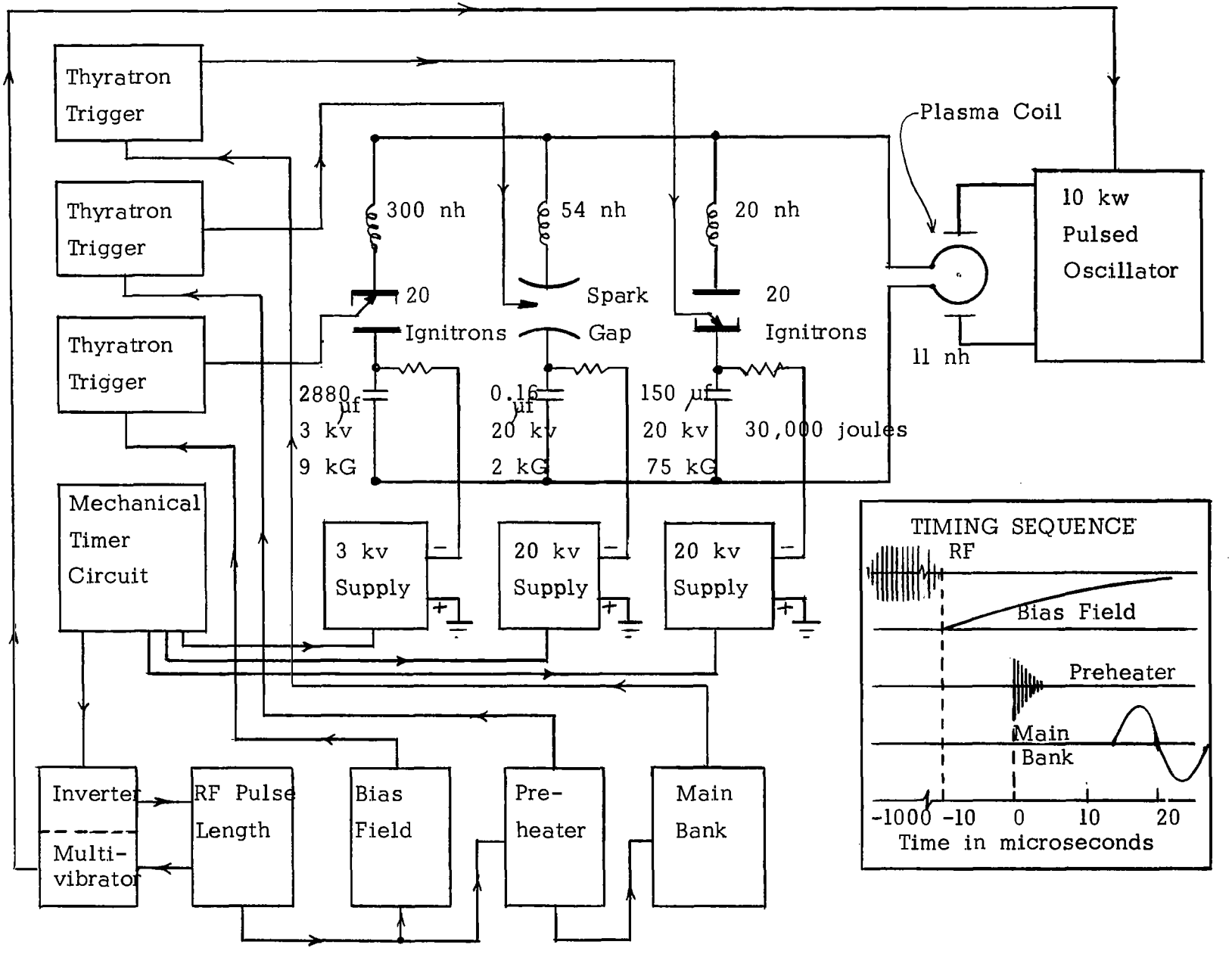

Fig. III-8. Extremely High Temperature Theta Pinch Experiment

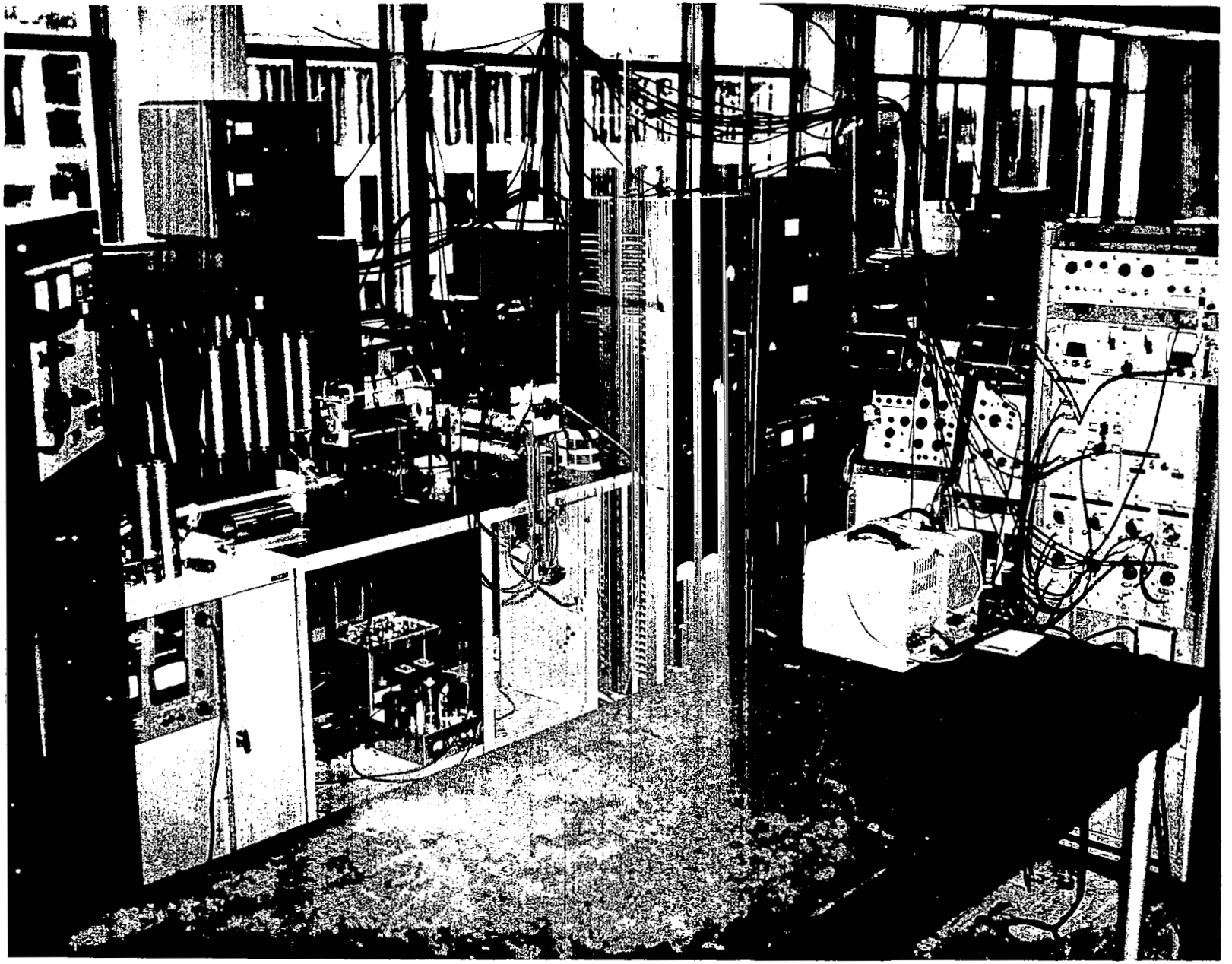

Fig. III-9. Photograph of Extremely High Temperature Theta Pinch

CHAPTER IV

INSTRUMENTATION

Several methods employed to investigate the properties of dynamic current sheaths are described in this chapter. These methods include infrared maser interferometry, electrostatic probes, Kerr cell high speed photography, piezoelectric pressure sensitive probes, magnetic probes, and voltage-current measurements.

A. Infrared Maser Interferometry

The recent development of intense, coherent visible and infrared light sources allows measurements of electron densities above 10^{14}/cc by extending familiar microwave diagnostic techniques to the optical wavelength range. The electron density is obtained by observing the resonant frequency shifts of a Fabry-Perot interferometer closely coupled to an infrared maser [1, 2]. King and Steward [3] observed that interference occurs if a maser beam is reflected back into the maser by an external mirror. If the mirror is moved, the interference modulates the maser beam.

---

[1] Dougal, Arwin A., "Optical Maser Probing Theory for Magneto-plasma Diagnostics", Proc. Fourth Symposium on MHD, IV, pp. 1-4, IEEE, 1963.

[2] Ashby, D.E.T.F., Jephcott, D.F., Malein, A., Raynor, F.A., "Performance of the He-Ne Gas Laser as an Interferometer for Measuring Plasma Density" Fifth Annual Meeting of the Division of Plasma Physics of the American Physical Society, San Diego, November, 1963.

[3] King, P.G.R., and Steward, G.J., New Scientist, 17, 180, 1963.

Intensity minima occur as the mirror moves through successive half-wavelengths. Due to the dispersion of a coherent infrared beam by electrons, varying electron densities located within the interferometer effect the maser in the same manner as the external mirror that moves. The phase shift $\Delta\phi$ for a given plasma length ℓ and electron density n_e is given by

$$\Delta\phi = \frac{\ell}{2}\omega_p^2/c\omega \quad , \qquad \text{(MKS units)} \qquad \text{(IV-1)}$$

where $\omega_p^2 = \frac{n_e e^2}{m_e \epsilon_o}$, n_e is the electron density, ω is the angular frequency of the maser, e is the electronic charge, c is the velocity of light, m_e is the mass of an electron, and ϵ_o is the free space permitivity. Thus, the phase shift is simply related to the electron density. The electron density is now obtained from the maser beam intensity modulation due to phase shifting.

The infrared maser used is a He-Ne gas maser operating at 3.39 micron wavelength. The mirror separation of the tuneable invar maser cavity is about 135 cm. A torsion bar mounting arrangement is used to provide angular adjustment for one mirror of the maser about two orthogonal axes. The other mirror assembly is mounted on linear ball bearings which allows about 4 cm variation in the mirror spacing. The He-Ne gas maser is operated in the visible 6328 Å laser mode to line up the optics in the system initially. The system is then adjusted to optimize the 3.39 micron infrared signal on an InAs detector. The Indium Arsenide detector is a Type M-8000 manufactured by Texas Instruments, Inc. The detector has a sensitive area of 1.54×10^{-2} cm^2, a detectivity D^* of 5.8×10^7 at 300^oK, a time constant less than 0.25 microseconds, and an incremental impedance of 15 ohms. Fig. IV-1 is a photograph of the

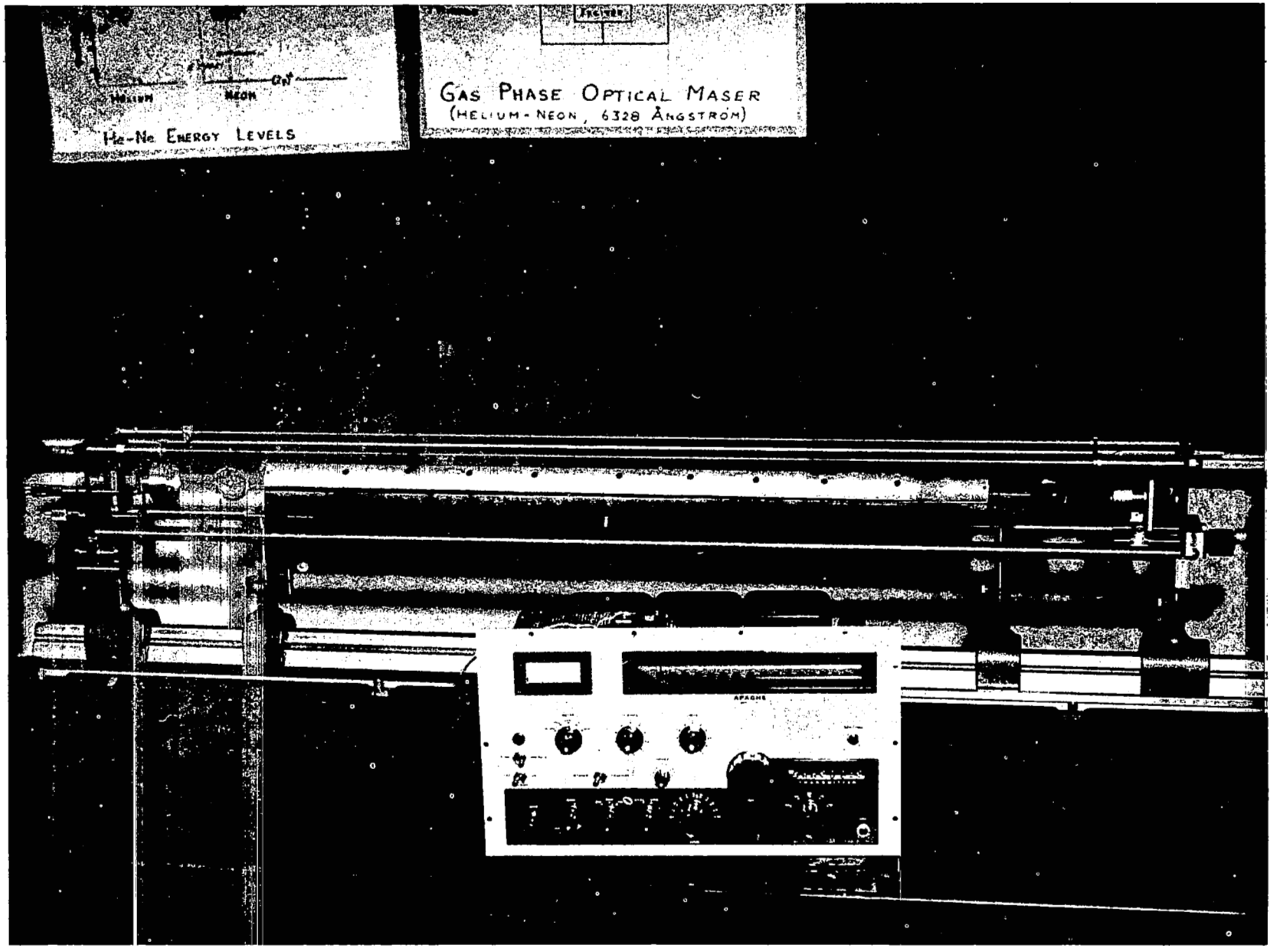

Fig. IV-1. Photograph of He-Ne Gaseous Maser

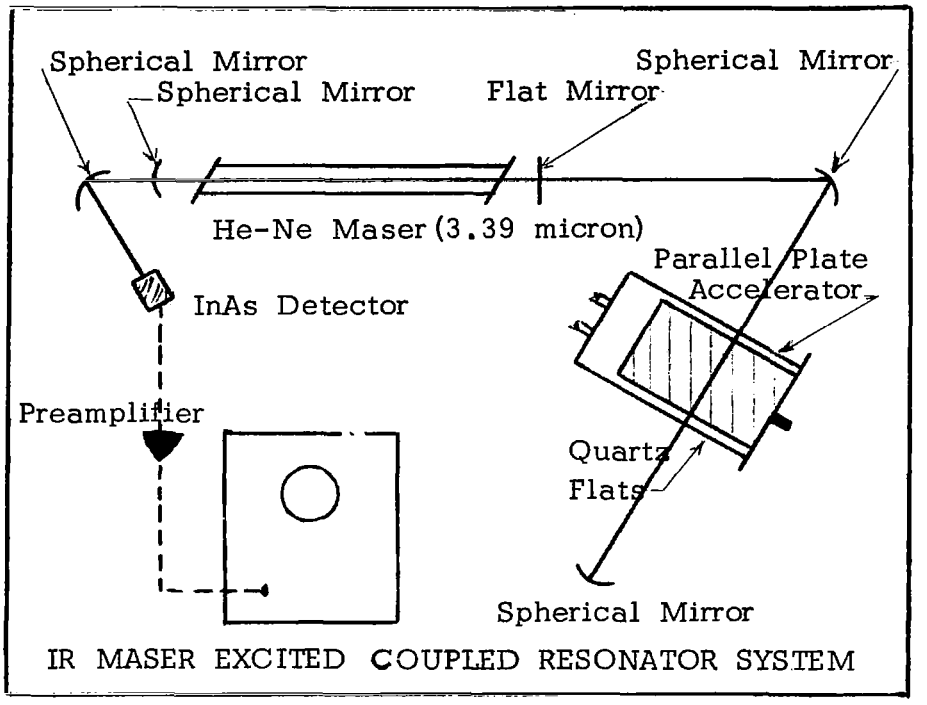

Fig. IV-2. IR Maser Excited Coupled Resonator System

He-Ne maser used. A sketch of the interferometer system is presented in Fig. IV-2.

B. Electrostatic Probes

In order to measure the electric fields produced by dynamic current sheaths in magnetoplasmas, small electrostatic probes were designed and constructed. R.H. Lovberg has reported [4] excellent measurements with a "ring and disc" type electrostatic probe employed to measure electric fields in coaxial guns. The "ring and disc" probe is constructed by forming soft solder electrodes (a ring and disc) at the center (disc formed) and outer (ring formed) conducting braid of a RG 196 coaxial cable. The spacing between the ring and the disc was either 5 mm or 10 mm. Similar electrostatic ring and disc probes formed with RG 174/U coaxial cable were constructed and employed to measure the radial electric fields in the stabilized inverse pinch at The University of Texas.

Several other small electrostatic probes were designed and constructed to measure the radial electric field (E_r), the axial electric field (E_z), and the azimuthal electric field (E_θ) in the stabilized inverse pinch. Small needle like electrodes spaced only 2 mm and 5 mm were used. The electrodes are 10 mil diameter, 2 mm long conductors. The RG 174/U coaxial cable attached to the small needle electrodes is lead out of the plasma region through a 5 mm O.D. Pyrex tube (a tube which moves radially in two O-ring vacuum seals) to a pulse transformer. Electrical insulation and a vacuum seal near the needle electrodes are accomplished

---

[4] Burkhardt, L.C., and Lovberg, R.H., "Current Sheet in a Coaxial Plasma Gun", Phys. Fluids, 5, 341, 1962.

with vacuum grade epoxy. Fig. IV-3 shows sketches of the electrostatic probes.

The pulse transformer is required for high voltage isolation of the recording oscilloscope from the plasma discharge tube and also for common mode signal rejection. High voltage isolation and common mode rejection are accomplished by winding a 10 turn primary and a 10 turn secondary pulse transformer with a powdered iron, toroidal core (manufactured by Arnold Engineering). Mylar sheets insulate the primary and secondary coils from the powdered iron core.

The properties of the current sheath that are measured with the electrostatic probes are: 1) space and time resolved electric fields, 2) the current sheath onset time, 3) an estimate of the width of the current sheath, and 4) an estimate of the energy of the expanding sheath's ions. Information of the stability of the current sheath is obtained from the electric field measurements in the azimuthal direction. Evidence of magnetosonic oscillations of the sheath can be investigated with the electric probes.

C. Kerr Cell High Speed Photography

The self-luminous fronts produced and accelerated in the parallel plate accelerator, the inverse pinch, and the theta pinch are photographed with a high speed Kerr cell system manufactured by Electro-Optical Instruments. The light from the discharge is electronically gated with a 100 ns Kerr cell shutter. A standard Crown Graflex 45 camera system with a Polaroid back with high speed Type 410 film (ASA 10,000 speed) is employed to record the self-luminous fronts.

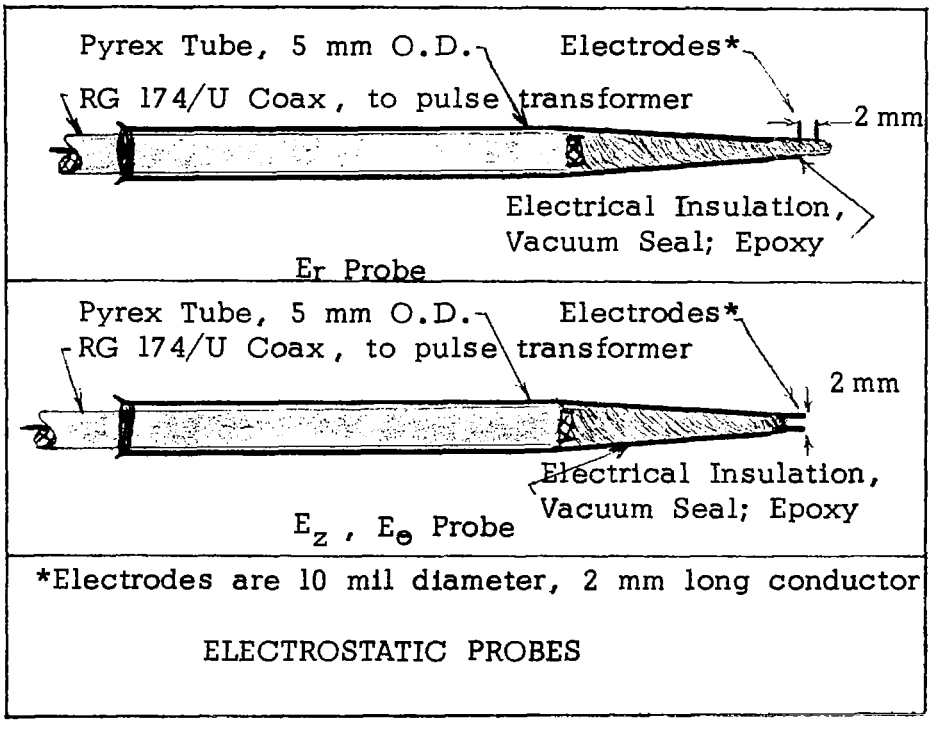

Fig. IV-3. Sketch of Electrostatic Probes, (E_r) and (E_z , E_θ) Probes.

D. Piezoelectric Pressure Sensitive Probes

Piezoelectric pressure sensitive probes [5,6,7] are used to investigate the gasdynamics associated with the dynamic current sheaths. A barium titanate disc 0.100" diameter x 0.040" thick is employed as the pressure sensitive element. The disc is cemented to a 3/32" O.D. solid, inertia rod and inserted into a 5 mm O.D. quartz tube. The piezoelectric element is electrically insulated from the plasma discharge by mylar. Vacuum seals are made with vacuum grade epoxy. The electrical signal is conducted from the barium titanate disc with a twisted pair of #42 enameled copper wires. These leads are then connected by RG 58/U coaxial cable to the recording oscilloscope. Fig. IV-4 shows the construction. A dynamic response of the piezoelectric probe is obtained by observing the probe signals for shock fronts produced by exploding a wire in air (air at atmospheric pressure). Fig. IV-5 shows the dynamic response of a piezoelectric probe. The onset of pressure fronts is readily observed with a piezoelectric probe in the stabilized inverse pinch with argon gas.

E. Magnetic Probes

Time and space resolved magnetic field measurements are made with small magnetic probes. The position of the current sheath in the stabilized

---

[5] Knight, H.T., "Piezoelectric Detector for Low-Pressure Shock Waves", Review of Scientific Instruments, 29, 174, 1958.

[6] Stern, M.O., and Dacus, E.N., "Piezoelectric Probe for Plasma Research", Review of Scientific Instruments, 32, 140, 1961.

[7] Filippov, N.V., "Investigation of Pressures in a Powerful Pulsed Gas Discharge using a Piezoelectric Measuring Device", Plasma Physics and the Problem of Controlled Thermonuclear Reactions, III, Pergamon Press, 280, 1959.

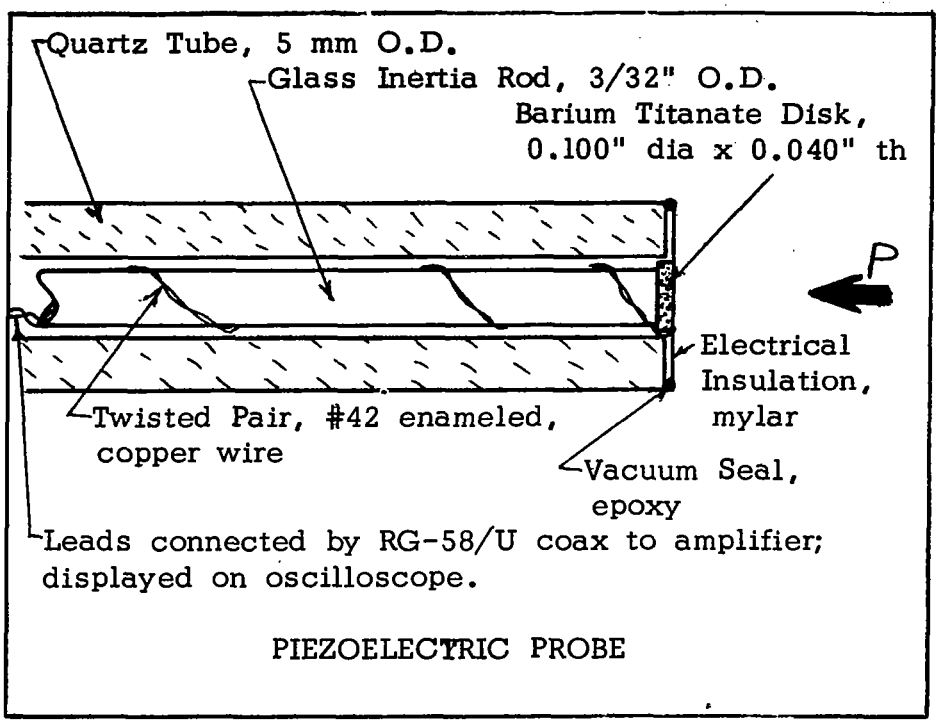

Fig. IV-4. Construction of Piezoelectric Probe

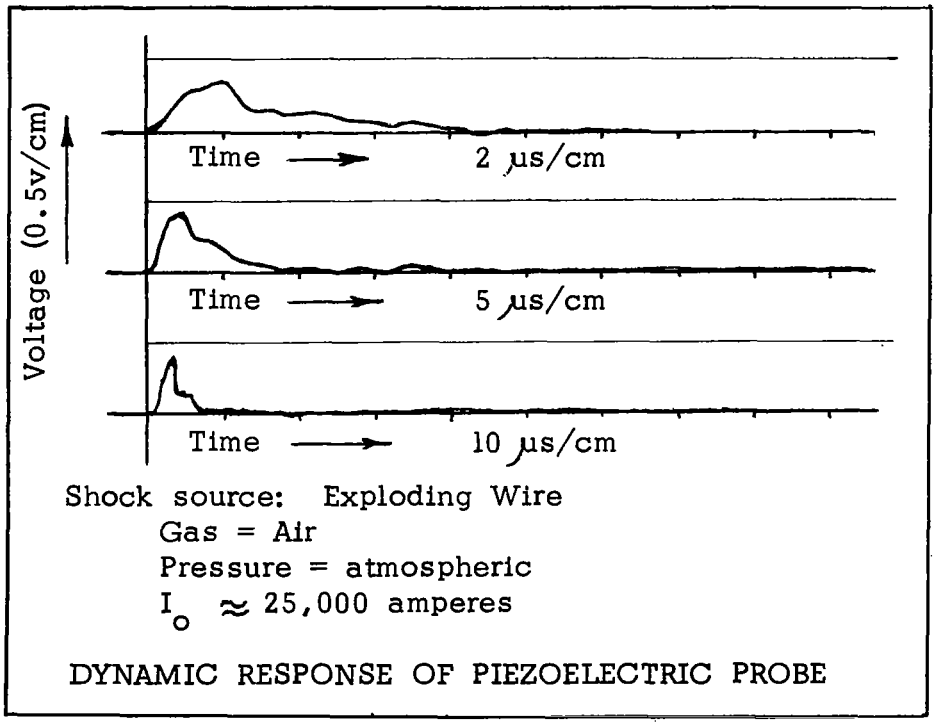

Fig. IV-5. Dynamic Response of Piezoelectric Probe

inverse pinch is determined by: 1) observing the "shielding" of the B_θ signal until the current sheath passes the probe coil; or 2) observing the B_z magnetic field buildup as the magnetic flux is swept by the current sheath. Magnetosonic oscillations of the current sheath in the stabilized inverse pinch predicted by an analytical analysis are observed on the B_z probe signals. Small coils of #36 (and #42) enameled copper wire wound on nylon rods 1/16" O.D. and machined to 50 mils are used to measure B_θ and also $\dot{B}_z$. Another coil is wound so as to measure $\dot{B}_r$. These signals are electronically integrated with a RC circuit to obtain B_θ, B_z, and B_r . From these measurements, the current distribution can be calculated with Maxwell's electromagnetic field equations. Fig. IV-6 shows the construction of magnetic probes.

F. Voltage-Current Input Measurements

The voltage at the input terminals of the parallel plate accelerator, the stabilized inverse pinch, and the theta pinch are measured with a Tektronix Type P6013 high voltage probe. The voltage signal is helpful in observing rapid changes in the inductance of the system. For example, in locating possible magnetosonic oscillations, voltage signals are employed. The current supplied to the discharge tube is obtained by measuring the magnetic field established around one of the current carrying conductors. A 1 cm diameter, 10 turn coil is employed to observe $\dot{B}_\theta$ which is electronically integrated before being displayed on the recording oscilloscope. These current measuring probes are also used to monitor the firing of various capacitor banks. The current derived signal can also be used to trigger other electronic units at preset current levels.

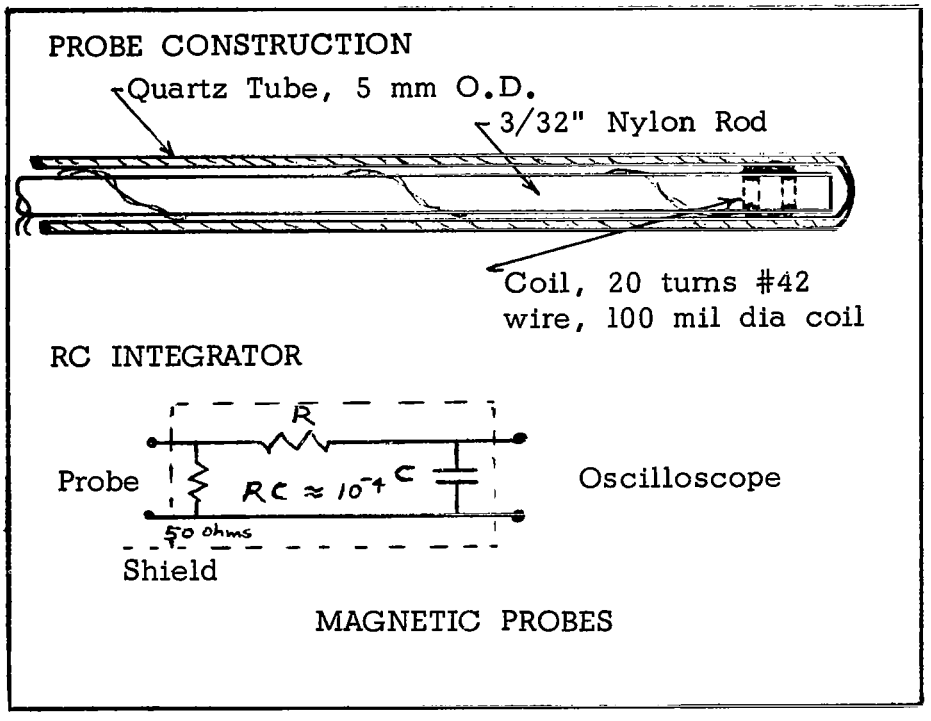

Fig. IV-6. Construction of Magnetic Probes

G. Other Diagnostics Employed

An image converter, high speed framing camera system was also employed to record self-luminous fronts produced in the stabilized inverse pinch and the extremely high temperature theta pinch. (The image converter camera system was on loan from the Space Technology Laboratory which manufactures the camera system for a one day period. Only a limited amount of data was recorded for each of the two systems.)

A time resolved neutron detector consisting of a NE-2 plastic scintillator block and an EMI 9531S photomultiplier tube was employed to look for possible neutrons emitted from the stabilized inverse pinch.

CHAPTER V

EXPERIMENTAL FINDINGS

Experimental results obtained with the diagnostic methods presented in Chap. IV (Instrumentation) on current sheaths produced in the experimental apparatus described in Chap. III are given in this chapter. Plasma breakdown and current sheath formation are presented first. Space and time resolved electron densities measured with an infrared maser interferometer in the parallel plate accelerator are given. Results of electric field, self-luminous fronts, pressure fronts, and magnetic fields associated with the current sheath are described. Magnetosonic oscillations observed in the stabilized inverse pinch are discussed.

A. Plasma Breakdown and Current Sheath Formation Between Planar Electrodes

The plasma breakdown path is that path which offers the minimum resistance and inductance. Therefore, breakdown should occur near the center return conductor in the stabilized inverse pinch and in the breech (along the ceramic insulator) in the parallel plate accelerator. Kerr cell high speed photography shows that the initial plasma breakdown occurs at these locations. Also, magnetic and electric measurements in the stabilized inverse pinch indicate that current sheaths do form near the center conductor. Electron density measurements with an infrared interferometer show the buildup of electron density in the breech of the gun initially.

The early formation of current sheaths is usually very difficult to

investigate due to the rapid rate at which formation occurs. Kerr cell photography, magnetic and electric field measurements, and electron density measurements indicate that the current sheaths often form in times much shorter than one microsecond. Due to the large current densities employed (current densities of the order of 10^4 amp/cm^2) , a high degree of ionization is accomplished. As observed by other researchers, current sheaths are produced at the beginning of each half-cycle of the current through the plasma discharge tube. These multiple current sheaths are observed with magnetic and electric probes in the stabilized inverse pinch and with an infrared maser interferometer, electron density measurement in the parallel plate accelerator.

No evidence of wall breakaway problems is present. Kerr cell photographs show that after the initial breakdown in the parallel plate accelerator, a current sheath with a flat, planar leading surface and a planar trailing surface is formed. Self-luminous fronts leave the breech of the accelerator and do not reappear during the acceleration process in the breech of the gun. Magnetic and electrostatic probe measurements indicate that the current sheaths formed in the stabilized inverse pinch at the center breakaway from the insulated center conductor and move radially outward. There is no evidence of continued breakdown near the insulated "wall" at the center.

B. Space and Time Resolved Electron Densities in the Parallel Plate Geometry

Space and time resolved electron densities in the parallel plate accelerator are measured with an infrared maser interferometer system. Fig. V-1 shows two infrared interferometer, intensity modulated signals

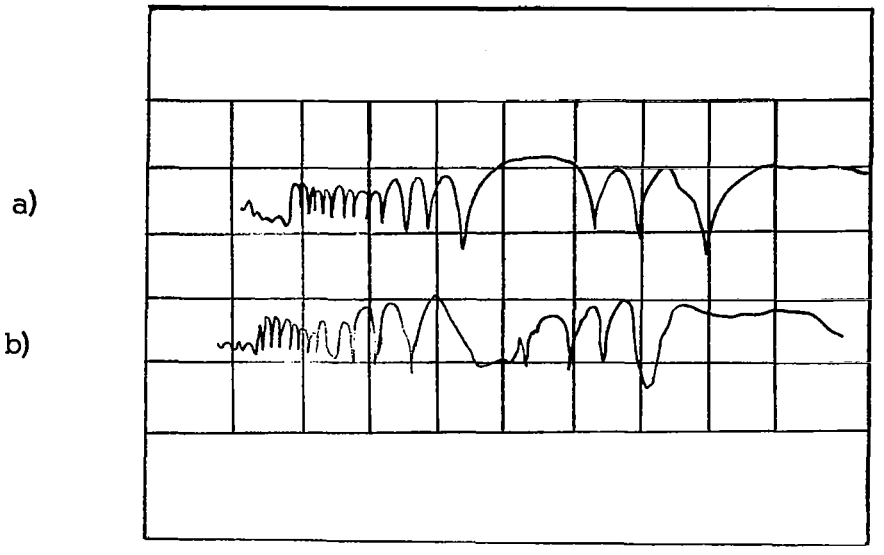

Fig. V-1. Infrared Maser Interferometry Signals. Parallel plate accelerator, driving current peak approximately 35,000 amperes. Axial location, 5 cm from breech. Time (across) 2 microseconds/division. Infrared intensity (ordinate) 200 millivolts/division.
a) Argon gas at initial pressure of 700 microns
b) Argon gas at initial pressure of 500 microns

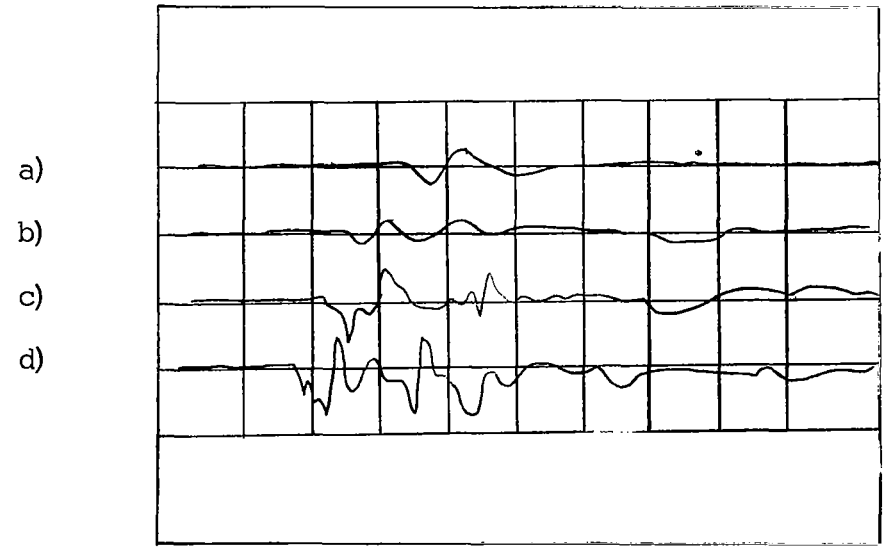

Fig. V-2. Plasma Inside Laser Cavity Signals. Parallel plate accelerator, argon gas at 1000 microns. Axial location, 5 cm from breech. Time (across) 5 microseconds/division. Infrared intensity (ordinate) 10 millivolts/division. a) Peak driving current 8,750 amperes, b) Peak driving current 17,500 amperes, c) Peak driving current 26,250 amperes, and d) Peak driving current 35,000 amperes.

for two different initial gas pressures. For these signals, the peak driving current in the parallel plate accelerator is approximately 35,000 amperes. The axial position of the probing maser beam is 5 cm from the breech (z = 5 cm) and between the two parallel plate electrodes. The coordinates of the figure are: time (across) 2 microseconds/division, and infrared intensity (ordinate) 200 millivolts/division. Signal a) is the interferometer signal for the case of argon gas at an initial pressure of 700 microns, and signal b) is for the case of 500 microns initial argon gas pressure. (Similar shape signals are obtained with deuterium gas at several hundred microns pressure in the parallel plate accelerator.) The delay in the onset of the large interference signals (approximately one microsecond more for the 700 micron initial gas pressure than for the 500 micron case) is shown in this figure.

A typical signal has the following characteristics: an initial onset of interference signal at the onset of the current sheath; a buildup of electron density indicated by a series of interference fringe signals with the appearance of rectified sine waves, a saddle where the electron density has reached its maximum, and then another series of interference fringe signals during the electron density decay. The infrared intensity signals are easiest explained[1] by considering the case in which the reflectivity of the laser mirrors is just sufficient to maintain maser action. If the output maser beam is reflected back through one of the maser mirrors, and it is in phase with the radiation in the cavity, then the maser will react as if the mirror reflectivity had increased; that is, the intensity

---

[1]Ashby, D.E.T.F. Jephcott, D.F., Malein, A., Raynor, F.A., "Performance of the He-Ne Gas Laser as an Interferometer for Measuring Plasma Density", Fifth Annual Meeting of the Division of Plasma Physics of the American Physical Society, San Diego, November, 1963.

of the beam will increase. If the return beam is out of phase with the radiation in the cavity, then the mirror reflectivity will effectively decrease and the maser intensity will decrease. The laser intensity remains highly sensitive to mirror reflectivity even when the reflectivity is above the threshold value. The nonlinear dependence of the maser intensity on mirror reflectivity is the reason for the pointed character of the fringes. Fringes more sinusoidal in shape can be obtained by reducing the reflected radiation[2]. The non-sinusoidal shape of the interference fringes makes the interferometer signals difficult to interpret for signals of less than one fringe.

Fig. V-2 shows infrared intensity modulated signals for the case of a dynamic plasma inside the maser cavity. The dynamic plasma is produced by peak driving currents of 8,750 to 35,000 amperes in argon gas at an initial pressure of 1000 microns. The location of the maser beam in the parallel plate accelerator is at the axial position 5 cm from the breech. The coordinates on the figure are: time (across) 5 microseconds/division, and infrared intensity (ordinate) 10 millivolts/division. The onset of dynamic current sheaths is readily observed on the signals. The signals are approximately zero until the arrival of the current sheath. As the driving current is increased (from signal a, to b, to c, to d), the onset occurs earlier as is expected. The interaction of the plasma with the masing action is very apparent. Notice that after the signal has decreased in intensity, sharp rising spikes often occur. The intensity often goes above the normal steady-state value during the spiking process. For low energy plasmas in the maser cavity, the interaction signals are

---

[2]Gribble, R.F., Craig, J.P., and Dougal, Arwin A., "Spatial Density Measurements in Fast Theta-Pinch Plasma by Maser Excitation of Coupled Infrared Resonators", Applied Physics Letters, 5, 60, August 1, 1964.

usually smoother, more sinusoidal than for energetic plasmas in the cavity. The details of the shape of the interaction signals require further investigation. This diagnostic method should be very helpful in studying turbulence in plasma media.

When breakdown occurs, the electron density initially builds up in the breech of the accelerator. The electron density profiles for various locations along the accelerator show the motion of the current sheath down the accelerator. Peak electron densities as high as 10^{17}/cc are obtained near the end of the discharge tube for initial deuterium gas at 500 microns.

The initial onset time as a function of axial position is readily measured with the infrared maser interferometer. Fig. V-3 and Fig. V-4 show experimental data obtained with the infrared maser interferometer system for the onset of current sheaths vs time in the parallel plate accelerator for a range of initial gas pressures and two driving currents. The peak driving current is 35,000 amperes in Fig. V-3 and 50,000 amperes in Fig. V-4. Notice that as the initial pressure is increased from 300 microns to 1,500 microns, the onset time at a given axial position is delayed as predicted by the analytical calculations presented earlier. Also, as the driving current is increased, the current sheaths move faster, as expected. In general, these onset times compare favorably with calculations based on a snowplow model.

Fig. V-5 through Fig. V-8 present time and space resolved electron densities measured in the parallel plate accelerator. The gas is deuterium at an initial pressure of 200 and 700 microns. The peak current is 50,000 amperes. The axial positions shown are at 0, 5 cm, 10 cm, and 15 cm from the breech in the accelerator. Fig. V-5 shows the initial breakdown and formation of the current sheath in the breech

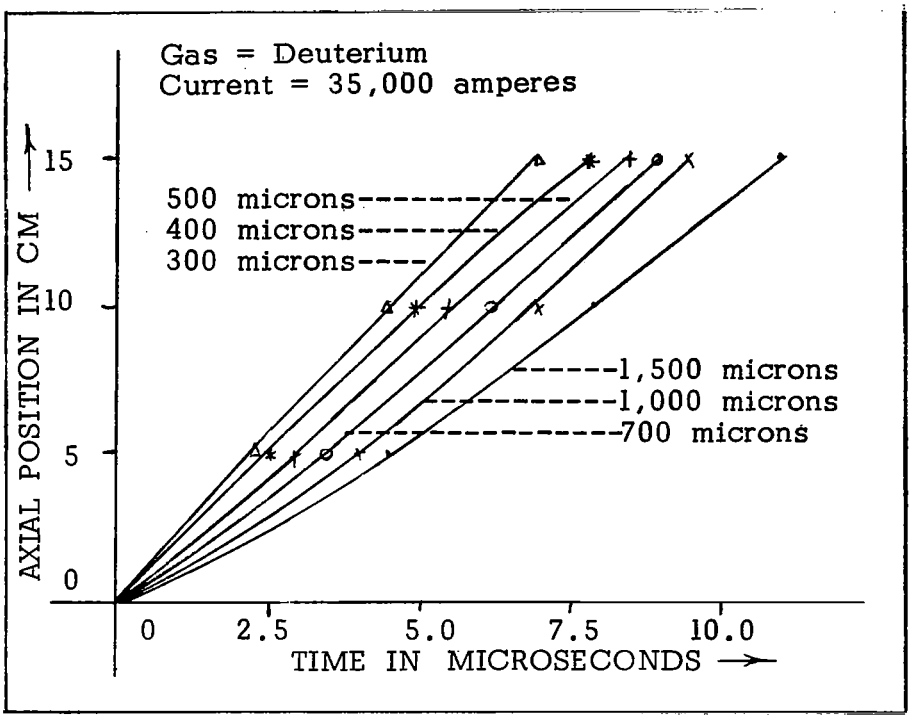

Fig. V-3. Current Sheath Position vs Time (35,000 amperes)

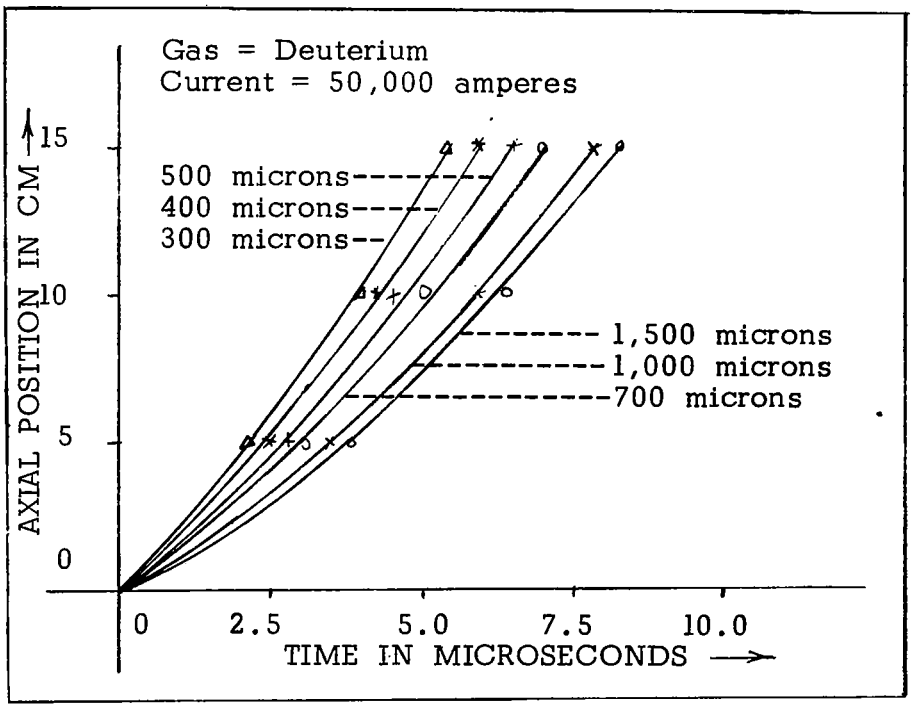

Fig. V-4. Current Sheath Position vs Time (50,000 amperes)

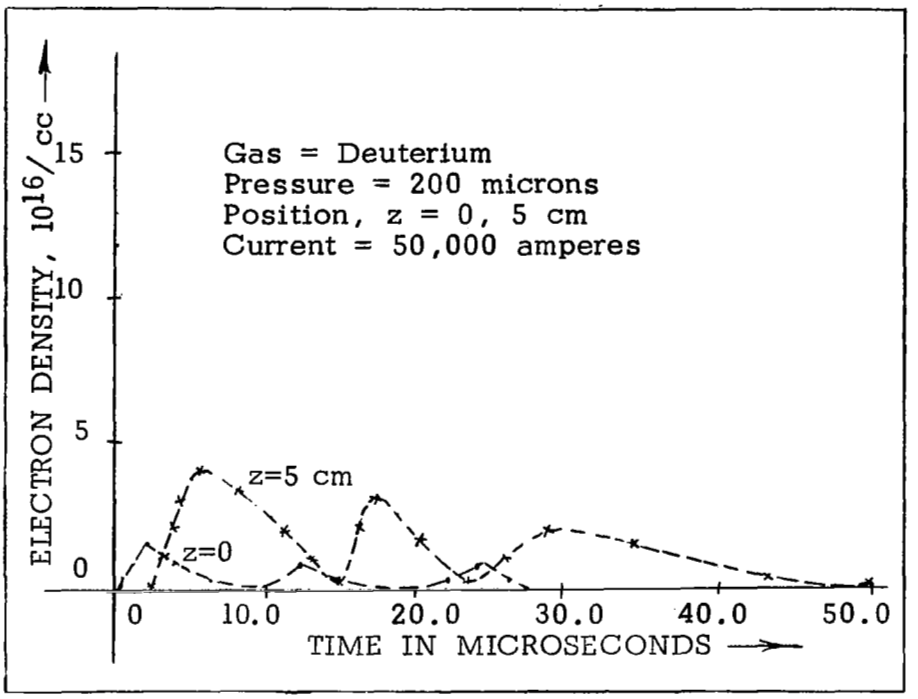

Fig. V-5. Electron Density vs Time (200 microns, z = 0, 5 cm).

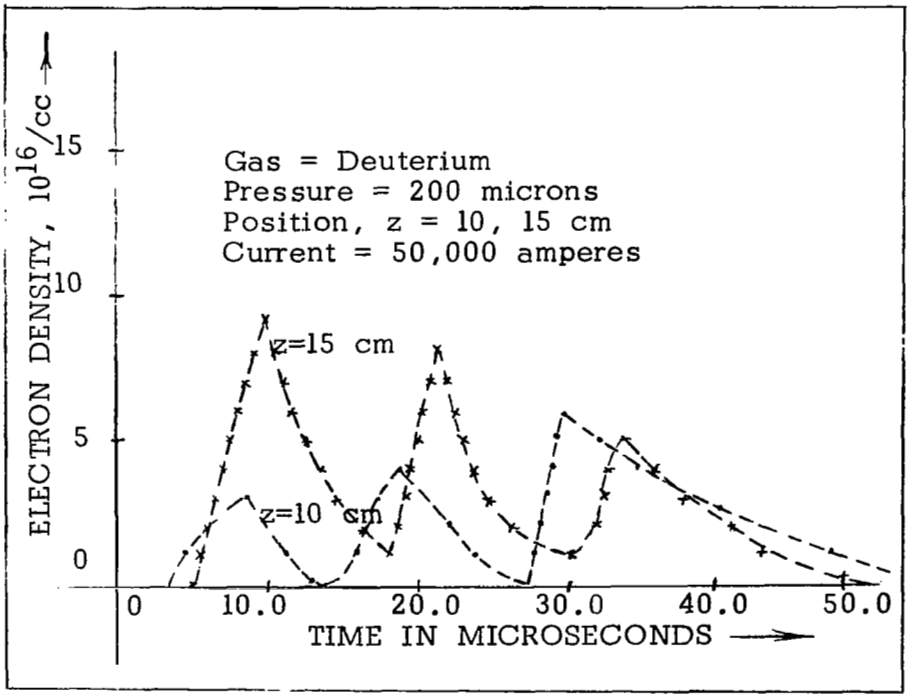

Fig. V-6. Electron Density vs Time (200 microns, z = 10 cm, 15 cm).

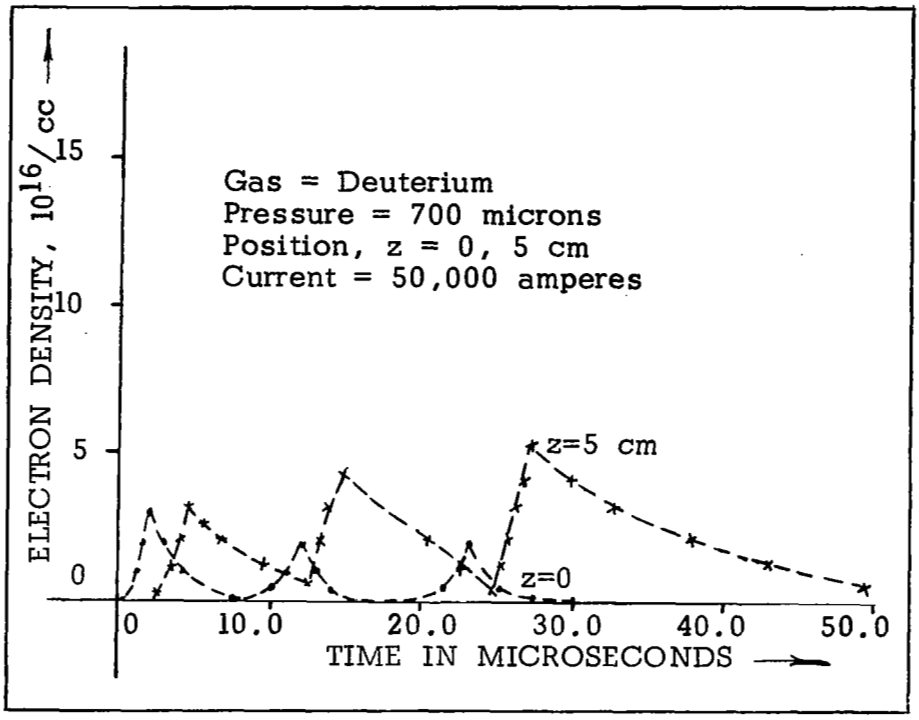

Fig. V-7. Electron Density vs Time (700 microns, z = 0, 5 cm).

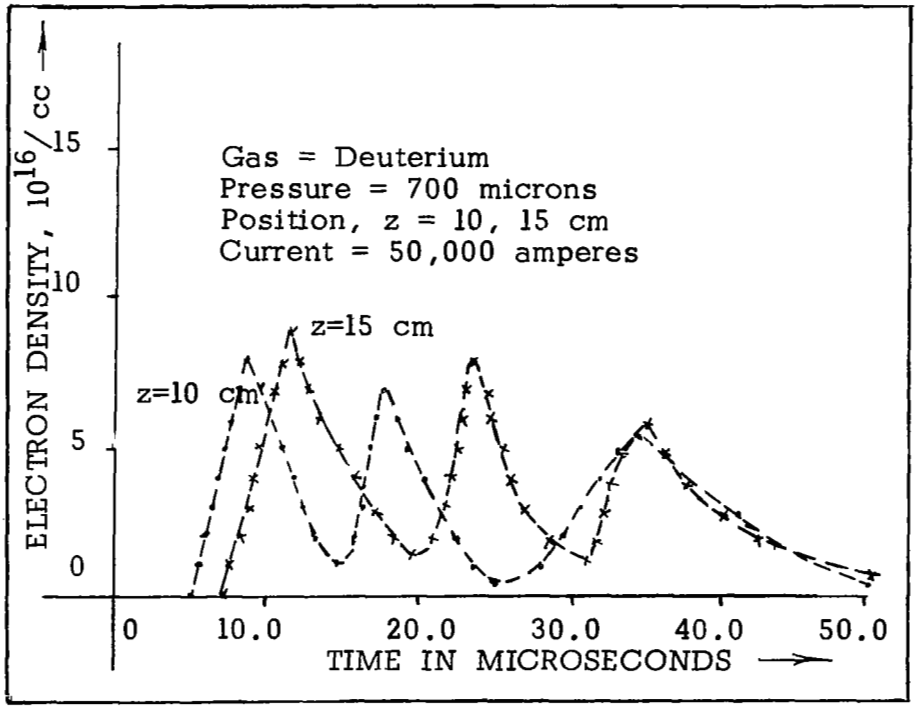

Fig. V-8. Electron Density vs Time (700 microns, z = 10 cm, 15 cm).

of the accelerator for an initial pressure of 200 microns. At a distance 5 cm down the accelerator, the electron density profile shows the onset is delayed a couple of microseconds, and then rises to a peak density of approximately 5 x 10^{16}/cc. A current sheath is formed at the beginning of each half-cycle of the driving current (i.e. at about 10 microsecond intervals). Fig. V-6 shows the delay of about 5 microseconds and then the buildup of electron density at the end of the discharge tube (15 cm from the breech). The electron densities buildup rapidly toward 10^{17}/cc, and then decay rapidly toward zero. The electron density in front of and behind the current sheaths indicate effective snowplowing by the current sheaths. The width of the current sheath as estimated from electron density profiles for deuterium of 700 microns initial pressure is the order of 2 cm thick.

C. Electric Fields Associated with Current Sheaths Formed in an Inverse Pinch

Small, double electrode, unbiased, electrostatic probes are used to measure the formation of electric fields associated with dynamic current sheaths produced in a stabilized inverse pinch geometry. The initial onset times at various radii are readily observed. Fig. V-9 through Fig. V-11 show reproductions of the actual signals recorded in the stabilized inverse pinch geometry. Note: the signals shown in these figures are after being sent through a pulse transformer which inverts and reduces the signals. The true electric field signal is thus obtained by multiplying the scales shown in the figures by (-5.0). These signals were recorded with a 5 mm spacing between the electrodes of the electrostatic probe. The large negative pulse on the actual

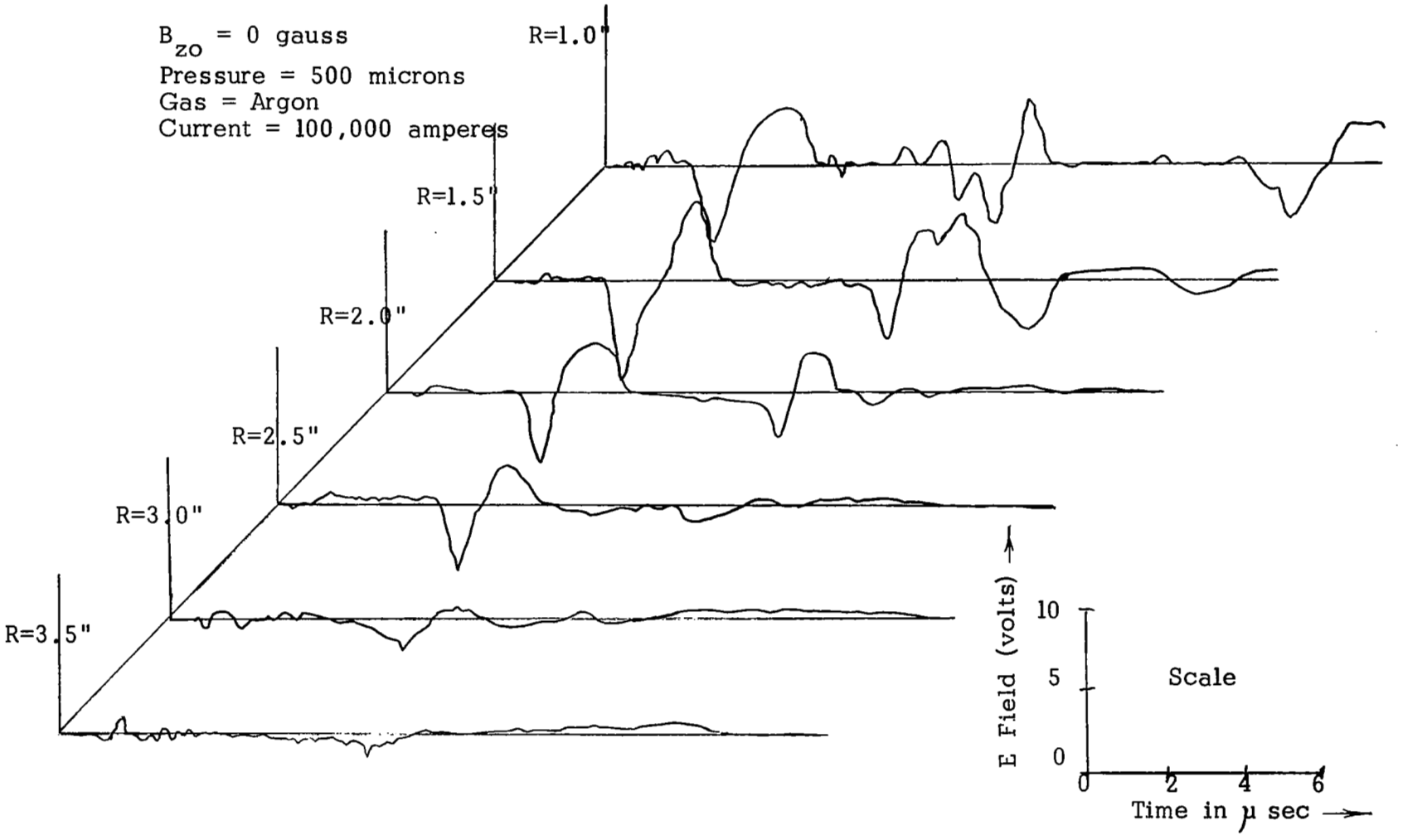

Fig. V-9. Radial Electric Field vs Time (B_{zo} = 0)

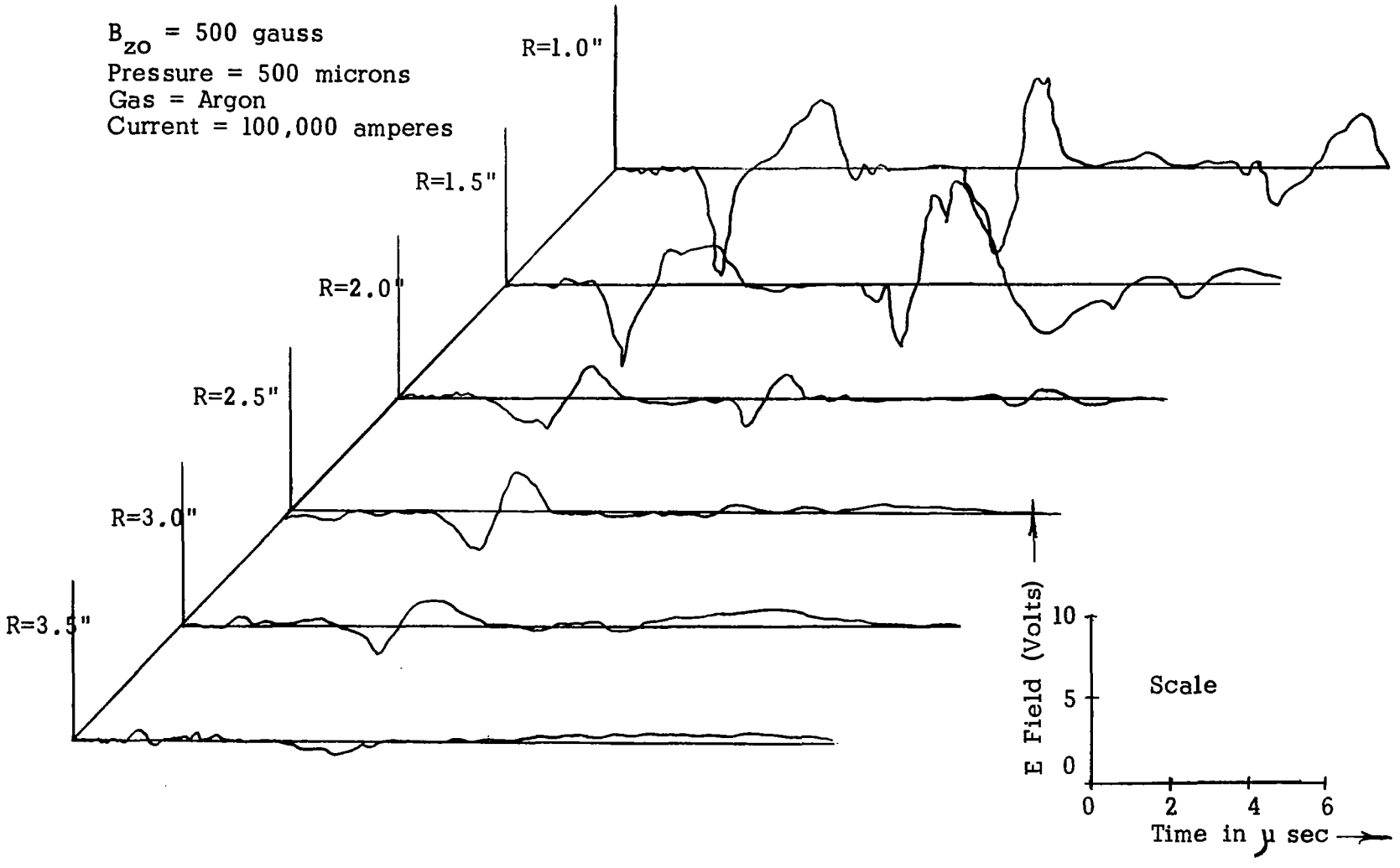

Fig. V-10. Radial Electric Field vs Time (B_{zo} = 500 gauss)

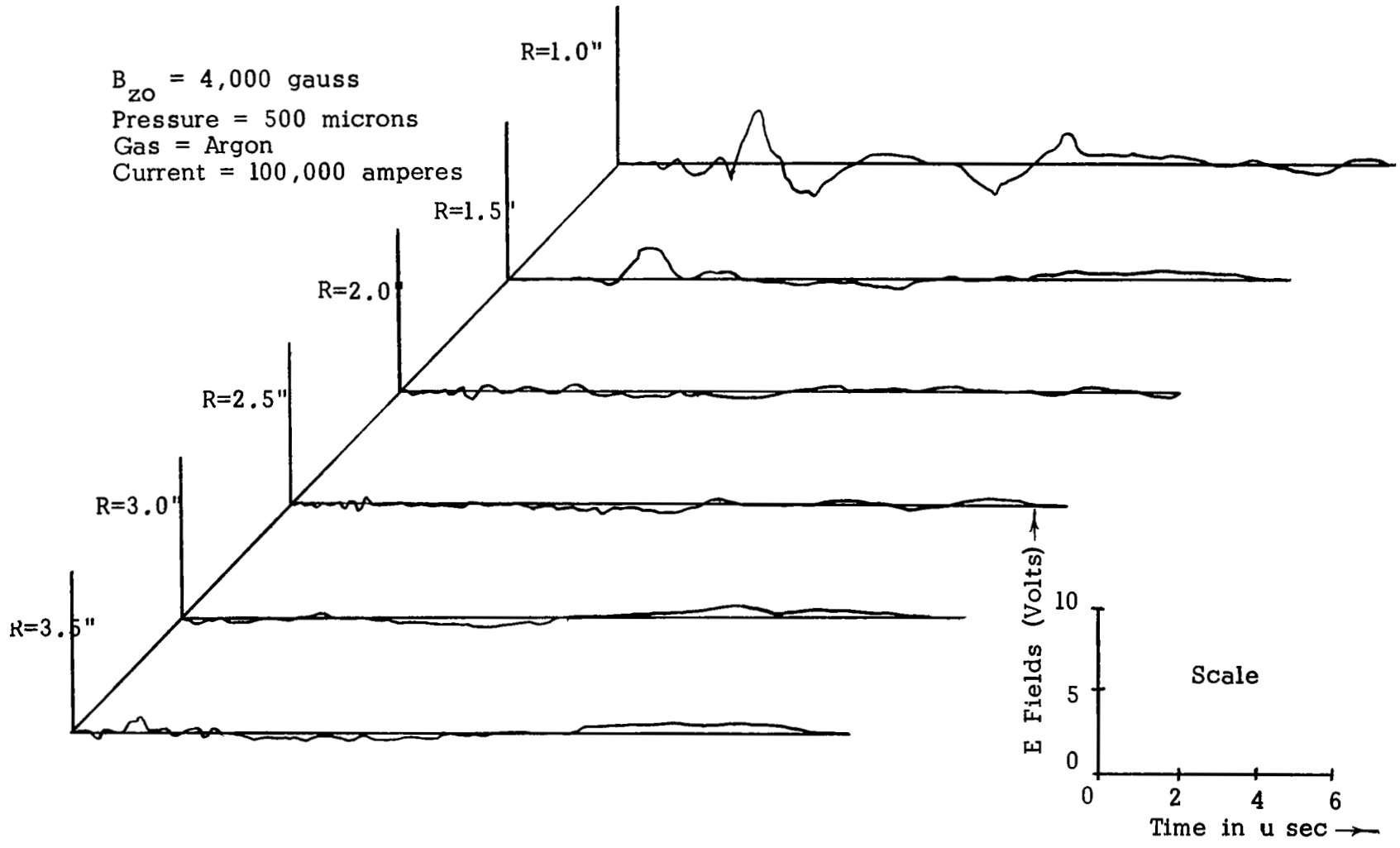

Fig. V-11. Radial Electric Field vs Time (B_{zo} = 4,000 gauss)

signals (a positive electric field when correction is made for the inverting transformer) followed by the positive peak for the case of small radii, and weak stabilizing magnetic fields indicates the onset and passage of the current sheath. Note that at approximately seven microseconds later, another current sheath due to the second half-cycle driving current is shown. With a series of electric field measurements at several radii, the formation of the current sheath as it moves radially outward can be investigated. For example, the peak value of the signals decreases as the radius increases (toward the outer boundary). Also, the current sheaths are prevented from reaching the outer wall as the stabilizing magnetic field is increased to several kilogauss.

Since the electric field in the radial direction is due primarily to charge separation caused by the accelerated electrons pulling the lagging ions (at least for the heavier gases and weak magnetic fields) [3], an estimate of the ion energy is given by the maximum electric fields measured with the electric probe as the current sheath reaches and passes the probe. The maximum electric field is the field required to accelerate ions entering the current sheath with low thermal velocities to the velocity of the moving sheath. Typical ion energies measured are 40 to 50 ev for argon gas at several hundred microns initial pressure, and with peak driving currents of 100,000 amperes. Compare this with an ion moving with the velocity of a typical current sheath of 2×10^4 m/sec, which corresponds to an ion with 42 ev energy. An estimate of the current sheath's thickness and other structural details are given by the

---

[3] Lovberg, R.H., "Acceleration of Plasma By Displacement Currents Resulting from Ionization", VIe Conference Internationale sur les Phenomenes D'Ionisation dans les Gaz, Vol. IV, 235, S.E.R.M.A., Paris, France, 1963.

width and shape of the charge separation, electric field measurement. A typical thickness for argon initially at 500 microns pressure, and with 100,000 ampere peak driving current is 3 cm.

The electric fields measured in the axial direction, along the current flow path, also give the time of onset of the current sheath. Some measure of the resistivity of the plasma in the current sheath can be obtained from these axial electric field measurements in the stabilized inverse pinch if one estimates the current density. For a current density of 5×10^3 amp/cm^2 , and axial electric field measurements at a radius of 3 cm for an argon gas at 500 microns pressure, the resistivity is estimated to be 2×10^{-4} ohm-meters.

The electric fields measured in the azimuthal direction are valuable for investigating the stability of current sheaths. Repeatable signals usually indicate macroscopic stability. For the conditions investigated in the stabilized inverse pinch, the azimuthal electric field measurements indicate macroscopic stability.

For certain initial conditions, magnetosonic oscillations are indicated on the radial electric probe signals. (Since these oscillations are small amplitude, the 2 mm electrode separation, electrostatic probe is employed to search for and to observe the magnetosonic oscillations.) Current sheath oscillations are also observed on the axial and azimuthal electric field signals with a 2 mm spacing electrode probe.

D. Self-Luminous Fronts Formed and Accelerated Between Planar Electrodes

High speed Kerr cell photography is employed to investigate the self-luminous fronts produced and accelerated in the parallel plate

accelerator, the stabilized inverse pinch, and the extremely high temperature theta pinch. The plasma light emitted indicates that the initial breakdown and formation of current sheaths is along the path of least resistance and inductance (in the breech of the parallel plate accelerator, near the center conductor in the inverse pinch, and near the tube wall in the theta pinch). The self-luminous fronts at various times after the application of the driving current for a wide range of initial gas pressures were recorded.

Self-luminous fronts produced near the insulating walls in the breech of the parallel plate accelerator are propelled down the gun with velocities of the order of 10^4 m/sec. These fronts often retain their planar leading surface during the acceleration process, and sometimes after leaving the 8 cm long electrodes are fairly flat when deuterium gas is used. The current sheath leaves the wall in the breech and the back surface often remains planar during the acceleration time. A luminous cathode sheath is also observed in deuterium. With argon gas, the leading edge of the self-luminous front is curved inward between the electrodes. Usually there is a leading "toe" formed along the anode. (A similar "toe" was observed in nitrogen by R.H. Lovberg [4]) An estimate of the thickness of the current sheath is obtained from the width of the luminous fronts; typically one or two centimeters for deuterium, and several centimeters for argon.

Fig. V-12 shows a series of Kerr cell photographs taken of the parallel plate accelerator with deuterium gas at an initial pressure of

---

[4] Lovberg, R.H., "Measurement of Plasma Density in a Rail Accelerator by Means of Schlieren Photography", IRE International Symposium on Plasma Phenomena and Measurement, San Diego, October 29-November 1, 1963.

t = 1.0 microseconds

t = 6.0 microseconds

t = 2.0 microseconds

t = 8.0 microseconds

t = 3.0 microseconds

t = 10.0 microseconds

t = 4.0 microseconds

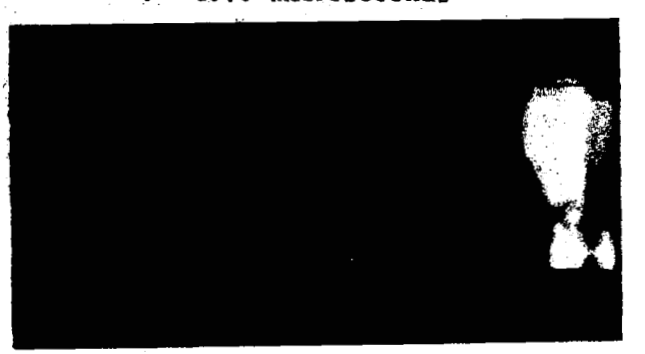

t = 12.0 microseconds

Fig. V-12. Kerr Cell Photographs (Parallel Plate Accelerator, 1000 microns, Deuterium gas, Current = 35,000 amperes).

1000 microns and a driving current of 35,000 amperes. The breech of the accelerator is on the left of the photograph (where the breakdown occurs initially). The parallel electrodes are horizontal and extend approximately half-way across the photograph. The top electrode is the cathode, and the bottom electrode is the anode during the first half-cycle. Fig. V-13 shows a series of Kerr cell photographs taken of the parallel plate accelerator with the same physical arrangement as above, but with argon gas at an initial pressure of 500 microns.

Some bending and stretching of the magnetic field lines is indicated for weak magnetic fields (several hundred gauss) in the stabilized inverse pinch. Fig. V-14 shows three Kerr cell photographs of the self-luminous fronts produced in argon at an initial pressure of 1000 microns in the stabilized inverse pinch for a weak magnetic field of 100 gauss. The current return, hard-core conductor, is at the lower portion of each picture. The stainless steel electrodes are vertical, on each end of the three photographs. The Kerr cell system was focused to look slightly into the electrode on the left side of the picture. Notice the curvature of the central luminous front in the pictures.

For large magnetic fields (several kilogauss) applied to the inverse pinch, the current sheath is confined to a column of only serveral centimeters diameter. Fig. V-15 shows three Kerr cell photographs of the self-luminous fronts produced in argon at an initial pressure of 1000 microns in the stabilized inverse pinch with a strong magnetic field of 2,000 gauss. The physical arrangement of the system is the same as above. Notice the confinement of the plasma.

Due to the rapid rate at which the magnetosonic oscillations occur and the fact that the Kerr cell system used only recorded one

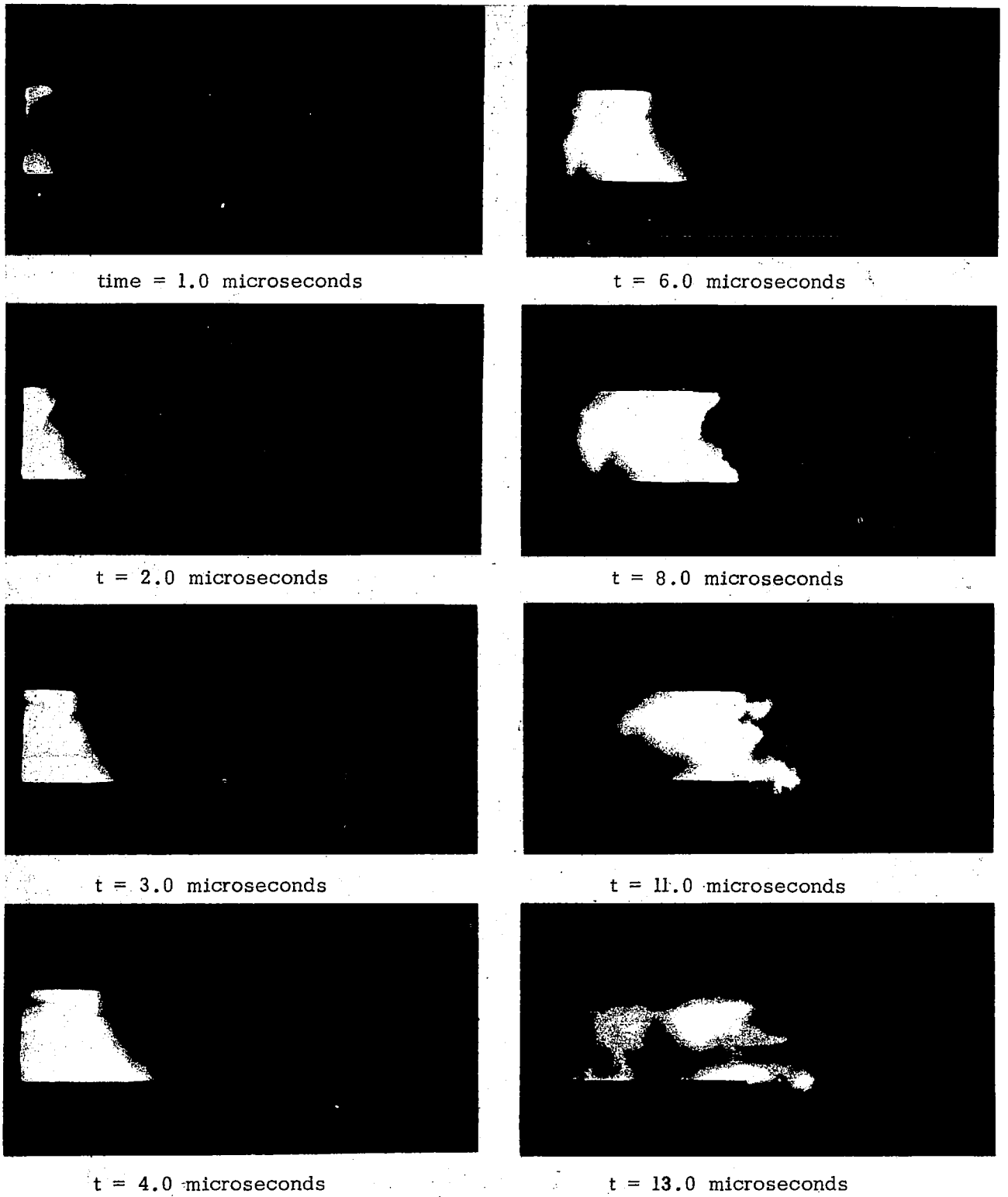

time = 1.0 microseconds

t = 6.0 microseconds

t = 2.0 microseconds

t = 8.0 microseconds

t = 3.0 microseconds

t = 11.0 microseconds

t = 4.0 microseconds

t = 13.0 microseconds

Fig. V-13. Kerr Cell Photographs (Parallel Plate Accelerator, 500 microns, Argon gas, Current = 35,000 amperes).

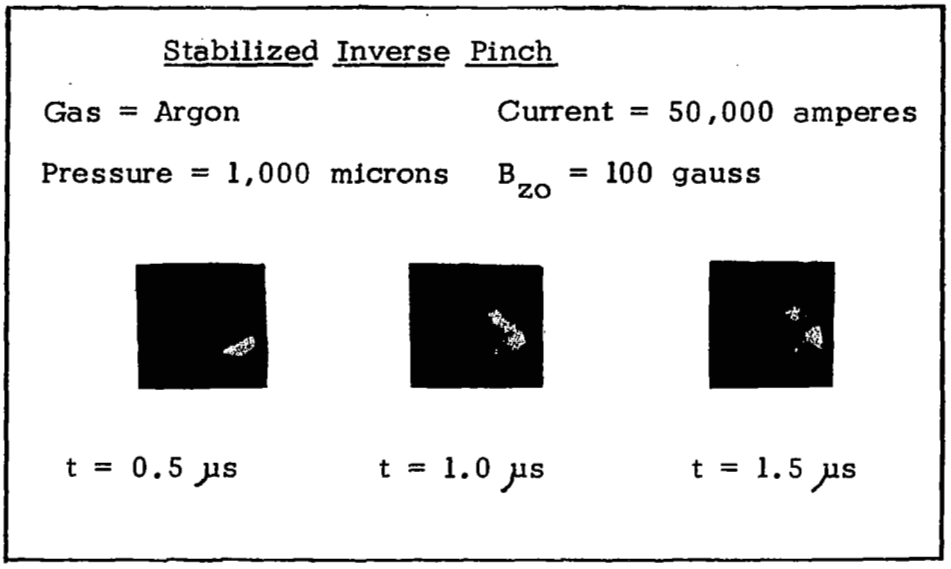

Fig. V-14. Kerr Cell Photographs (Stabilized Inverse Pinch, 100 gauss)

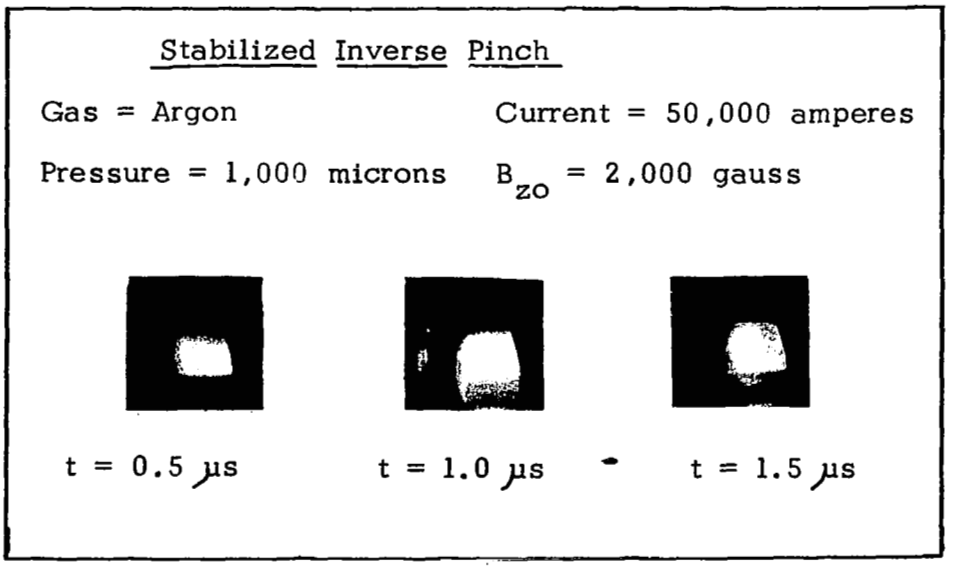

Fig. V-15. Kerr Cell Photographs (Stabilized Inverse Pinch, 2000 gauss)

frame at a preset time per shot of the experiment, no concrete statement of observing magnetosonic oscillations in the stabilized inverse pinch with the Kerr cell system can be made. Although there is strong indication of these oscillations on many Kerr cell photographs.

Self-luminous fronts produced in an extremely high temperature theta pinch were photographed. The onset times of the luminous fronts are compared with the computed position of maximum electron density computed with the Hain-Roberts code. Fig. V-16 shows the theoretical curve and experimental points for 2 kilogauss reverse bias, 100 micron initial deuterium pressure, and 15 kv on the main compression capacitor bank. The experimental data shows good agreement with the initial radial pinch and then indicates radial oscillations. Fig. V-17 shows the theoretical curve and experimental data for 4 kilogauss reverse bias and other similar conditions.

E. Pressure Fronts Associated with Current Sheaths in an Inverse Pinch Geometry

Piezoelectric pressure sensitive probes are employed to determine the onset time and to investigate the structure of pressure fronts associated with the dynamic current sheaths produced in the stabilized inverse pinch [5]. The dynamic response of the probe is checked by exploding a wire in air at atmospheric pressure with approximately 25,000 amperes of current from an ignitron switched capacitor bank. The pressure front onset times for various radii for a range of initial pressures

---

[5] Vlases, G.C., "Experiments in a Cylindrical Magnetic Shock Tube", Journal of Fluid Mechanics, 16, Part 1, 82, 1963.

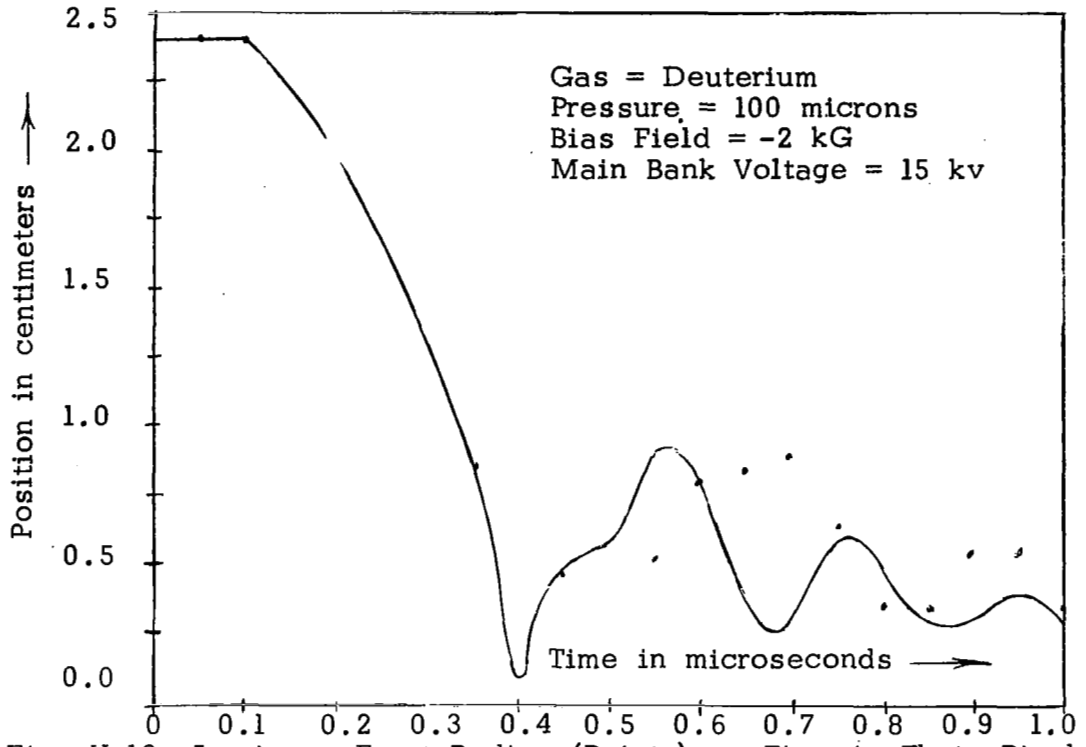

Fig. V-16. Luminous Front Radius (Points) vs Time in Theta Pinch (2 kilogauss Reverse Bias). Calculated Position of Peak Density (Curve).

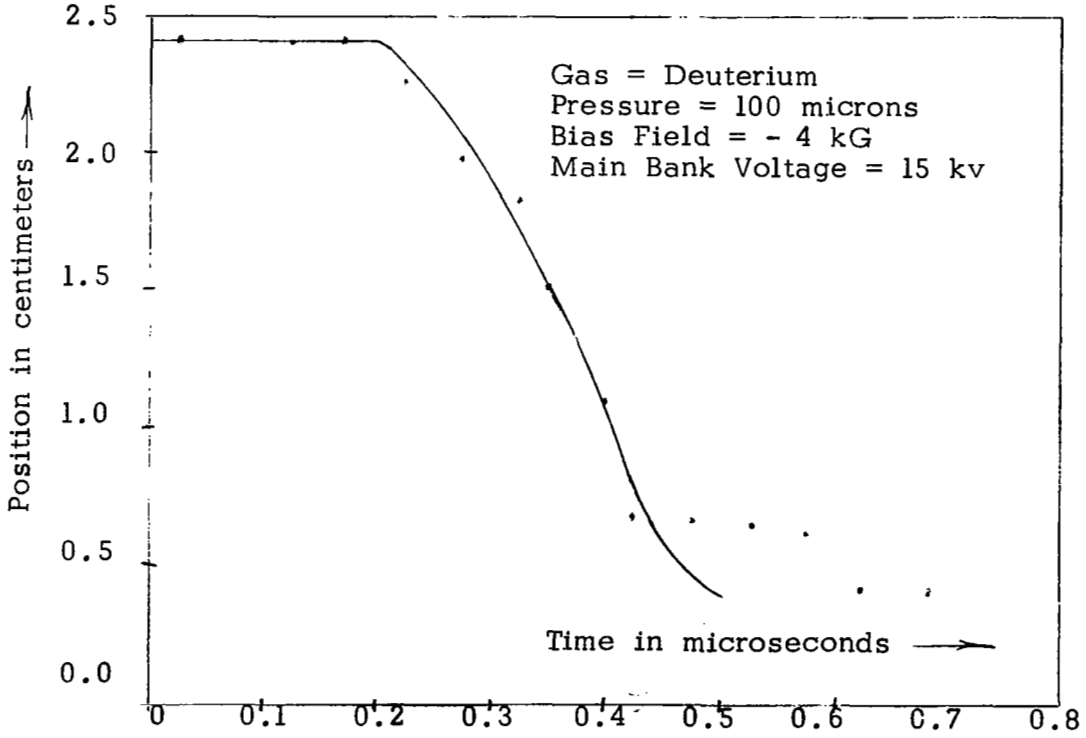

Fig. V-17. Luminous Front Radius (Points) vs Time in Theta Pinch (4 kilogauss Reverse Bias). Calculated Position of Peak Density (Curve).

of hydrogen, and argon gas were obtained. Fig. V-18 shows the pressure front onset times for various radii for an argon gas at initially 500 microns pressure, a driving current of 104,000 amperes, and several different values of stabilizing magnetic fields. The effect of the external stabilizing magnetic field on slowing down, stopping, and confining the expanding current sheath is observed with the piezoelectric probe. These probe signals also indicate that possibly two pressure fronts impact onto the pressure sensitive probe. But due to the natural ringing of the probe, no concrete statement can be made at this time for the present probes employed. For certain conditions of pressure, driving current, and stabilizing magnetic fields, the dynamic current sheaths may consist of a shock wave (a pressure front) followed by the magnetic piston (another pressure front). A further reason for believing that two pressure fronts are being observed is that the separation between these two pressure signals changes slightly with various experimental conditions.

The subsequent oscillations of the signals are most likely natural oscillations of the piezoelectric crystal. (Reflections of the pressure wave in the inertia rod require much longer times.) The magnetosonic oscillations of the current sheath are therefore difficult to observe with the piezoelectric probes with natural frequencies of the same order of magnitude.

Fig. V-19 shows typical piezoelectric probe signals for argon gas at an initial pressure of 500 microns, zero stabilizing magnetic field, and 100,000 amperes driving current peak. Notice the onset of pressure fronts, a possible second pressure front, passage of the pressure front, and subsequent small oscillations. Also, note that as the probe is moved radially inward (smaller radius), the onset times are earlier as

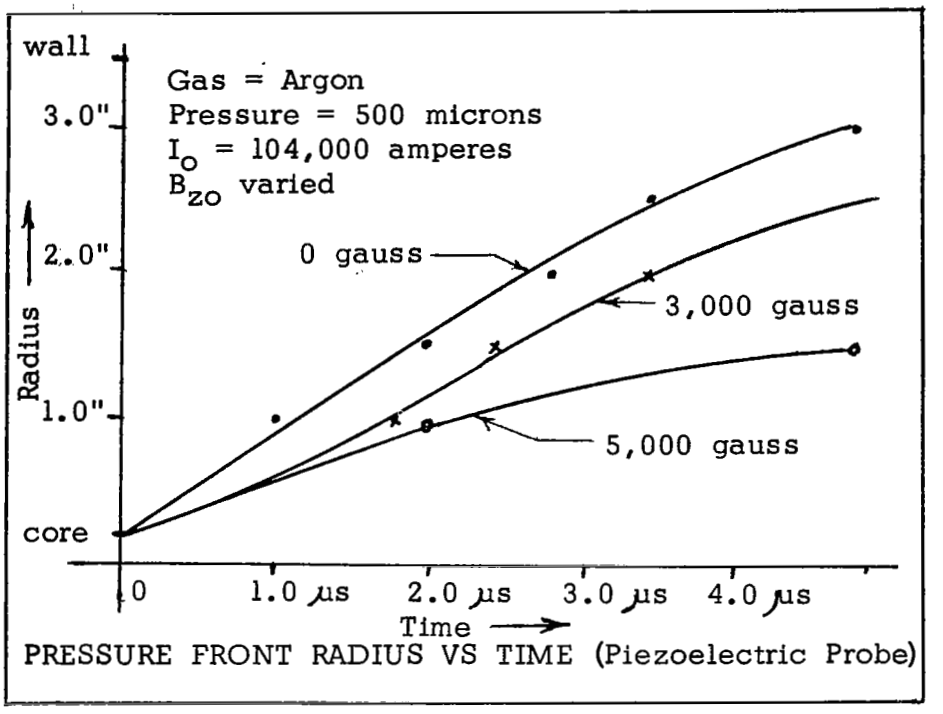

Fig. V-18. Pressure Front Position vs Time as Measured with a Piezoelectric Probe in a Stabilized Inverse Pinch

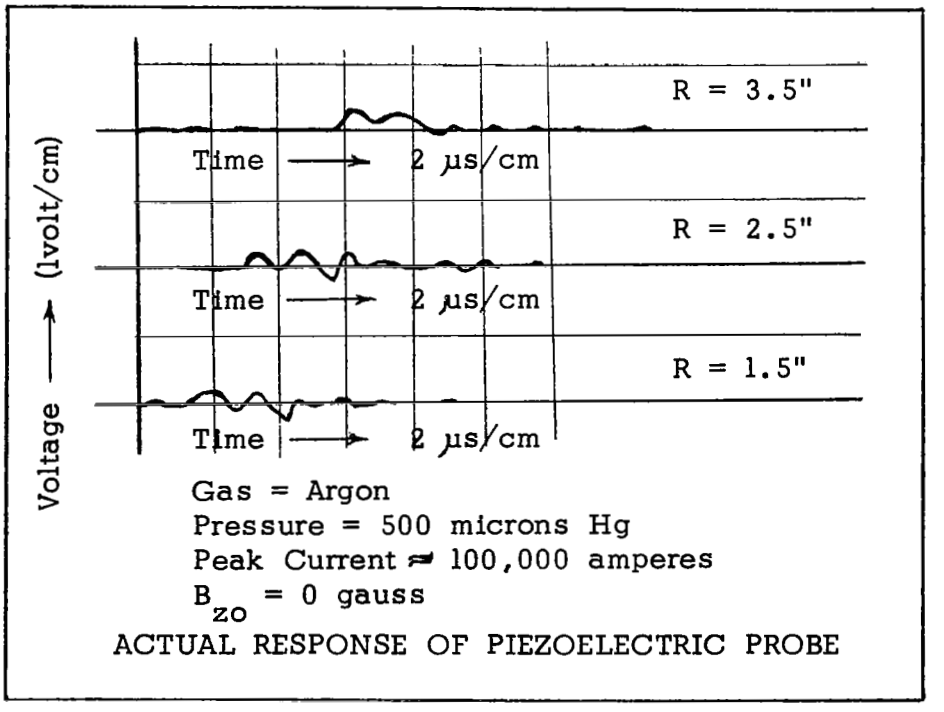

Fig. V-19. Actual Response of Piezoelectric Probe to Pressure Fronts Produced in a Stabilized Inverse Pinch

expected. Signals indicating pressure fronts of 4×10^4 nt/m^2 are observed under certain conditions. (A signal of 1 volt represents a pressure of approximately 5×10^4 nt/m^2.)

F. Magnetic Fields in an Inverse Pinch Geometry

Small magnetic probe coils are employed to measure B_θ, B_z, and B_r fields in the stabilized inverse pinch. The B_θ magnetic field is shielded until after the current sheath passes the probe. Fig. V-20 shows a typical B_θ magnetic field signal for hydrogen gas at initially 200 microns, with the probe located at a radius of 2.5 inches, with a peak driving current of 104,000 amperes, and a stabilizing magnetic field of 1,000 gauss. The initial onset time is approximately 1.8 microseconds.

The B_z magnetic field is swept up and compressed by the radially expanding current sheath. Fig. V-20 shows a typical B_z magnetic field signal for hydrogen gas at 200 microns initial pressure, the probe located at a radius of 2.5 inches, a peak driving current of 104,000 amperes, and a stabilizing magnetic field of 1,000 gauss. Notice the initial buildup of the B_z signal (starting at about 1.4 microseconds) indicating compression of the magnetic flux by the expanding current sheath. As the sheath passes, the B_z signal returns to zero and then goes negative as the current sheath sweeps out the magnetic flux. For strong stabilizing magnetic fields of several kilogauss, the current sheath is slowed down, stopped, and confined.

From the B_θ and B_z signals, the onset of the current sheath was determined for a wide range of gas pressures. Fig. V-21 shows the experimentally measured current sheath position vs time for hydrogen gas

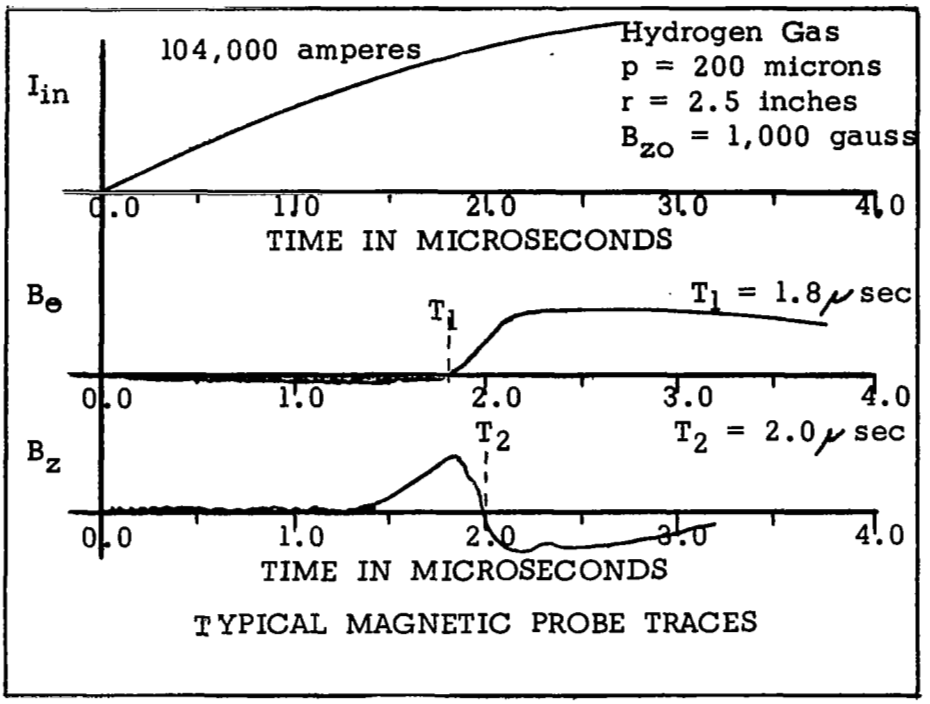

Fig. V-20. Experimental Magnetic Probe Traces

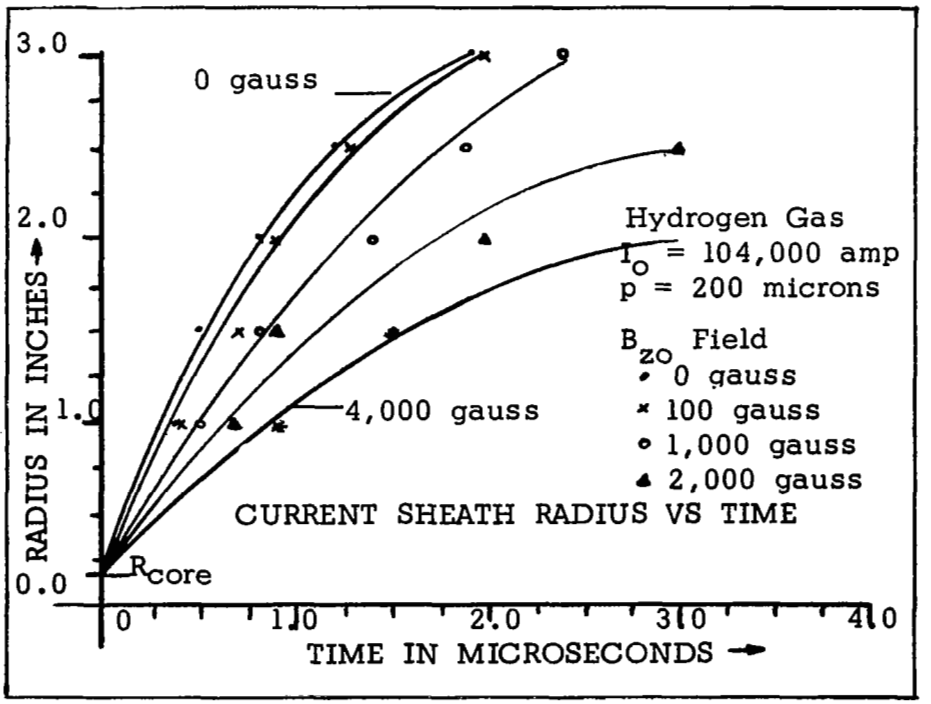

Fig. V-21. Experimentally Measured Current Sheath Radius vs Time

initially at 200 microns, a peak driving current of 104,000 amperes, and a range of stabilizing magnetic fields.

Structural details of the current sheath are also given by the magnetic probe signals. The thickness of the current sheath is the order of one centimeter for hydrogen gas at initially several hundred microns, peak driving currents of 100,000 amperes, and weak magnetic fields. For very strong stabilizing magnetic fields, and a location near the stopping radius, the B_θ field signals show a diffusion of the magnetic field through the current sheath for a range of pressures of hydrogen, and argon.

A larger (1 cm diameter) magnetic probe placed near an electrode to measure $\dot{B}_z$ indicates that the external stabilizing magnetic field lines are tied to the metal electrodes of the inverse pinch tube during the formation and acceleration process. (This was one of the assumptions made in the analytical model described earlier.)

The small magnetic probes indicate magnetosonic oscillations occur for certain ranges of gas pressure, driving currents, and stabilizing magnetic fields. These oscillations are easiest observed on the B_z probe signals in the compression, expansion, and then re-compression and re-expansion of magnetic flux. The frequency of these oscillations is of the order of 500 kc to 1 Mc. Fig. V-22 shows experimental data relating the measured frequency of magnetosonic oscillations in the stabilized inverse pinch vs the initial gas pressure (or density).

The hydrodynamic instabilities that might be present for the current sheath are investigated by measuring the radial magnetic field, B_r. The B_r signal should be small and repeatable for a stable current sheath. For the conditions investigated in the stabilized inverse pinch, most of the B_r probe signals indicate hydrodynamic stability for the current sheaths.

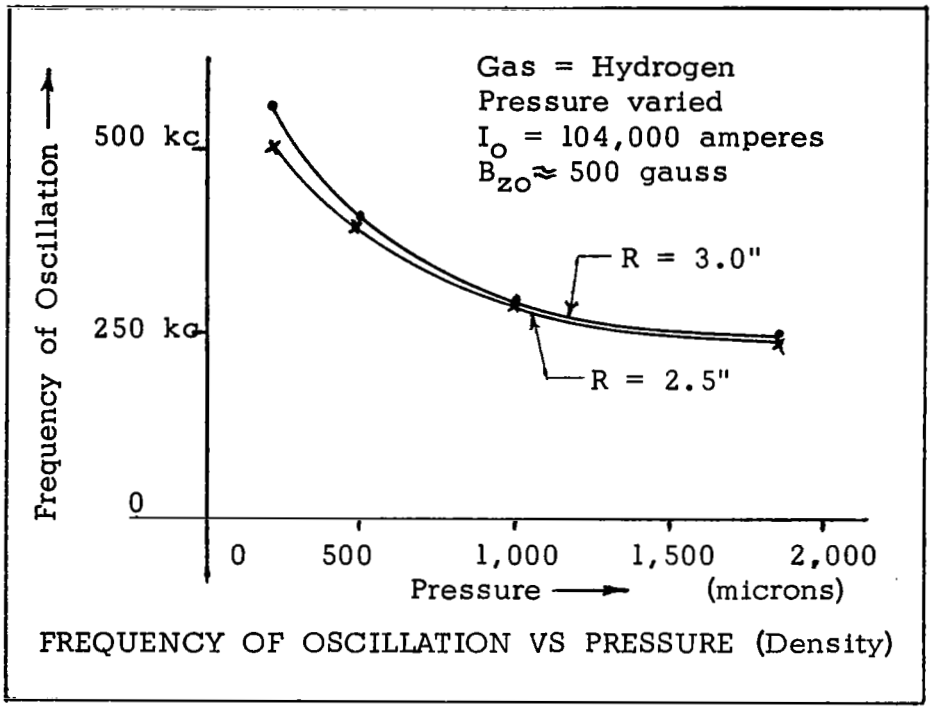

Fig. V-22. Magnetosonic Oscillation in a Stabilized Inverse Pinch. Frequency of Oscillation is Plotted vs Pressure (Density)

G. Macroscopic Behavior of Current Sheaths Formed Between Planar Electrodes

The voltage at the input terminals to the discharge tube measured with a high voltage oscilloscope probe, and the current forming and accelerating the current sheaths measured with an integrated magnetic probe coil are very useful in observing macroscopic effects. The time of gas breakdown is readily determined from these signals. Often, these signals are used as time reference markers for other events. Since the inductance of the system is reflected in the voltage-current measurements, macroscopic changes in the discharge tubes such as an expanding current sheath in the stabilized inverse pinch and an axial moving current sheath in the parallel plate accelerator are observable. Indications of magnetosonic oscillations in the stabilized inverse pinch are present on the voltage-current signals. The formation of multiple current sheaths, one at the beginning of each half-cycle of the current, is also detected. If present, gross macroscopic instabilities should be detectable on the voltage-current signals. No evidence of gross instabilities is measured for the conditions investigated in the stabilized inverse pinch.

CHAPTER VI

CONCLUSIONS

In the light of the analytical investigations and experimental results presented in the first five chapters, the following major topics will be considered in this chapter: 1) gas breakdown, current sheath formation, and structure, 2) current sheath acceleration, propulsion, and dynamics, and 3) magnetosonic oscillations and macroscopic stability.

A. Breakdown, Formation, and Structure

The gas breakdown path is the path of minimum impedance. In the stabilized inverse pinch, this path is along the insulation surrounding the center current return conductor. In the parallel plate accelerator, gas breakdown occurs in the breech along the ceramic insulation. The relative time of breakdown for various conditions of pressure, voltage, and magnetic fields is obtained from voltage-current measurements. Kerr cell photographs indicate that the initial breakdown and current sheath formation is near the paths of minimum impedance. Infrared maser interferometer data shows that the initial electron density buildup is in the breech of the parallel plate accelerator. Electric, magnetic, and piezoelectric pressure probe measurements show that gas breakdown and initial current sheath formation occurs near the central current return conductor in the stabilized inverse pinch. The time required for formation of the current sheath is very small compared to one microsecond

in most cases as indicated by infrared maser interferometer, Kerr cell, electric, and magnetic measurements.

Details of the structure of the dynamic current sheath formed and accelerated between planar electrodes are also obtained with the previously mentioned diagnostic techniques. Kerr cell photographs show a planar leading luminous front and a planar trailing edge for a wide range of hydrogen gas pressures in the parallel plate accelerator. With argon gas, the leading front forms a projecting "toe" on the anode electrode. The current sheath's thickness appears larger in argon than in hydrogen. Often, indications of turbulence are present as the argon current sheaths leave the accelerator electrodes. Kerr cell photographs taken of the self-luminous fronts in the stabilized inverse pinch show some curvature of the leading front for weak stabilizing magnetic fields. (For strong stabilizing magnetic fields, little motion occurs and the current sheath is confined.)

Electrostatic probe measurements in the stabilized inverse pinch indicate that electron current dominates for argon plasmas. Ions enter the moving current sheath and are accelerated by radial electric fields due to radial charge separation. (The energy of the ions is estimated by the maximum radial electric fields established.) A thickness for the current sheath can also be given from these signals. The electric fields along the driving current (axial fields in the stabilized inverse pinch) also give an estimate of the thickness of the sheath.

The shape of the magnetic probe signals indicate the sharpness of the front of the current sheath, the thickness, and the shape of the trailing edge. As the initial gas pressure is increased to 1 mm Hg, the current sheath front is less sharp and the magnetic field diffuses through

the current sheath.

Piezoelectric pressure sensitive probes indicate that possibly two pressure fronts are associated with the current sheath in the stabilized inverse pinch. Again some idea of the sharpness and thickness of the pressure fronts is given by the shape of the piezoelectric probe signals.

B. Electron Densities in a Parallel Plate Accelerator

The measurement of the high electron densities produced in a parallel plate accelerator has heretofore been impossible by conventional microwave and other methods. Thus, this separate section is being devoted to discuss the infrared maser interferometer electron density measurements. The initial breakdown and buildup of electron density is easily obtained. The onset time of current sheaths is readily determined with the infrared maser interferometry method. Measured electron densities indicate a high degree of ionization in the current sheath area for current densities of the order of 10^4 amp/cm^2 and initial gas pressures of several hundred microns. The results indicate effective sweeping (good snowplowing) of the electrons as the current sheath moves down the parallel plate accelerator. Peak electron densities of 10^{17}/cc are obtained in some cases. The rapid rise of the electron density indicates fairly sharp current sheaths. The electron density decay is slower, as might be expected, except near material boundaries and regions where the current sheath passes very rapidly.

Infrared intensity modulated signals are obtained with a dynamic plasma inside the maser cavity. The interaction of the plasma with the masing action is very apparent. Onset of current sheaths is readily

observed. Intensity spikes occur in which the intensity of the spikes is often larger than the steady-state intensity of the maser. For low energy plasmas in the maser cavity, the interaction signals are usually smooth, sinusoidal. The details of the shapes of the interaction signals require further investigation. This diagnostic method should be very helpful in studying plasma turbulence.

C. Acceleration, Propulsion, and Dynamics

The self-luminous fronts associated with the current sheaths observed with a Kerr cell system show the acceleration of current sheaths in the stabilized inverse pinch and the parallel plate accelerator. Electric, magnetic, piezoelectric pressure, and voltage-current measurements define the expanding current sheath in the stabilized inverse pinch. Infrared maser interferometer results show the acceleration of current sheaths formed in the parallel plate accelerator.

Kerr cell photographs and infrared maser interferometer results show that the current sheath separates from the electrodes and travels to the end of the discharge tube for certain initial pressures, and driving currents. With reference to possible pulsed plasma propulsion systems, no critical problems related to current sheath separation from the electrodes for the conditions investigated in the parallel plate accelerator appear. The electron density measurements and velocity measurements indicate effective snowplowing in the parallel plate accelerator. Therefore, high mass efficiency for propulsion appears possible in the parallel plate accelerator geometry.

Most experimental results of the dynamics of the current sheath

indicate good agreement with predicted snowplow results. Some data shows faster movement of the current sheath in the stabilized inverse pinch than predicted. This may be due to incomplete snowplowing. The velocity in the parallel plate accelerator is sometimes slow compared to the calculated velocity. This may be due to electrode drag effects, decoupling of the driving forces, and/or increasing mass pickup.

D. Magnetosonic Oscillations and Macroscopic Stability

Magnetosonic oscillations predicted by the analytical analysis based on a snowplow model for the stabilized inverse pinch are indicated in voltage-current measurements. Magnetic probe signals show the onset of dynamic current sheaths and subsequent oscillations for weak stabilizing magnetic fields and certain initial gas pressures and driving currents. Electrostatic probe data shows oscillations of the current sheath. Piezoelectric pressure sensitive probes and Kerr cell photographs indicate possible magnetosonic oscillations, but due to limitations of the measuring technique and equipment, no concrete statement of observation of magnetosonic oscillations by the piezoelectric method is made at this time in the stabilized inverse pinch. Radial hydromagnetic oscillations are indicated in the extremely high temperature theta pinch by Kerr cell photographs.

The inverse pinch geometry is hydrodynamically stable. Voltage-current measurements indicate that the stabilized inverse pinch is macroscopically stable for the conditions investigated. Most magnetic field measurements of the radial component, B_r, also indicate macroscopic stability. Photographs obtained with the Kerr cell again indicate macroscopic stability in the stabilized inverse pinch, and also in the

parallel plate accelerator under certain conditions. Kerr cell photographs of the extremely high temperature theta pinch show periods of hydrodynamic instability.

APPENDIX A

INITIAL CONDITIONS FOR STABILIZED INVERSE PINCH

The simultaneous equations employed to compute the initial conditions for the stabilized inverse pinch are written in this appendix. Also, the listing of the FORTRAN computer code and a portion of a typical computer printout are presented.

The five finite difference equations employed to compute the degree of ionization, the ion energy (temperature), electron energy (temperature), resistivity, and current density are:

degree of ionization

$$\Delta f = \Delta t\,(c_4 f)(1-f)\,\theta_e^{1/2}\left\{\left[0.8 + \tfrac{4}{3}\theta_e - 0.8\,\theta_e^2\right]e^{-1/\theta_e} + \left[-0.16 + 0.987\,\theta_e + 0.8\,\theta_e^2\right]e^{-4/\theta_e} + \left[0.8 + 0.08\,\theta_e\right]e^{-20/\theta_e}\right\}, \tag{A-1}$$

ion energy (temperature)

$$\Delta\theta_i = \Delta t\,(c_5 f)(\theta_e - \theta_i)/\theta_e^{3/2}, \tag{A-2}$$

electron energy (temperature)

$$\frac{\Delta\theta_e}{\Delta t} = -\left(\tfrac{2}{3}\alpha + \theta_e + \theta_i\right)\frac{1}{f}\frac{\Delta f}{\Delta t} + \left(\frac{2}{3}\frac{\eta_0}{n_0 \epsilon_0 f}\right)\eta j^2 - \frac{\Delta\theta_i}{\Delta t}, \tag{A-3}$$

resistivity

$$\eta = c_2\left(\frac{1}{f} - 1\right)\theta_e^{1/2} + c_3\,1/\theta_e^{3/2}, \tag{A-4}$$

current density

$$\frac{j_\ell^{n+1} - j_\ell^n}{\Delta t} = \frac{1}{2\pi R^2}\frac{\Delta I}{\Delta t} + \frac{1}{\mu_0(\Delta R)^2}\left[\eta_{\ell+1}^n\, j_{\ell+1}^n - 2\eta_\ell^n\, j_\ell^n + \eta_{\ell-1}^n\, j_{\ell-1}^n\right]. \tag{A-5}$$

```
..    FRIEDRICH, O. M., JR.   PROGRAM B-LF--HCP              MASTER DECK
      PROGRAM BXLF
C         THIS IS A PROGRAM TO COMPUTE THE VARIOUS PARAMETERS (I.E. THE
C     ELECTRON AND ION TEMPERATURES, RESISTIVITY, DEGREE OF IONIZATION,
C     AND CURRENT DENSITY) FOR THE INITIAL, BOUNDARY-LAYER FORMATION FOR
C     THE HCP.
C
C     MAXWELL,S FIELD EQUATIONS AND THE PLASMA EQUATIONS ARE USED TO
C     GIVE FIVE PARTIAL DIFFERENTIAL EQUATIONS IN TIME AND SPACE
C     COORDINATES.
C
C     FINITE DIFFERENCE EQUATIONS ARE WRITTEN TO SOLVE THE SYSTEM OF
C     PARTIAL DIFFERENTIAL EQUATIONS.
C
C     THE PARAMETERS USED ARE THE FOLLOWING (GENERAL NAMES)
C     DEGREE---THE FRACTION OF IONIZATION
C     THETAXE---THE MEASURE OF THE ELECTRON TEMPERATURE
C     THETAXI---THE MEASURE OF THE ION TEMPERATURE
C     RESIST---THE NORMALIZED RESISTIVITY FUNCTION
C     CURRENT---THE CURRENT DENSITY FUNCTION
C
C     THE CONSTANTS REQUIRED ARE THE FOLLOWING
C     C2---A CONSTANT CONNECTED WITH RESISTIVITY FOR A PARTIALLY IONIZED
C     PLASMA
C     C3---ANOTHER CONSTANT CONNECTED WITH THE RESISTIVITY FOR A PARTIALLY
C     IONIZED PLASMA
C     C4---A CONSTANT USED IN THE RELATION FOR THE CHANGE IN DEGREE OF
C     IONIZATION WITH THE ELECTRON TEMPERATURE
C     C5---A CONSTANT FOR THE ENERGY TRANSFER OF ELECTRONS TO IONS
C     A MU---THE PERMEABILITY
C     ETA---A RESISTIVITY UNIT
C     EPSILON---AN IONIZATION POTENTIAL UNIT
C     A---A CONSTANT ( = 2.0 )
C
C     THE INITIAL VALUES TO BE INPUT ARE THE FOLLOWING
C     EO---ELECTRIC FIELD APPLIED
C     A NO---THE GAS DENSITY  (PER CC)
C
C     THE STEP INCREMENTS AND INTERVAL MAXIMUMS ARE THE FOLLOWING
C     T INIT---THE INITIAL TIME PARAMETER, STARTING POINT
C     R INIT---THE INNER, I.E. INITIAL, RADIUS
C     DEL T---THE TIME INCREMENT FOR THE STEP INTEGRATION, I.E. MESH SIZE
C     DEL R---THE RADIAL INCREMENT FOR SPACIAL STEPS
C     T MAX---THE MAXIMUM TIME TO BE CONSIDERED.
C     CURNT O---THE CURRENT THROUGH THE CORE
C     CURNT M---THE MAXIMUM CURRENT THROUGH THE CORE
C     OMEGA---THE RADIAN FREQUENCY OF THE MAIN CURRENT
C
C     FORMAT STATEMENTS
 40   FORMAT(4E20.8)
 41   FORMAT(8E15.8)
C     FORMAT NOS. 42 THROUGH 49 ARE LEFT FOR DATA DISPLAY
C     FORMAT NOS. 75 THROUGH 85 ARE LEFT FOR HEADINGS AND TITLES
 75   FORMAT(30H FRIEDRICH IDENT B-LF--HCP        )
 76   FORMAT(35H SOLUTIONS USING FINITE DIFFERENCE          )
 77   FORMAT(// 11H DATA INPUT          )
 78  0FORMAT(6X, 2H T, 13X, 2H R, 10X, 7H DEGREE, 8X, 8H THETAXE, 5X,
     1 8H THETAXI, 8X, 12H RESISTIVITY, 3X, 8H CURRENT      )
 79   FORMAT(1H1)
      PRINT 75
```

```
      PRINT 76
 1    READ 40, C2, C3, C4, C5
 2    READ 40, A MU, ETA, EPSILON, A
 3    READ 40, EO, A NO, CURNT M, OMEGA
 4    READ 40, T INIT, R INIT, DEL T, DEL R
 5    READ 40, T MAX, R MAX
C
C     DATA CHECK
      PRINT 77
 45  0FORMAT(5H C2 =, E15.8,/ 5H C3 =, E15.8,/ 5H C4 =, E15.8,/
     1 5H C5 =, E15.8 )
 46  0FORMAT(7H A MU =, E15.8, 6H ETA =, E15.8, 10H EPSILON =, E15.8,
     1 4H A =, E15.8 )
 47  0FORMAT( 5H EO =, E15.8, 10X, 7H A NO =, E15.8, / 10H CURNT M =,
     1  E15.8, 10X, 8H OMEGA =, E15.8)
 48  0FORMAT( 9H T INIT =, E15.8, 9H R INIT =, E15.8, 8H DEL T =, E15.8,
     1 8H DEL R =, E15.8)
 49   FORMAT(8H T MAX =, E15.8, 8H R MAX =, E15.8)
 7    PRINT 45, C2, C3, C4, C5
 8    PRINT 46, A MU, ETA, EPSILON, A
      PRINT 47, EO, A NO, CURNT M, OMEGA
      PRINT 48, T INIT, R INIT, DEL T, DEL R
      PRINT 49, T MAX, R MAX
      PRINT 78
C     THE DOUBLE SUBSCRIPTS ARE USED ON THE FIVE PARAMETERS TO BE
C     DETERMINED.  THE FIRST SUBSCRIPT GIVES THE RADIAL POSITION  OR
C     SPACE MODE AND THE SECOND SUBSCRIPT GIVES THE TIME LOCATION.
      DELTA = 1.0
      R = R INIT
     0DIMENSION DEGREE(105,3), THETAXE(105,3), THETAXI(105,3),
     1  RESIST(105,3), CURRENT(105,3), CURNT O(105)
C
C     INITIALIZATION  (PARAMETERS, VARIABLES, CONDITIONS)
      DO 200  I = 1, 100
      J = 1
      DEGREE(I,J) = 1.0E-02
      THETAXE(I,J) = 1.0E-01
      THETAXI(I,J) = 1.0E-05
      RESIST(I,J) = 1.0E-01
      AAA = I - 1
 200  CURRENT(I,J) = 1.0E+03 * EXPF( - AAA/DELTA)
      COUNT = 3.0
      CURNT O(1) = CURNT M * OMEGA * 1.0 * DEL T
      CURNT O(2) = CURNT M * OMEGA * 2.0 * DEL T
      T = T INIT
      J = 1
      R = R INIT - DEL R
      DO 320  I = 1, 100
      R = R + DEL R
 320 0PRINT 41, T, R, DEGREE(I,J), THETAXE(I,J), THETAXI(I,J),
     1RESIST(I,J), CURRENT(I,J)
      PRINT 79
      PRINT 78
      DO 400 INDEX = 1, 10
      DO 360 I COUNT = 1, 20
      DO 300  I = 1, 100
      K = I + 1
      L = J + 1
C
C     CALCULATIONS USING FINITE DIFFERENCE METHODS
100   0 DEGREE(I,L) = DEGREE(I,J) + (DEL T)*(C4*DEGREE(I,J)*(1.0 -
```

```
     1  DEGREE(I,J))*SQRTF(ABSF(THETAXE(I,J)))*((0.8+1.333*THETAXE(I,J)
     2  - 0.8*THETAXE(I,J)*THETAXE(I,J))*EXPF(-1.0/THETAXE(I,J))
     3  + (-0.16 + 0.987*THETAXE(I,J) + 0.8*THETAXE(I,J)*THETAXE(I,J))
     4  *EXPF(-4.0/THETAXE(I,J))
     5  + (0.8 + 0.08*THETAXE(I,J))*EXPF(-20.0/THETAXE(I,J))))
 101 0THETAXI(I,L) = THETAXI(I,J) + (DEL T)*C5*DEGREE(I,J)*(THETAXE(I,J)
     1 - THETAXI(I,J))/(ABSF(THETAXE(I,J)))**1.5
      DER DEG = DEGREE(I,L) - DEGREE(I,J)
      DER TI = THETAXI(I,L) - THETAXI(I,J)
C     NOTE---THE DERIVATIVE ROUTINE MUST FOLLOW STATEMENT 101 BUT THE
C     RESULTS ARE REQUIRED IN STATEMENT 102.
 102 0THETAXE(I,L) = THETAXE(I,J) + (DEL T)*(-(0.6667*A + THETAXE(I,J)
     1 + THETAXI(I,J))*1.0/DEGREE(I,J)*(DER DEG) + (0.6667*ETA/(A NO
     2 *EPSILON * DEGREE(I,J)))*RESIST(I,J)*CURRENT(I,J)*CURRENT(I,J))
     3  - DER TI
 103 0RESIST(I,L) = C2*(1.0/DEGREE(I,J) - 1.0)*SQRTF(ABSF(THETAXE(I,J)))
     1 + C3*1.0/(THETAXE(I,J)**1.5)
 300  CONTINUE
C     THE FOLLOWING COMPUTES THE CURRENT DENSITY USING FORWARD FINITE
C     DIFFERENCE METHODS.
      DO 350  I = 1, 100
      R = FLOATF(I)*DEL R
      L = J + 1
      K = I + 1
      M = I - 1
 350 0CURRENT(I,L) = CURRENT(I,J) + 1.0/(6.2832*R*R)*(CURNT O(L) -
     1CURNT O(J)) + (DEL T)/(A MU)*(CURRENT(K,J)*RESIST(K,J) - 2.0*
     2CURRENT(I,J)*RESIST(I,J) + CURRENT(M,J)*RESIST(M,J))/
     3(DEL R*DEL R)
      T = T + DEL T
      DO 360 I = 1, 100
      DEGREE(I,J) = DEGREE(I,L)
      THETAXI(I,J) = THETAXI(I,L)
      THETAXE(I,J) = THETAXE(I,L)
      RESIST(I,J) = RESIST(I,L)
      CURRENT(I,J) = CURRENT(I,L)
      CURNT O(J) = CURNT O(L)
      CURNT O(L) = CURNT M * OMEGA * COUNT * DEL T
      COUNT = COUNT + 1.0
 360  CONTINUE
      R = R INIT - DEL R
      DO 390  I = 1, 100
      R = R + DEL R
 390 0PRINT 41, T, R, DEGREE(I,L), THETAXE(I,L), THETAXI(I,L),
     1RESIST(I,L), CURRENT(I,L)
      PRINT 79
      PRINT 78
 400  CONTINUE
1001  END
1002  END
```

.. FRIEDRICH, O. M., JR. PROGRAM B-LF--HCP RUN NO. 1
FRIEDRICH IDENT B-LF--HCP
SOLUTIONS USING FINITE DIFFERENCE

DATA INPUT
C2 = .31300000E-05
C3 = .16100000E-05
C4 = .83000000E+08
C5 = .17200000E+04
A MU = .12400000E-05 ETA = .10000000E+01 EPSILON = .26000000E-17 A = .20000000E+01
E0 = .20000000E+05 A NO = .35000000E+22
CURNT M = .10000000E+05 OMEGA = .45000000E+06
T INIT = .00000000E+00 R INIT = .75000000E-02 DEL T = .10000000E-08 DEL R = .10000000E-02
T MAX = .50000000E-05 R MAX = .90000000E-01

T	R	DEGREE	THETAXE	THETAXI	RESISTIVITY	CURRENT
.00000000E+00	.75000000E-02	.10000000E-01	.10000000E+00	.10000000E-04	.10000000E+00	.10000000E+04
.00000000E+00	.85000000E-02	.10000000E-01	.10000000E+00	.10000000E-04	.10000000E+00	.36787944E+03
.00000000E+00	.95000000E-02	.10000000E-01	.10000000E+00	.10000000E-04	.10000000E+00	.13533528E+03
.00000000E+00	.10500000E-01	.10000000E-01	.10000000E+00	.10000000E-04	.10000000E+00	.49787068E+02
.	.	.	.	.	.	.
.	.	.	.	.	.	.
.	.	.	.	.	.	.

T	R	DEGREE	THETAXE	THETAXI	RESISTIVITY	CURRENT
.50000000E-06	.75000000E-02	.10000000E+01	.29077447E+02	.17795141E-03	.10288062E-07	.70672167E+10
.50000000E-06	.85000000E-02	.10000000E+01	.15180793E+02	.21813487E-03	.27222215E-07	.67875702E+09
.50000000E-06	.95000000E-02	.10000000E+01	.93798271E+01	.27084500E-03	.56045683E-07	.17370398E+09
.50000000E-06	.10500000E-01	.10000000E+01	.54385532E+01	.34705720E-03	.12694220E-06	.69144866E+08
.50000000E-06	.11500000E-01	.10000000E+01	.30163992E+01	.45004873E-03	.30732526E-06	.34684220E+08
.50000000E-06	.12500000E-01	.10000000E+01	.16785392E+01	.56422270E-03	.74034827E-06	.19443237E+08
.50000000E-06	.13500000E-01	.99999977E+00	.99122781E+00	.62155764E-03	.16314552E-05	.11535020E+08
.50000000E-06	.14500000E-01	.97901481E+00	.64787452E+00	.44319327E-03	.31424974E-05	.71310851E+07
.50000000E-06	.15500000E-01	.26741546E+00	.47933000E+00	.99092651E-04	.10841516E-04	.26870794E+07
.50000000E-06	.16500000E-01	.50885647E-01	.39403091E+00	.41153312E-04	.43335698E-04	.96824022E+06
.50000000E-06	.17500000E-01	.23214989E-01	.34490514E+00	.32757596E-04	.85525469E-04	.61743833E+06
.50000000E-06	.18500000E-01	.15876522E-01	.31098441E+00	.31094444E-04	.11768808E-03	.51723117E+06
.50000000E-06	.19500000E-01	.12972127E-01	.28342391E+00	.31100085E-04	.13761116E-03	.48297452E+06
.50000000E-06	.20500000E-01	.11573606E-01	.25874918E+00	.31650759E-04	.14829812E-03	.47161808E+06
.50000000E-06	.21500000E-01	.10839237E-01	.23580803E+00	.32383941E-04	.15280418E-03	.46857353E+06
.50000000E-06	.22500000E-01	.10443811E-01	.21442591E+00	.33151068E-04	.15354773E-03	.46688816E+06
.50000000E-06	.23500000E-01	.10232570E-01	.19479665E+00	.33881409E-04	.15233319E-03	.46239195E+06
.50000000E-06	.24500000E-01	.10122159E-01	.17719026E+00	.34539549E-04	.15040790E-03	.45259647E+06
.50000000E-06	.25500000E-01	.10065694E-01	.16180877E+00	.35109417E-04	.14853744E-03	.43649049E+06
.50000000E-06	.26500000E-01	.10037159E-01	.14872408E+00	.35586929E-04	.14710742E-03	.41436476E+06
.50000000E-06	.27500000E-01	.10022686E-01	.13786965E+00	.35975769E-04	.14623490E-03	.38744405E+06
.50000000E-06	.28500000E-01	.10015198E-01	.12906678E+00	.36284429E-04	.14587253E-03	.35739724E+06
.50000000E-06	.29500000E-01	.10011194E-01	.12206678E+00	.36523935E-04	.14589462E-03	.32589274E+06
.50000000E-06	.30500000E-01	.10008965E-01	.11659305E+00	.36706091E-04	.14615892E-03	.29431931E+06

APPENDIX B

THEORETICAL MODELS

1. Snowplow Model

Consider a unit length cylinder, with an initial radius, R_o, a variable radius, r, and a mass density, ρ_o .

a. Continuity Equation

$$m_i = \rho_o [\pi R_o^2 - \pi r^2] = m(r) \tag{B-1}$$

where, m_i is mass accumulated by the snowplow.

b. Momentum Equation

$$\frac{d}{dt}\left(m \frac{dr}{dt}\right) = -2\pi r p_m \tag{B-2}$$

where, p_m is magnetic pressure.

c. Energy Equation

$$\frac{d}{dt} E_p = \frac{I^2}{2} \frac{dL}{dt} = m U \frac{dU}{dt} + \frac{dm}{dt} U^2 \tag{B-3}$$

where, E_p is plasma energy, U is velocity, I is current, and L is inductance.

d. Circuit Equation

$$-\frac{d}{dt}(L_p I) = L_o \frac{dI}{dt} + V - \frac{1}{C}\int_o^t I\,dt \tag{B-4}$$

where, L_p is variable plasma inductance, L_o is constant external inductance, C is constant external capacitance, and V is voltage due to external resistance.

2. Quasi-Steady State Model

Consider a unit length cylinder with a piston radius, r_b, a shock radius, r_s, and initial radius, R_o.

a. Continuity Equation

$$\rho_1 \pi (r_b^2 - r_s^2) = \rho_o \pi (R_o^2 - r_s^2) \tag{B-5}$$

where, ρ_1 is mass density behind shock, ρ_o is initial mass density.

b. Momentum Equation

$$p_m = \rho_0 U_s^2 - \rho_1 (U_s - U_1)^2 \qquad \text{(B-6)}$$

where, p_m is magnetic pressure, U_s is velocity of shock, and U_1 is velocity behind shock.

c. Energy Equation

$$\left(\frac{\gamma}{\gamma-1}\right)\frac{p_0}{\rho_0} + \frac{U_s^2}{2} = \left(\frac{\gamma}{\gamma-1}\right)\frac{p_m}{\rho_1} + \frac{1}{2}(U_s - U_1)^2 \qquad \text{(B-7)}$$

$(p_m >> p_0)$

where, γ is ratio of specific heats c_p/c_v, and p_0 is initial pressure.

d. Circuit Equation

For constant external capacitance, resistance, and total inductance with circuit elements in series,

$$0 = L_0 \frac{dI}{dt} + V - \frac{1}{C}\int_0^t I\,dt \qquad \text{(B-8)}$$

where, L_0 is constant inductance (total).

3. Slug Model

Consider a slug of total mass m_T, and velocity U.

a. Continuity Equation

$$m_T = m_0 = \text{constant} \qquad \text{(B-9)}$$

where, m_0 is initial mass.

b. Momentum Equation

$$m_0 \frac{d^2 r}{dt^2} = -2\pi r p_m \qquad \text{(B-10)}$$

where, p_m is magnetic pressure.

c. Energy Equation

$$\frac{d}{dt} E_p = \frac{1}{2} I^2 \frac{dL}{dt} = \frac{d}{dt}\left(\frac{1}{2} m_0 U^2\right) \qquad \text{(B-11)}$$

where, E_p is plasma energy.

d. Circuit Equation

For constant external capacitance, resistance, and inductance but variable plasma inductance due to the motion of the slug,

$$-\frac{d}{dt}(L_p I) = L_0 \frac{dI}{dt} + V - \frac{1}{C}\int_0^t I\,dt\,. \qquad \text{(B-12)}$$

4. Gasdynamic Model

Consider a shock with velocity U and mass density ρ .

a. Continuity Equation (for one dimensional flow)

$$\frac{\partial}{\partial t}\rho + \frac{\partial}{\partial r}(\rho U) = 0 \quad . \tag{B-13}$$

b. Momentum Equation (for one dimensional flow)

$$0 = \frac{\partial}{\partial t}(\rho U) + \frac{\partial}{\partial r}(\rho U^2) + \frac{\partial p}{\partial r} \quad . \tag{B-14}$$

c. Energy Equation (for one dimensional flow)

$$0 = \frac{\partial}{\partial t}(\text{energy}) + \frac{\partial}{\partial r}(\text{energy}\, U + pU) \tag{B-15}$$

where, $\text{energy} = \left(\frac{p}{\gamma - 1}\right) + \frac{1}{2}\rho U^2$.

d. Circuit Equation

For constant external capacitance, resistance, and inductance, with plasma inductance and resistance variable,

$$-\frac{d}{dt}(L_p I) = L_0 \frac{dI}{dt} + V - \frac{1}{C}\int_0^t I\,dt \quad . \tag{B-16}$$

APPENDIX C

CURRENT SHEATH DYNAMICS CALCULATIONS FOR PARALLEL PLATE ACCELERATOR

The finite difference equations employed to calculate the position and velocity of the current sheath during the initial acceleration process for small velocities are:

$$\Delta v = \frac{\Delta t}{\rho x} \left(\mu_0 I^2 / (2 w^2) \right) , \qquad \text{(C-1)}$$

and

$$\Delta x = v \Delta t , \qquad \text{(C-2)}$$

where I is the current and w is the width of the parallel plate accelerator. A listing of the FORTRAN computer code is presented on the following pages.

```
EE020147 FRIEDRICH      PPGUN
..     FRIEDRICH, O. M., JR.   PROGRAM PPGUN
       PROGRAM PPGUN
C      THE COUPLED DIFFERENTIAL EQUATIONS DESCRIBING THE ACCELERATION OF
C      PLASMA IN AN EM GUN ARE SOLVED
C      FINITE DIFFERENCE METHODS ARE EMPLOYED TO SOLVE THE CIRCUIT  EQUATION
C      WITH THE EQUATION OF MOTION SIMULTANEOUSLY.*
C      * EQUATION 211 WAS NOT EMPLOYED FOR RESULTS SHOWN
C      THE VOLTAGE ON THE CAPACITOR, THE VOLTAGE ON THE GUN, AND/OR THE
C      CURRENT IN THE GUN ARE REQUIRED.
C      THE SPECIFICATIONS FOR THE ACCUMULATION OF MASS, THE GUN IMPEDANCE,
C      AND THE GUN RESISTANCE ARE REQUIRED.
C      THE MASS MAY BE CONSTANT, LINEARLY COLLECTED, SNOW PLOW COLLECTED,
C      OR SPECIFIED BY A FUNCTIONAL RELATION OF TIME OR POSITION
C      THE GUN INDUCTANCE IS DEFINED TO INCREASE WITH DISTANCE.
C      THE GUN RESISTANCE MAY BE CONSTANT, OR SPECIFIED BY A FUNCTIONAL
C      RELATION.
      0DIMENSION VCAP(49), AMASS(49,49), A INDUCT(49), CURRENT(49),
      1  RESIST(49)
   40 FORMAT(4E20.8)
   41 FORMAT(10I5)
   42 FORMAT(6E20.8)
   45 FORMAT(10E12.5)
   460FORMAT(4H R =, E16.8, 5X, 5H AL =, E16.8, 5X, 5H AM =, E16.8, 5X,
     1  4H W =, F16.8)
   470FORMAT(5H VC =, E16.8, 5X, 8H OMEGA =, E16.8, 5X, 11H ALPHA VC =,
     1 E16.8, 5X, 6H CUR =, E16.8)
   48 FORMAT(9H X INIT =, E16.8, 10X, 9H V INIT =, F16.8)
   490FORMAT(9H T INIT =, E16.8, 10X, 8H DEL T =, E16.8, 10X, 8H T MAX =
     1  , E16.8)
   500FORMAT(11H ALPHA AM =, F16.8, 5X, 11H ALPHA AA =, E16.8, 4X, /
     1  11H ALPHA AL =, E16.8, 5X, 10H ALPHA R =, E16.8)
   51 FORMAT(11H ALPHA CV =, E16.8, 5X, 7H A MU =, E16.8)
   55 FORMAT(16H VALUES OF VCAP         )
   56 FORMAT(16H CURRENT VALUES         )
   57 FORMAT(16H AMASS VALUES           )
   58 FORMAT(20H A INDUCT VALUES        )
   59 FORMAT(16H RESIST VALUES          )
   60 FORMAT(45H THE VALUE OF X CANNOT BE LESS THAN 1.0E-04          )
   61 FORMAT(25H I COUNT MINIMUM IS 1        )
   62 FORMAT(25H I COUNT MAXIMUM IS 48       )
   760FORMAT(9X, 2H X, 18X, 2H V, 18X, 8H CURRENT, 12X, 6H V CAP, 14X,
     1  5H TIME  )
C     DATA INPUT
    10READ 41, I VCAP, I CURNT, I MASS, I INDUCT, I RESIST, I CONT,
     1I COUNT
    2 IF(I VCAP)1001, 4,3
    3 READ 40, VCAP
    4 IF(I CURNT)   6,6,5
    5 READ 40, CURRENT
    6 IF(I MASS)1001,8,7
    7 READ 40, AMASS
    8 IF(I INDUCT)1001,10,9
    9 READ 40, A INDUCT
   10 IF(I RESIST)1001,12,11
   11 READ 40, RESIST
   12 CONTINUE
   20 READ 40, R, AL, AM, W
   21 READ 40, VC, OMEGA, ALPHA VC, CUR
   22 READ 40, X INIT, V INIT
```

```
   23 READ 40, T INIT, DEL T, T MAX
   24 READ 40, ALPHA AM, ALPHA AA, ALPHA AL, ALPHA R
   25 READ 40, ALPHA CV, A MU
C     DATA CHECK
  101 IF(I VCAP)1001,104,103
  103 PRINT 55
      PRINT 45, VCAP
  104 IF(I CURNT) 106,106,105
  105 PRINT 56
      PRINT 45, CURRENT
  106 IF(I MASS)1001,108,107
  107 PRINT 57
      PRINT 45, AMASS
  108 IF(I INDUCT)1001,110,109
  109 PRINT 58
      PRINT 45, A INDUCT
  110 IF(I RESIST)1001,112,111
  111 PRINT 59
      PRINT 45, RESIST
  112 CONTINUE
  120 PRINT 46, R, AL, AM, W
  121 PRINT 47, VC, OMEGA, ALPHA VC, CUR
  122 PRINT 48, X INIT, V INIT
  123 PRINT 49, T INIT, DEL T, T MAX
  124 PRINT 50, ALPHA AM, ALPHA AA, ALPHA AL, ALPHA R
  125 PRINT 51, ALPHA CV, A MU
      PHI1 = 0.0
      PHI2 = 0.0
      M = 1
      N = 1
      V = V INIT
      X = X INIT
      T = T INIT
      PRINT 40, T , T INIT
      K = 0
      L = 0
      IF(ABSF(X) - 1.0E-04) 180,180,181
  180 PRINT 60
      X = 1.0E-04
  181 IF(I COUNT - 1)182,183,183
  182 PRINT 61
      I COUNT = 1
  183 IF(I COUNT - 48)185, 185, 184
  184 PRINT 62
      I COUNT = 48
  185 CONTINUE
C     PRINT HEADINGS
C     M WILL BE THE COUNTER INDEX USED
C     N WILL BE A COUNTER INDEX USED
      PRINT 76
C     CALCULATIONS BEGIN
  199 CONTINUE
      T = T INIT
      IF(I CURNT) 200,200,201
  200 CURRENT(0) = CUR
```

```
  201 DO 420 I = 1, 48
      DO 400 J = 1, I COUNT
      K = K + 1
      L = L + 1
      IF(I VCAP)1001,202,203
  202 VCAP(M) = VC*SINF(OMEGA*T + PHI1)*EXPF(-ALPHA VC*T)
  203 IF(I MASS)1001,204,205
 2040AMASS(M,N) = AM*EXPF(-ALPHA AM*FLOATF(K))*EXPF(-ALPHA AA*FLOATF(
     1  L))
  205 IF(I INDUCT)1001,206,207
  206 A INDUCT(N) = AL*EXPF(-ALPHA AL*FLOATF(L))
  207 IF(I RESIST)1001,208,209
  208 RESIST(N) = R*EXPF(-ALPHA R*FLOATF(L))
  209 IF(I CURNT)210,211,212
  210 CURRENT(M) = CUR*SINF(OMEGA*T + PHI2)*EXPF(-ALPHA CV*FLOATF(K))
      GO TO 212
  211 STOP
 2120V = V + (DEL T/(AMASS(M,N)*X))*(A MU*CURRENT(M)*CURRENT(M)/(2.0*
     1  W*W))
  213 X = X + V*DEL T
      T = T + DEL T
  400 CONTINUE
C     PRINT OUTPUT
      T = T - DEL T
  250 PRINT 42, X, V, CURRENT(M), VCAP(M), T
      T = T + DEL T
      M = M + 1
      N = N + 1
  420 CONTINUE
      IF(T - T MAX)260,1001,1001
C     260 IS TO BE USED TO SHIFT AND / OR TO READ IN DATA
  260 GO TO 422
  422 IF(I VCAP)1001,424,423
  423 READ 40, VCAP
  424 VCAP(0) = VCAP(48)
      IF(I CURNT) 426,426,425
  425 READ 40, CURRENT
  426 CURRENT(0) = CURRENT(48)
      IF(I MASS)1001,428,427
  427 READ 40, AMASS
  428 IF(I INDUCT)1001,430,429
  429 READ 40, A INDUCT
  430 IF(I RESIST)1001,432,431
  431 READ 40, RESIST
  432 CONTINUE
      M = 1
      N = 1
      GO TO 201
 1001 END
 1002 END
```

.. FRIEDRICH, O. M., JR. PROGRAM PPGUN

R = .10000000E-03 AL = .33000000E-06 AM = .30000000E-02 W = .60000000E-01

VC = .40000000E+04 OMEGA = .31400000E+06 ALPHA VC = .00000000E+00 CUR = .35000000E+05

X INIT = .10000000E-02 V INIT = .00000000E+00

T INIT = .10000000E-08 DEL T = .10000000E-08 T MAX = .10000000E-04

ALPHA AM = .00000000E+00 ALPHA AA = .00000000E+00

ALPHA AL = .00000000E+00 ALPHA R = .00000000E+00

ALPHA CV = .00000000E+00 A MU = .12570000E-05

.10000000E-08 .10000000E-08

X	V	CURRENT	V CAP	TIME
.10000000E-02	.27060555E-02	.10989982E+03	.12559979E+02	.10000000E-07
.10000001E-02	.20172290E-01	.21979856E+03	.25119835E+02	.20000000E-07
.10000005E-02	.66455417E-01	.32969512E+03	.37679443E+02	.30000000E-07
.10000017E-02	.15561096E+00	.43958844E+03	.50238679E+02	.40000000E-07
.10000040E-02	.30169261E+00	.54947743E+03	.62797420E+02	.50000000E-07
.10000081E-02	.51875144E+00	.65936099E+03	.75355542E+02	.60000000E-07
.10000149E-02	.82083508E+00	.76923806E+03	.87912921E+02	.70000000E-07
.10000252E-02	.12219867E+01	.87910754E+03	.10046943E+03	.80000000E-07
.10000402E-02	.17362437E+01	.98896835E+03	.11302495E+03	.90000000E-07
.10000609E-02	.23776366E+01	.10988194E+04	.12557936E+03	.10000000E-06
.10000889E-02	.31601871E+01	.12086596E+04	.13813253E+03	.11000000E-06
.10001255E-02	.40979061E+01	.13184880E+04	.15068434E+03	.12000000E-06
.10001724E-02	.52047919E+01	.14283033E+04	.16323466E+03	.13000000E-06
.10002314E-02	.64948275E+01	.15381045E+04	.17578337E+03	.14000000E-06
.10003044E-02	.79819775E+01	.16478906E+04	.18833035E+03	.15000000E-06
.10003934E-02	.96801849E+01	.17576604E+04	.20087547E+03	.16000000E-06
.10005006E-02	.11603368E+02	.18674129E+04	.21341861E+03	.17000000E-06
.10006283E-02	.13765415E+02	.19771469E+04	.22595965E+03	.18000000E-06
.10007790E-02	.16180182E+02	.20868615E+04	.23849846E+03	.19000000E-06
.10009553E-02	.18861484E+02	.21965555E+04	.25103492E+03	.20000000E-06
.10011600E-02	.21823092E+02	.23062279E+04	.26356890E+03	.21000000E-06
.10013959E-02	.25078729E+02	.24158775E+04	.27610028E+03	.22000000E-06
.10016660E-02	.28642057E+02	.25255033E+04	.28862895E+03	.23000000E-06
.10019735E-02	.32526678E+02	.26351042E+04	.30115476E+03	.24000000E-06
.10023217E-02	.36746116E+02	.27446791E+04	.31367761E+03	.25000000E-06
.10027140E-02	.41313821E+02	.28542269E+04	.32619736E+03	.26000000E-06
.10031539E-02	.46243148E+02	.29637466E+04	.33871390E+03	.27000000E-06
.10036452E-02	.51547355E+02	.30732371E+04	.35122710E+03	.28000000E-06
.10041917E-02	.57239590E+02	.31826973E+04	.36373683E+03	.29000000E-06
.10047973E-02	.63332881E+02	.32921261E+04	.37624298E+03	.30000000E-06
.10054660E-02	.69840122E+02	.34015224E+04	.38874542E+03	.31000000E-06
.10062022E-02	.76774064E+02	.35108852E+04	.40124403E+03	.32000000E-06
.10070101E-02	.84147299E+02	.36202134E+04	.41373868E+03	.33000000E-06
.10078943E-02	.91972249E+02	.37295059E+04	.42622925E+03	.34000000E-06
.10088592E-02	.10026115E+03	.38387617E+04	.43871562E+03	.35000000E-06
.	.	.	.	.
.	.	.	.	.
.	.	.	.	.

APPENDIX D

CURRENT SHEATH DYNAMICS CALCULATIONS FOR STABILIZED INVERSE PINCH

The method of Runge-Kutta with Gill's coefficients is used to solve the stabilized inverse pinch's equation of motion. The method approximates the increment in "y", Δy, by the relation,

$$\Delta y = \frac{f_3 \Delta t}{6} - \frac{q_3}{3} , \qquad \text{(D-1)}$$

where f_3 is the function, f_i, evaluated after three repetitive steps, and q_3 is the result of evaluation of a function, q_i, after several steps. The relations for the modified Runge-Kutta method with Gill's coefficients are,

$$y_i = y_{i-1} + a_i \left(f_{i-1} \Delta t - q_{i-1} \right) , \qquad \text{(D-2)}$$

$$q_i = 2 a_i f_{i-1} \Delta t + \left(1 - 3 a_i \right) q_{i-1} , \qquad \text{(D-3)}$$

where i goes from 1 to 3. The values of the constants, a_i, are:

$$a_1 = 1/2 \qquad \text{(D-4)}$$

$$a_2 = 1 - 1/\sqrt{2} \qquad \text{(D-5)}$$

and

$$a_3 = 1 + 1/\sqrt{2} \qquad \text{(D-6)}$$

The second order equation describing the current sheath's motion is reduced to a set of two first order equations, which are then solved by applying the above iterations simultaneously to the two first order differential equations. A listing of the FORTRAN computer code employed to determine the position and velocity of the dynamic current sheath is presented on the following pages.

```
** 1   FRIEDRICH, O.M. JR.   PROGRAM HCP-U1, ORIGINAL PHYSICAL PARAMETERS MASTER
      PROGRAM HCP                                                              2
C     THIS IS A PROGRAM TO CALCULATE THE POSITION                              3
C     OF A PLASMA CURRENT SHEATH AS A FUNCTION                                 4
C                                                                              5
C     THE RUNGE-KUTTA METHOD IS USED IN THIS RUN                               6
C     TO SOLVE THE NONLINEAR DIFFERENTIAL EQUATION.                            7
C     RHO IS THE FLUID DENSITY, KG/METER**3                                    8
C     A MU IS THE PERMEABILITY, MKS UNITS                                      9
C     A LEN IS THE ELECTRODE SEPARATION, METERS                               10
C     R M IS THE OUTER RADIUS, METERS                                         11
C     R C IS THE INNER RADIUS, METERS                                         12
C     B ZO IS THE STABILIZING FIELD IN WEBERS/SQ. METER                        13
C     W IS THE RINGING FREQUENCY, RADIANS/SEC                                 14
C     CUR N T IS THE PEAK CURRENT, AMPS                                       15
C     R IS THE DEPENDENT VARIABLE, INITIAL RADIUS, METERS                     16
C     Y1 IS THE INITIAL CURRENT SHEATH RADIUS, METERS                         17
C     Y2 IS THE INITIAL CURRENT SHEATH VELOCITY                               18
C     T INIT IS THE INITIAL TIME INDEPENDENT PARAMETER,SEC                    19
C     DEL T IS THE INCREMENT TIME , SEC                                       20
C     T MAX IS THE MAXIMUM  TIME LIMIT, SEC                                   21
C     A MASS IS A PARAMETER USED TO INITIALLY LIMIT THE SHEATH-S MOTION       22
C     COUNTER IS THE PRINTING INTERVAL PARAMETER                              23
   40 FORMAT (4E20.8)                                                         24
   41 FORMAT( 7H RHO = , E16.8,/ 16H PERMEABILITY = , F16.8,//       )        25
  420FORMAT(24H ELECTRODE SEPARATION = , E16.8,/ 24H R MAX.(OUTER RADIU      26
     1S) = , E16.8,/ 25H R CORE (INNER RADIUS) = , E16.8,//          )       27
  430FORMAT(21H STABILIZING FIELD = , E16.8,/ 21H RINGING FREQUENCY = ,      28
     1E16.8,/ 16H PEAK CURRENT = , E16.8,/ 29H INITIAL SHEATH RADIUS = ,     29
     2F16.8,//                                                       )       30
  440FORMAT(24H INITIAL DISPLACEMENT = , E16.8,/ 20H INITIAL VELOCITY =      31
     1 , E16.8,//                                                    )       32
  450FORMAT(16H INITIAL TIME = , E16.8,/ 18H INCREMENT TIME = , E16.8        33
     1,/ 16H MAXIMUM TIME = , E16.8,//                               )       34
   46 FORMAT(5E20.8, 14H OSCILLATION    )                                     35
   47 FORMAT(5E20.8, 15H PEAK, LEVELING      )                                36
   48 FORMAT(5E20.8, 11H INCREASING     )                                     37
   49 FORMAT ( I4 )
   74 FORMAT(27H FRIEDRICH IDENT HCP-U1          )                           38
   75 FORMAT (// 27H SOLUTION USING RUNGE-KUTTA  )                           39
   76 FORMAT (// 11H INPUT DATA)                                             40
  780FORMAT ( 5X,  2H T, 18X,  6H DEL T, 14X,  3H Y1, 17X,  3H Y2,           41
  781  17X, 7H DEL Y1, 5X, 9H COMMENTS          )                           42
   79 FORMAT (95X, 14H DAMPING USED    , I3  )                               43
   80 FORMAT( 13H NEED TO DAMP          )                                    44
   81 FORMAT( 30H ERROR IN DAMPING  -A MASS-      )                          45
   82 FORMAT ( // 14H A MASS = 1.0                )                          46
   83 FORMAT (1H1     )
      PRINT 74                                                               47
      PRINT 75                                                               48
C                                                                            49
C     DATA INPUT                                                             50
    1 READ 40, RHO, A MU                                                     51
    2 READ 40, A LEN, R M, R C                                               52
    3 READ 40, B ZO, W, CUR N T, R                                           53
    4 READ 40, Y1, Y2                                                        54
      READ 40, T INIT, DEL T, T MAX                                          55
      READ 49, I CODE
C                                                                            56
C     DATA CHECK                                                             57
```

```
      PRINT 83
      PRINT 76                                                          58
    6 PRINT 41, RHO, A MU                                               59
    7 PRINT 42, A LEN, R M, R C                                         60
    8 PRINT 43, B ZO, W, CUR N T, R                                     61
    9 PRINT 44, Y1, Y2                                                  62
      PRINT 45, T INIT, DEL T, T MAX                                    63
C                                                                       64
C     DIMENSIONING, INIALIZING, AND HEADINGS                            65
   10 DIMENSION Q(3), BBBB(2), Y(2), A(3)                               66
   11  A(1) = 0.50000                                                   67
       A(2) = 0.29280                                                   68
       A(3) = 1.70700                                                   69
      AAAA = 0.0                                                        70
       Y(1) = Y1                                                        71
       Y(2) = Y2                                                        72
      COUNTER = 10.0                                                    73
      N DAMP = 1                                                        74
      A MASS = 1.0 E -20                                                75
      INIT M = 5
      PRINT 78                                                          77
C                                                                       78
C     CALCULATIONS USING RUNGE - KUTTA                                  79
C     THE FLOATING POINT VARIABLE  -A MASS-  IS USED TO DAMP THE        80
C     INITIAL ACCELERATION OF THE LIGHT CURRENT SHEATH.                 81
C     THE FLOATING POINT VARIABLE  -COUNTER-  IS USED TO DETERMINE      82
C     THE PRINTING INTERVAL RATE.                                       83
  108 CONTINUE                                                          84
      A MASS = A MASS * 10.0                                            85
  110 CONTINUE                                                          86
  129   DO 130  I = 1, 3                                                87
  130 Q(I) = 0.0                                                        88
        DO 143  J = 1, 3                                                89
      TERMM1 = -(2.0*Y(1)*Y(2)**2*RHO*3.14159)                          90
99900TERMM2 = A MU*((CUR N T**2)*(SINF(W*T INIT))**2)/(4.0*3.14159*Y(1)  91
     1 )                                                                92
99910TERMM3 = - (4.0*3.14159*(B ZO**2)*((R M**2) - (R**2))**2*(Y(1) -   93
     1  R)*Y(1))/(A MU*A LEN* (R M**2 - Y(1)**2)**2)                     94
99920TERMM4 = - (3.14159*(B ZO**2)*((R M**2 - R**2)**2*Y(1)))/(A MU*     95
     1  ((R M**2 - Y(1)**2)**2))                                         96
99930TERMM5 =   (3.14159*(B ZO**2)*((R C**2 - R**2)**2)*Y(1))/(A MU*     97
     1  ((Y(1)**2 - R C**2)**2))                                         98
  132 BBBB(1) = Y(2)                                                    99
 1330BBBB(2) =  (TERMM1 + TERMM2 + TERMM3 + TERMM4 + TERMM5)/(RHO*      100
     1 3.14159*(Y(1)**2 - R**2))                                        101
      IF ( INIT M ) 502, 502, 501                                       102
  502 CONTINUE                                                          103
      IF(BBBB(2) - 5.0E+18) 136, 134, 134                               104
  501 CONTINUE                                                          105
  134 IF ( A MASS - 1.0 ) 137, 137, 601                                 106
  601 IF ( A MASS - 5.0 ) 602, 602, 138                                 107
  602 A MASS = 1.0                                                      108
      PRINT 82                                                          109
  137 CONTINUE                                                          110
      N DAMP = N DAMP + 1                                               111
      BBBB(2) = BBBB(2)* A MASS                                         112
  136 CONTINUE                                                          113
        DO 143  I = 1, 2                                                114
  142 Y(I) = Y(I) + A(J)*(BBBB(I)*DEL T - Q(I))                         115
  143 Q(I) = 2.0*A(J)*BBBB(I)*DEL T + (1.0 - 3.0*A(J))*Q(I)             116
        DO 155  I = 1, 2                                                117
```

```
155 Y(I) = Y(I) + 0.1666667*BBBB(I)*DEL T - 0.3333333*Q(I)                118
    T INIT = T INIT + DEL T                                              119
    T MAX = T MAX - DEL T                                                120
    COUNTER = COUNTER - 1.0                                              121
    IF(COUNTER) 112,112, 110                                             122
112 CONTINUE                                                             123
    INIT M = INIT M - 1                                                  124
    IF (N DAMP - 1) 115, 115, 114                                        125
114 PRINT 79, N DAMP                                                     126
    N DAMP = 1                                                           127
    GO TO 115                                                            128
115 CONTINUE                                                             129
    DEL Y1 = Y(1) - AAAA                                                 130
    IF(DEL Y1) 200, 201, 202                                             131
200 PRINT 46, T INIT, DEL T, Y(1), Y(2), DEL Y1                          132
    GO TO 205                                                            133
201 PRINT 47, T INIT, DEL T, Y(1), Y(2), DEL Y1                          134
    GO TO 205                                                            135
202 PRINT 48  T INIT, DEL T, Y(1), Y(2), DEL Y1                          136
205 CONTINUE                                                             137
    AAAA = Y(1)                                                          138
    IF(T MAX) 1001, 1001, 111                                            139
111 COUNTER = 10.0                                                       140
    GO TO 110                                                            141
138 PRINT 81                                                             142
    GO TO 1001                                                           143
1001 IF ( I CODE ) 1002, 1002, 1
1002 END                                                                 145
     END
```

```
..      FRIEDRICH, O.M. JR.    PROGRAM HCP-UT, ORIGINAL PHYSICAL PARAMETERS     A1
FRIEDRICH IDENT HCP-UT


  SOLUTION USING RUNGE-KUTTA

INPUT DATA
RHO =     .28800000E-04
PERMEABILITY =     .12600000E-05


ELECTRODE SEPARATION =     .66000000E-01
R MAX.(OUTER RADIUS) =     .95250000E-01
R CORE (INNER RADIUS) =     .47500000E-02


STABILIZING FIELD =     .90000000E-01
RINGING FREQUENCY =     .44800000E+06
PEAK CURRENT =     .10000000E+06
INITIAL SHEATH RADIUS =     .70000000E-02


INITIAL DISPLACEMENT =     .75000000E-02
INITIAL VELOCITY =     .00000000E+00


INITIAL TIME =     .00000000E+00
INCREMENT TIME =     .10000000E-07
MAXIMUM TIME =     .50000000E-05

      T                  DEL T              Y1                 Y2                 DEL Y1       COMMENTS
  .10000000E-06      .10000000E-07      .73258957E-02      .65952170E+04      .73258957E-02 INCREASING
  .20000000E-06      .10000000E-07      .87708110E-02      .18835201E+05      .14449153E-02 INCREASING
  .30000000E-06      .10000000E-07      .10917507E-01      .23716337E+05      .21466956E-02 INCREASING
  .40000000E-06      .10000000E-07      .13439019E-01      .26470407E+05      .25215122E-02 INCREASING
  .50000000E-06      .10000000E-07      .16166567E-01      .27939652E+05      .27275487E-02 INCREASING
  .60000000E-06      .10000000E-07      .19001325E-01      .28673535E+05      .28347573E-02 INCREASING
  .70000000E-06      .10000000E-07      .21886411E-01      .28977544E+05      .28850864E-02 INCREASING
  .80000000E-06      .10000000E-07      .24787785E-01      .29015695E+05      .29013738E-02 INCREASING
  .90000000E-06      .10000000E-07      .27683686E-01      .28876617E+05      .28959016E-02 INCREASING
  .10000000E-05      .10000000E-07      .30559025E-01      .28608644E+05      .28753387E-02 INCREASING
  .11000000E-05      .10000000E-07      .33402339E-01      .28237840E+05      .28433139E-02 INCREASING
  .12000000E-05      .10000000E-07      .36204080E-01      .27777355E+05      .28017405E-02 INCREASING
  .13000000E-05      .10000000E-07      .38955591E-01      .27232397E+05      .27515117E-02 INCREASING
  .14000000E-05      .10000000E-07      .41648464E-01      .26602925E+05      .26928728E-02 INCREASING
  .15000000E-05      .10000000E-07      .44274090E-01      .25885149E+05      .26256256E-02 INCREASING
```

APPENDIX E

HAIN-ROBERTS CALCULATIONS

A set of hydromagnetic equations based on a two fluid model often employed to describe the dynamic plasma is presented in this appendix. A continuity equation, a momentum equation, an equation of state, an equation for the electron temperature, an equation for the ion temperature, an Ohm's Law, and Maxwell's electromagnetic field equations are usually required to completely define the problem.

1. Continuity Equation

The conservation of material is described by an equation of continuity. In general,

$$\frac{\partial \rho}{\partial t} + \bar{\nabla} \cdot \rho \bar{v} = 0 \qquad \text{(E-1)}$$

where, ρ is the fluid density, and $\bar{v}$ is the fluid velocity.

For cylindrical symmetry with only radial variations, the continuity equation often is written

$$\frac{\partial \rho}{\partial t} + \frac{1}{r} \frac{\partial}{\partial r} (r \rho v) = 0. \qquad \text{(E-2)}$$

2. Momentum Equation

Conservation of momentum states that the rate of gain of momentum in a fluid element is equal to the forces that act on the element. In general, the conservation of momentum is given by

$$\rho \left(\frac{\partial \bar{v}}{\partial t} + \bar{v} \cdot \bar{\nabla} \bar{v} \right) = - \bar{\nabla} p + \bar{F} \qquad \text{(E-3)}$$

where, p is the pressure, and $\bar{F}$ is the arbitrary volume force.

For the case of cylindrical symmetry and only radial variations, the momentum equation reduces to

$$\rho \left(\frac{\partial v}{\partial t} + v \frac{\partial v}{\partial r} \right) = - \frac{\partial}{\partial r} \left(p_e + p_i + q_i \right) + F , \qquad \text{(E-4)}$$

where, p_e is the electron pressure term, p_i is the ion pressure term, and q_i is an artificial shockwave term introduced by von Neumann to widen the shock fronts and to permit numerical calculations through shock fronts.

3. Equation of State

An expression relating the pressure, density, and temperature of a fluid is called an equation of state for the fluid. In general, the equation of state is symbolized by

$$\phi(p, \rho, T) = 0. \tag{E-5}$$

The equation of state for an ideal gas is written

$$pV = MRT. \tag{E-6}$$

The internal energy, u, is given by

$$u = \frac{p}{\rho}\left(\frac{1}{\gamma - 1}\right) \tag{E-7}$$

and the temperatures, T_e and T_i, vary as

$$T \propto p/\rho. \tag{E-8}$$

Two expressions for the transport of internal energy are required to complete the set of hydrodynamic equations describing the electron and the ion fluid. These relations are discussed below.

4. Electron Temperature Equation

The electron temperature is obtained from an expression relating the energy gains and energy losses by the electron fluid. Usually the change in the electron temperature is determined by hydrodynamic effects, heat conduction, joule (or ohmic) heating, heat radiation, and heat exchange with the ion fluid. In general,

$$c_v\left(\frac{\partial T_e}{\partial t} + \bar{v}\cdot\bar{\nabla}T_e\right) = -p\bar{\nabla}\cdot\bar{v} + k\nabla^2 T_e + \varepsilon_{joule} - \varepsilon_{radiation} - \frac{T_e - T_i}{2\tau_{eq}} \tag{E-9}$$

where, c_v is the specific heat at constant volume, k is the thermal conductivity, ε_{joule} is energy added by joule heating, $\varepsilon_{radiation}$ is energy

loss by radiation. For the case of cylindrical symmetry with only radial variation, an equation for the electron temperature is given by

$$\frac{\partial T_e}{\partial t} + v \frac{\partial T_e}{\partial r} = -(\gamma-1) T_e \frac{1}{r} \frac{\partial}{\partial r}(rv) + \frac{1}{\rho} \frac{1}{r} \frac{\partial}{\partial r}\left(K_e r \frac{\partial T_e}{\partial r}\right) + \frac{(\gamma-1)}{\rho} \varepsilon_j - \frac{T_e - T_i}{2 t_{eq}} \tag{E-10}$$

where γ is specific heat ratio.

5. Ion Temperature Equation

The equation relating energy gains and losses by the ion fluid is very similar to the electron temperature equation. For the particular case of cylindrical symmetry with only radial variations,

$$\frac{\partial T_i}{\partial t} + v \frac{\partial T_i}{\partial r} = -(\gamma-1)\left(T_i + \frac{q_i}{\rho}\right) \frac{1}{r} \frac{\partial}{\partial r}(rv) + \frac{1}{\rho} \frac{1}{r} \frac{\partial}{\partial r}\left(K_i r \frac{\partial T_i}{\partial r}\right) + \frac{T_e - T_i}{2 t_{eq}} \tag{E-11}$$

where, q_i is the von Neumann shockwave term.

The differences between the equation for the ion temperatures and the preceding equation for the electron temperatures are:

1) an artificial shockwave term appears in the ion temperature equation,

$$-(\gamma-1) \frac{q_i}{\rho} \frac{1}{r} \frac{\partial}{\partial r}(rv) \tag{E-12}$$

2) the joule heating term is absent in the ion temperature expression, and 3) the sign of the electron-ion exchange term is positive in the ion temperature equation,

$$\frac{T_e - T_i}{2 t_{eq}} \tag{E-13}$$

6. Ohm's Law

In a plasma immersed in a strong magnetic field, the electrical resistivity parallel to the magnetic field is about one-half that of the perpendicular resistivity. A two dimensional symmetric tensor, $\vec{\eta}^2$ is often employed to describe the resistivity. Thus, Ohm's Law can be written

$$\vec{E} = \vec{\eta}^2 \cdot \vec{J} \tag{E-14}$$

7. Maxwell's Equations

Maxwell's electromagnetic field equations must also be satisfied in the conducting dynamic plasma. Therefore,

$$\bar{\nabla} \times \bar{B} = \bar{J}, \qquad \bar{\nabla} \times \bar{E} = -\frac{\partial \bar{B}}{\partial t} \tag{E-15}$$

These are the electromagnetic field equations with the preceding fluid equations and Ohm's Law that describe the dynamic plasma problem. Boundary conditions defining the initial temperatures, density, and magnetic fields are required to now determine the solution to the set of hydromagnetic equations. Also, the variables at the walls must be specified at all times. Boundary conditions for a one dimensional model with azimuthal symmetry and infinite axial dimension will be presented.

A typical initial density employed in present codes for hydrodynamic pinches is 10^{15}/cc. Initial ion temperatures and electron temperatures of 1 ev to 5 ev are often used. Near the walls ($r = R_{wall}$) numerical difficulties often arise. Due to the sweeping action by inward pinches on the particles (snowplow effect) and also gas expansion, the particle density near the walls is lowered. Thus, fewer particles near the wall receive proportionally more energy. As a result, the electrical conduction near the walls increases; then the current increases causing a still higher electrical conductivity. A run-away phenomena results in which the current is concentrated in a narrow layer near the wall. (This run-away can often be avoided by introduction of a thermal conductivity to remove energy and to limit the electrical conductivity.)

When an explicit method is employed to solve the differential equations, low densities near the walls cause computational difficulties. The time step used in the explicit method is governed by the Alfvén or the magnetosonic speeds in the plasma at the mesh point in question.

The lower the density of the plasma, the smaller the time step must be for numerical stability.

Two alternatives are available for the wall density problem: 1) the magnetic field equations describing the region near the wall can be adjusted to accommodate the "vacuum" region produced near the wall, or 2) an artificial source of particles can be placed near the wall. In most cases, the continuously emitting wall approximates the true situation better than the "vacuum" field method. The particle emitting wall prevents the problem of current concentration near the wall from arising and allows explicit methods of integration to be employed. But, instabilities due to the increase in inward pressure from the wall emitted particles has been experienced in computer codes. (The extra pressure due to the emitted wall particles causes the plasma to move inward faster, which in turn demands a larger wall particle pressure, and thus run-away, or instability, occurs.)

Initially, forward or reverse bias magnetic fields are often present in the plasma. As stated in the preceding paragraph, the wall boundary problem can be satisfied if the magnetic fields near the wall (in the lower density region) are assumed to be "vacuum" fields. If the particle emitting wall model is used, provision for a discontinuity in the magnetic field must be made so that conservation of momentum at the wall exists. (This requirement results in a current sheath at the wall.)

For the case of reversed bias magnetic field, the magnetic field just within the plasma is set equal to the value in the insulating wall, (to eliminate surface currents). Therefore, the plasma initially moves outward as the external magnetic field first decreases to zero before going to its peak value. There are still limitations on the reversed bias

field that will allow a stable numerical calculation. Presently the value for the magnetic field is about 5 kilogauss for the reversed bias field.

Two popular methods for specifing the variables of a plasma exist, the Eulerian method and the Lagrangian method. Also, two methods of solving the partial differential equations are presently employed, the explicit and the implicit methods.

In the Eulerian method, the variables describing the plasma fluid are specified as functions of fixed points in space and equal time steps are often taken. (Note: These points are often moved between time iterative operations in solving the differential equations so as to optimize the location of the space mesh points.) In the other method, the Lagrangian method, the variables are functions specified in a moving system that moves with the plasma fluid. Due to difficulty in specifing wall emission effects and some shock phenomena, the Eulerian method is usually employed.

In the explicit method of specifing space derivatives for the differential equations, only differences at the time t are involved. But in the implicit method for specifing space derivatives, differences at both t and $t + \triangle t$ are required. The explicit method (due to its mathematical formulation) only allows for a numerical influence to propagate a limited distance in the step time $\triangle t$. Thus, when the Alfven speed becomes large due to low density or strong magnetic fields, the explicit numerical method fails to give the correct solution. The solution is usually then unstable. The advantage of the implicit method is that no such velocity-of-propagation limit exists. Thus, the step size, $\triangle t$, is not restricted for the implicit method.

BIBLIOGRAPHY

1. Ashby, D.E.T.F., Jephcott, D.F., Malein, A., Raynor, F.A., "Performance of the He-Ne Gas Laser as an Interferometer for Measuring Plasma Density", Fifth Annual Meeting of the Division of Plasma Physics of the American Physical Society, San Diego, November, 1963.

2. Burkhardt, L.C. and Lovberg, R.H., "Current Sheet in a Coaxial Plasma Gun", Phys. Fluids, 5, 341, 1962.

3. Colgate, Stirling A., "Initial Conditions for the Dynamic Pinch", Lawrence Radiation Laboratory, University of California, Livermore, California, UCRL-4895, 1957.

4. Dougal, Arwin A., "Optical Maser Probing Theory for Magneto-plasma Diagnostics", Proc. Fourth Symposium on MHD, IV, pp. 1-4, IEEE, 1963.

5. Filippov, N.V., "Investigation of Pressures in a Powerful Pulsed Gas Discharge using a Piezoelectric Measuring Device", Plasma Physics and the Problem of Controlled Thermonuclear Reactions, III, Pergamon Press, 280, 1959.

6. Friedrich, Otto M., Jr., "Analysis of the Plasma Current Sheath's Motion for an Inverse or 'Hard-Core' Pinch", Master's Thesis, The University of Texas, 1962.

7. Granet, Irving and Guman, William J., "The Application of the Pinch Process for Space Propulsion", Z. Flugwiss, 10, Heft 3, 83, 1962.

8. Granet, Irving and Guman, William J., "Some Engineering Aspects of the Magnetohydrodynamic Pinch Process for Space Propulsion", Republic Aviation Corporation, Farmingdale, N.Y., AFOSR TN 60-86, (PPL # 120), November, 1959.

9. Gribble, R.F., Craig, J.P., and Dougal, Arwin A., "Spatial Density Measurements in Fast Theta-Pinch Plasma by Maser Excitation of Coupled Infrared Resonators", Applied Physics Letters, 5, 60, August 1, 1964.

10. Gribble, R.F., Roberts, H.N., and Dougal, Arwin A., "Diagnostics of Experimental Extreme Temperature Plasma", Quarterly Progress Report No. 1 on Research on Plasma Diagnostic Methods for High Temperature Plasma Research, (Contract No. AF 33(657)-11073), Plasma Dynamics Research Laboratory, The University of Texas, Austin, Texas, July 15, 1963.

11. Guman, William J., and Granet, Irving, "Pinch Dynamics with Nonuniform Conditions", Republic Aviation Corporation, Farmingdale, N.Y., PPL-TR-60-6, January, 1960.

12. Hain, K., Hain, G., Roberts, K.V., and Roberts, S.J., "Fully Ionized Pinch Collapse", Z. Naturforschg. 15a, 1039-1050, 1960.

13. Killeen, J., Gibson, G., and Colgate, S.A., "Boundary-Layer Formation in the Pinch", Phys. Fluids, 3, 387, 1960.

14. King, P.G.R., and Steward, G.J., New Scientist, 17, 180, 1963.

15. Knight, H.T., "Piezoelectric Detector for Low-Pressure Shock Waves", Review of Scientific Instruments, 29, 174, 1958.

16. Lovberg, R.H., "Acceleration of Plasma by Displacement Currents Resulting from Ionization", VIe Conference Internationale sur les Phenomenes D'Ionisation dans les Gaz, vol. IV, 235, S.E.R.M.A., Paris, France, 1963.

17. Lovberg, R.H., "Measurement of Plasma Density in a Rail Accelerator by Means of Schlieren Photography", IRE International Symposium on Plasma Phenomena and Measurements, San Diego, October 29-November 1, 1963.

18. Mostov, Philip M., Neuringer, Joseph L., and Rigney, Donald, "Electromagnetic Acceleration of a Plasma Slug", Republic Aviation Corporation, Farmingdale, N.Y., PPL-TR-61-5, February, 1961.

19. Pai, Shih-I, Magnetogasdynamics and Plasma Dynamics, Prentice-Hall, 1962.

20. Roberts, K.V., Hertweck, F., and Roberts, S.J., "Thetatron, A Two-Dimensional Magnetohydrodynamic Computer Programme, Part 1, General Discussion", Culham Laboratory, UKAEA, CLM-R 29, 1963.

21. Rosenbluth, M., Garwin, R., and Rosenbluth, A., "Infinite Conductivity Theory for the Pinch", Los Alamos Scientific Laboratory, Los Alamos, New Mexico, LA-1850, 1954.

22. Stern, M.O., and Dacus, E.N., "Piezoelectric Probe for Plasma Research", Review of Scientific Instruments, 32, 140, 1961.

23. Vlases, G.C., "Experiments in a Cylindrical Magnetic Shock Tube", Journal of Fluid Mechanics, 16, Part 1, 82, 1963.

24. Wyld, N.W., and Watson, K.M., "Ionization and Heating of a Plasma in a Magnetic Field", Conference on Controlled Thermonuclear Reactions, June 4-7, 1956, Gatlinburg, Tennesse, U.S.A.E.C. Report TID-7520 (Part 2), 1956.